THE STABILITY OF TWO-DIMENSIONAL LINEAR FLOWS

Thesis by

Ronald Robert Lagnado

In Partial Fulfillment of the Requirements

for the Degree of

Doctor of Philosophy

California Institute of Technology

Pasadena, California

1985

(Submitted January 9, 1985)

ACKNOWLEDGEMENTS

I am grateful to Professor L. Gary Leal for the guidance and encouragement he has provided as my research advisor and for his personal interest in my professional development. His insight in research and his excellence as a teacher have enhanced my own abilities tremendously. He has also been a very good friend.

I thank Dr. Nhan Phan-Thien for his substantial contributions to this investigation. My friends Jeff Simmen, Doug Lynch, Paul Dunlap, Ed Ascoli, and Howard Stone offered many helpful suggestions which I gratefully acknowledge. The interaction with all of the members of my research group has been of great benefit to me as well.

Special thanks go to Ms. Kathy Lewis for an excellent job of typing a difficult manuscript and to Mr. Seichi Nakawatase for modifying the four-roll mill.

ABSTRACT

This thesis presents the results of a theoretical and experimental investigation concerned with the hydrodynamic stability of extensional flows. In particular, model extensional flows in the class of two-dimensional linear flows are considered. These flows may be classified by a parameter λ ranging from $\lambda = 0$ for simple shear flow to $\lambda = 1$ for pure extensional flow.

In Chapter I, a linear stability analysis is given for an unbounded Newtonian fluid undergoing two-dimensional linear flows. The linearized velocity disturbance equations are analyzed to yield the large-time asymptotic behavior of spatially periodic initial disturbances. The results confirm the established fact that simple shear flow ($\lambda = 0$) is linearly stable. However, it is found that unbounded extensional flows in the range $0 < \lambda \leq 1$ are unconditionally unstable. Spatially periodic initial disturbances which have lines of constant phase parallel to the inlet streamline of the basic flow and have sufficiently small wavenumbers in the direction normal to the plane of the basic flow must grow exponentially in time. A complete analytical solution of the vorticity disturbance equation is obtained for the case of pure extensional flow ($\lambda = 1$).

Chapter II presents a linear stability analysis for an Oldroyd-type fluid undergoing two-dimensional linear flows throughout an unbounded region. The effects of fluid elasticity on extensional-flow stability are considered. The time derivatives in the constitutive equation can be varied continously from co-rotational to co-deformational as a parameter β varies from 0 to 1. It is again found that unbounded flows in the range $0 < \lambda \leq 1$ are unconditionally unstable with respect to spatially periodic intitial disturbances that have lines of constant phase parallel to the inlet streamline in the plane of the basic flow. For small values of the Weissenberg number, only disturbances with sufficiently small wavenumbers α_3 in the direction normal to the plane of the basic flow give rise

to instability. However, for certain values of β, there exist critical values of the Weissenberg number above which flows are unstable for all values of the wavenumber α_3.

The results of an experimental investigation of the flow of a Newtonian fluid in a four-roll mill are found in Chapter III. The four-roll mill may be used to generate an approximation to two-dimensional linear flow in a central region between the rollers. A photographic flow-visualization technique was employed to study the stability of a pure extensional flow ($\lambda = 1$). Two four-roll mills with different ratios of roller length to gap width between adjacent rollers (namely, $L/d = 3.39$ and 12.73) were used in order to study end effects on flow stability. At sufficiently small Reynolds numbers the flow in both devices is essentially two-dimensional throughout most of the region between the rollers, except near the top and bottom bounding surfaces where three-dimensional flow involving four symmetrically positioned vortices appears. The vertical extent of this two-dimensional flow gradually diminishes and the vortices grow in size and strength as the Reynolds number is increased up to a quasi-critical range. An increase in Reynolds number through this quasi-critical range results in an abrupt transition to a steady three-dimensional flow throughout the entire region between the rollers. The three-dimensionality is significantly less pronounced in the device with $L/d = 12.73$, however. At sufficiently high Reynolds numbers beyond the quasi-critical range, the flow becomes unsteady in time and eventually turbulent.

TABLE OF CONTENTS

CHAPTER I

THE STABILITY OF TWO-DIMENSIONAL LINEAR FLOWS OF A NEWTONIAN FLUID

The text of Chapter I consists of an article which appeared in *The Physics of Fluids*, Volume 27, pages 1094-1101, May 1984.

The Stability of Two-Dimensional Linear Flows

by

R. R. Lagnado, N. Phan-Thien†, and L. G. Leal

Department of Chemical Engineering
California Institute of Technology
Pasadena, California 91125

† Permanent address: Mechanical Engineering Department, Sydney University, N. S. W. 2006, Australia.

Abstract

A theoretical investigation is made of the linear stability of a viscous incompressible fluid undergoing a steady, unbounded two-dimensional flow in which the velocity field is a linear function of position. Such flows are approximately generated by a four-roll mill device which has many experimental applications, and can be characterized completely by a single parameter λ which ranges from $\lambda = 0$ for simple shear flow to $\lambda = 1$ for pure extensional flow. The linearized velocity disturbance equations are analyzed for an arbitrary spatially periodic initial disturbance to give the asymptotic behavior of the disturbance at large time for $0 \leq \lambda \leq 1$. In addition, a complete analytical solution of the vorticity disturbance equation is obtained for the case $\lambda = 1$. It is found that unbounded flows with $0 < \lambda \leq 1$ are unconditionally unstable. An instability criterion relating the initial disturbance wave vector $\boldsymbol{\alpha}$ to the steady flow strain rate E, kinematic viscosity ν, and the parameter λ is obtained. This criterion shows that for all admissible values of E and ν, a wave vector $\boldsymbol{\alpha}$ may be found which corresponds to disturbances that grow exponentially in time. The growth of these disturbances is accompanied by a growth of vorticity oriented along the principal axis of extensional strain in the case $\lambda = 1$. The results of this investigation also confirm the established fact that simple shear flow ($\lambda = 0$) is stable to all infinitesimal spatially periodic disturbances.

I. Introduction

A linear stability analysis is the usual first step taken to investigate the physical realizability ("stability") of a laminar flow. Although nonlinear effects and/or the presence of boundaries will generally lead to a discrepancy between linearized theory and experimental observations of instability in real systems,[1-3] the linear stability analysis can still contribute to an understanding of the processes which lead to a departure from the base flow (i.e., an "instability") as well as at least a qualitative estimate of conditions for this change in the flow. The majority of linear stability analyses of flows are simplified by the fact that the base flow is unidirectional, and the flow domain unbounded in one or more directions in space.

We consider here a linear stability analysis for an unbounded incompressible Newtonian fluid which is undergoing a two-dimensional flow in which the velocity varies linearly with position. The analysis applies to a class of two-dimensional linear flows ranging from simple shear flow to pure extensional flow which can be produced approximately in the region between the rollers of two- and four-roll mills. The four-roll mill was invented in 1932 by G. I. Taylor[4] and consists basically of four cylindrical rollers which are positioned at the corners of a square and immersed in a tank of fluid. The two-roll mill is a simpler version of this device with two of the rollers removed. One reason for interest in the two-dimensional linear flows produced by the two- and four-roll mills is their application as models for the flows occurring in real polymer processes such as calendering and extrusion. Another reason is the increasing experimental use of two- and four-roll mills for the study of such phenomena as drop deformation and breakup,[4-7] flow-induced changes in the conformation of macromolecules in solution,[8,9] and floc stability in flow.

In spite of the importance of these flows, relatively few basic fluid mechanical investigations have been made. The stability of actual two- and four-roll mill flows has never undergone a thorough theoretical or experimental study, though it is generally recognized that the onset of instability at quite small roller speeds is one of the main limitations in the use of these devices for the studies mentioned earlier. Furthermore, even the *idealized* model of an *unbounded* two-dimensional linear flow has not been subjected to a rigorous stability analysis except in the limiting cases of simple shear flow and pure extensional flow.

The stability of simple shear flow between parallel plane boundaries (plane Couette flow) has undergone thorough investigation. A linear stability analysis for this flow requires solution of the Orr-Sommerfeld equation that governs infinitesimal disturbances which are periodic in the direction of the basic flow. Hopf[10] carried out an asymptotic analysis of solutions for very small and very large values of αRe (where α is the wavenumber of the disturbance and Re is the Reynolds number of the basic flow). Gallagher and Mercer[11] obtained numerical solutions for values of αRe up to 1000. An exact analytical solution of the Orr-Sommerfeld equation was given by Reid[12] who also considered semi-bounded plane Couette flow. Asymptotic and numerical investigations were carried out by many other authors, as well. All of these studies indicate that plane Couette flow is stable to all infinitesimal disturbances at all Reynolds numbers.

The specific case of pure extensional flow has been considered (indirectly) by Pearson[13] in a paper concerned with the behavior of weak homogeneous turbulence subjected to a uniform distortion. Pearson found that the total energy associated with the turbulence increases without limit when the mean flow is an unbounded pure extensional flow. This result was obtained by an analysis of a linearized form of the Navier-Stokes equations. It may be inferred from this analysis that an unbounded pure extensional flow is unconditionally unstable to

infinitesimal disturbances.

In the present paper, we report a straightforward linear stability analysis for a general, one-parameter class of unbounded two-dimensional linear flows which range from simple shear flow to pure extensional flow. Our purpose is to investigate the effect of flow type (e.g.,the ratio of strain-rate to vorticity) on stability in order to provide a link between the results obtained for the two limiting cases. We shall obtain criteria for determining the stability of the basic flow with respect to spatially periodic disturbances as well as a qualitative interpretation of the physical mechanism for instability.

II. The Basic Flow

The velocity field **U** for a steady *linear* flow can be expressed in the form

$$\mathbf{U} = \Gamma \cdot \mathbf{x} \ , \tag{1}$$

where Γ is a second-order tensor which is independent of the position vector $\mathbf{x}$. It has been demonstrated by Marrucci and Astarita[14] that this general form of the equations defining steady two-dimensional linear flow of an incompressible fluid can be reduced to a form which contains only two parameters. In particular, a Cartesian coordinate system can be selected relative to which the matrix of components of Γ is

$$[\Gamma] = \frac{E}{2}\begin{bmatrix} 1+\lambda & 1-\lambda & 0 \\ -(1-\lambda) & -(1+\lambda) & 0 \\ 0 & 0 & 0 \end{bmatrix} . \tag{2}$$

Here, $E \geq 0$ is the magnitude of the local velocity gradient, and λ a parameter which specifies the type of flow as it varies between ± 1. The cases $\lambda = -1$, $\lambda = 0$, and $\lambda = 1$ correspond to pure rotational flow, simple shear flow, and pure extensional (straining) flow, respectively.

From Eqs. (1) and (2), the Cartesian components of the basic velocity field

are found to be

$$U_1 = \frac{E}{2}[(1+\lambda)x_1 + (1-\lambda)x_2] ,$$

$$U_2 = -\frac{E}{2}[(1-\lambda)x_1 + (1+\lambda)x_2] , \tag{3}$$

$$U_3 = 0 .$$

The family of curves

$$(x_1 + x_2)^2 - \lambda(x_1 - x_2)^2 = C , \tag{4}$$

where C is an arbitrary constant comprises the streamlines for this flow field. Figure 1 depicts streamlines of the basic flow for several values of λ. All flows possess a stagnation point at $\mathbf{x} = 0$. The cases $-1 \leq \lambda < 0$ and $0 \leq \lambda \leq 1$ correspond to closed- and open-streamline flows, respectively.

The principal strain-rates and principal axes of strain for the basic flow are determined by the eigenvalues and eigenvectors, respectively, of the rate-of-strain tensor $\Gamma + \Gamma^T$. With Γ in the form of (2), we find that the principal axes of strain coincide with the x_1–, x_2–, and x_3–axes, and the associated principal strain-rates are $E(1+\lambda)$, $-E(1+\lambda)$, and 0, respectively. The basic vorticity field $\Omega = \nabla \times \mathbf{U}$ has Cartesian components

$$\Omega_1 = 0, \quad \Omega_2 = 0, \quad \Omega_3 = -E(1-\lambda) . \tag{5}$$

Hence, the magnitude of the vorticity relative to the largest strain-rate is given by $(1-\lambda)/(1+\lambda)$. This ratio varies monotonically from $+\infty$ to 0 as λ ranges from -1 to +1.

The flows for which $0 < \lambda \leq 1$ are called "strong" flows because the strain-rate is greater than the vorticity.[15–17] In this flow regime, the streamlines form a family of hyperbolas with two streamlines as asymptotes. These asymptotes are

straight lines intersecting at the central stagnation point with slopes of $(\sqrt{\lambda}+1)/(\sqrt{\lambda}-1)$ and $(\sqrt{\lambda}-1)/(\sqrt{\lambda}+1)$ and shall be referred to as the "inlet" and "outlet" streamlines, respectively. The streamlines for a typical strong flow are shown in Fig. 2. It is apparent that flow is directed toward the stagnation point along the inlet streamline and away along the outlet streamline.

III. The Linearized Disturbance Equations

We consider an unbounded incompressible Newtonian fluid with constant density ρ and kinematic viscosity ν which is undergoing the steady two-dimensional linear flow given by Eqs. (1) and (2). This steady velocity field $\mathbf{U}(\mathbf{x})$, and the corresponding steady pressure field $P(\mathbf{x})$ satisfy the Navier-Stokes equation

$$\mathbf{U}\cdot\nabla\mathbf{U} = -\frac{1}{\rho}\nabla P + \nu\nabla^2\mathbf{U} \ , \tag{6}$$

and the incompressibility condition

$$\nabla\cdot\mathbf{U} = 0 \ . \tag{7}$$

Suppose that this steady flow is disturbed at some initial time $t = 0$. Let $\mathbf{u}'(\mathbf{x},t) = \mathbf{U}(\mathbf{x}) + \mathbf{u}(\mathbf{x},t)$ and $p'(\mathbf{x},t) = P(\mathbf{x}) + p(\mathbf{x},t)$ denote, respectively, the velocity and pressure fields of the subsequent altered flow.

Restricting our attention in this paper to the assumption, $\|\mathbf{u}\| << \|\mathbf{U}\|$, the resulting linearized disturbance equation for the solenoidal disturbance velocity $\mathbf{u}$ is

$$\frac{\partial\mathbf{u}}{\partial t} + (\Gamma\cdot\mathbf{x})\cdot\nabla\mathbf{u} = -\Gamma\cdot\mathbf{u} - \frac{1}{\rho}\nabla p + \nu\nabla^2\mathbf{u} \ , \tag{8}$$

where (1) has been used.

In order to determine the stability of the unbounded flow, we must find all solutions $\mathbf{u}(\mathbf{x},t)$ of Eq. (8) for $\mathbf{x} \in \mathbb{R}^3$ and $t \geq 0$ which satisfy the initial condition

$$\mathbf{u}(\mathbf{x},0) = \mathbf{u}^{\circ}(\mathbf{x}) \quad . \tag{9}$$

The vector field $\mathbf{u}^{\circ}(\mathbf{x})$ specifies the arbitrary initial disturbance and is assumed for physical reasons to be solenoidal and spatially bounded.

The usual approach in a linear stability analysis is to seek disturbance solutions of the form

$$\mathbf{u}(\mathbf{x},t) = e^{-\sigma t}\, \mathbf{f}(\mathbf{x}) \ ,$$

$$p(\mathbf{x},t) = e^{-\sigma t}\, p(\mathbf{x}) \ ,$$

and solve the resulting spectral problem for the eigenvalues σ and eigenfunctions $(\mathbf{f},p)$. Stability is then judged by the sign of the real parts of the eigenvalues. In the case of two-dimensional linear flow, the basic flow is a function of two spatial variables (except for simple shear flow), and this spectral problem is difficult to solve analytically. We circumvent this difficulty by seeking an alternative representation of the solutions of (8). The fact that we seek solutions of the velocity disturbance equations on an unbounded domain in space suggests the use of spatial Fourier transforms. We follow this suggestion in the following section. After application of the spatial Fourier transform to the velocity disturbance equations, we obtain a system of first-order linear partial differential equations which can be solved by the method of characteristics. The velocity disturbance Fourier transform so obtained can then be inverted to yield the desired general solution.

IV. General Solution of Linearized Disturbance Equations

A general solution of the linearized disturbance Eq. (8) will now be obtained following the procedure outlined at the end of the preceding section. Our solution is general in the sense that the initial disturbance $\mathbf{u}^{\circ}(\mathbf{x})$ is left unspecified.

A later consideration of specific forms for $\mathbf{u}^o(\mathbf{x})$ will lead to the establishment of flow stability criteria.

Since we are considering the flow of an unbounded fluid, the disturbance velocity $\mathbf{u}(\mathbf{x},t)$ and disturbance pressure $p(\mathbf{x},t)$ are defined for all values of $\mathbf{x}$ in $\mathbb{R}^3$. The Fourier transforms of $\mathbf{u}(\mathbf{x},t)$ and $p(\mathbf{x},t)$ are defined as

$$\hat{\mathbf{u}}(\mathbf{k},t) = \int \exp(i\mathbf{k}\cdot\mathbf{x})\mathbf{u}(\mathbf{x},t)d\mathbf{x} \ , \tag{10}$$

$$\hat{p}(\mathbf{k},t) = \int \exp(i\mathbf{k}\cdot\mathbf{x})p(\mathbf{x},t)d\mathbf{x} \ .$$

Thus, formally taking the Fourier transform of Eq. (8), we obtain

$$\frac{\partial\hat{\mathbf{u}}}{\partial t} - (\Gamma^T\cdot\mathbf{k})\cdot\nabla_k\hat{\mathbf{u}} = -\Gamma\cdot\hat{\mathbf{u}} + \frac{i}{\rho}\hat{p}\mathbf{k} - \nu k^2\hat{\mathbf{u}} \ , \tag{11}$$

while incompressibility and the initial condition require

$$\mathbf{k}\cdot\hat{\mathbf{u}} = 0 \ , \tag{12}$$

$$\hat{\mathbf{u}}(\mathbf{k},0) = \hat{\mathbf{u}}^o(\mathbf{k}) \ . \tag{13}$$

In (11)-(13), $\hat{\mathbf{u}}^o(\mathbf{k})$ is the Fourier transform of $\mathbf{u}^o(\mathbf{x})$, $\nabla_k\hat{\mathbf{u}}$ is the gradient of $\hat{\mathbf{u}}(\mathbf{k},t)$ with respect to the wave vector $\mathbf{k}$, and $k^2 = \mathbf{k}\cdot\mathbf{k}$. The pressure term in Eq. (11) can be eliminated by first forming the inner product of Eq. (11) with $\mathbf{k}$ and using the condition (12) to obtain

$$\frac{i}{\rho}\hat{p}\mathbf{k} = \frac{2}{k^2}(\mathbf{k}\cdot\Gamma\cdot\hat{\mathbf{u}})\mathbf{k} \ . \tag{14}$$

which is then substituted for the pressure term in Eq. (11). We obtain the following equation for the Fourier transform of the velocity disturbance:

$$\frac{\partial \hat{\mathbf{u}}}{\partial t} - (\Gamma^T \cdot \mathbf{k}) \cdot \nabla_k \hat{\mathbf{u}} = - \Gamma \cdot \hat{\mathbf{u}} + \frac{2}{k^2} (\mathbf{k} \cdot \Gamma \cdot \hat{\mathbf{u}}) \mathbf{k} - \nu k^2 \hat{\mathbf{u}} \, . \tag{15}$$

Equation (15) represents a system of first-order linear partial differential equations for the components of $\hat{\mathbf{u}}(\mathbf{k},t)$. The solution of Eq. (15) satisfying the initial condition (13) can be obtained using the method of characteristics which are obtained by solving the linear system

$$\frac{d\mathbf{k}}{dt} = - \Gamma^T \cdot \mathbf{k} \, , \tag{16}$$

subject to the initial condition

$$\mathbf{k}(o) = \boldsymbol{\alpha} \, . \tag{17}$$

The solution for $t \geq 0$ is

$$\mathbf{k}(t) = e^{-t\Gamma^T} \cdot \boldsymbol{\alpha} \, , \tag{18}$$

where $e^{-t\Gamma^T}$ is the fundamental matrix solution for the linear system (16). The characteristic curve of Eq. (15) which passes through the point $\boldsymbol{\alpha}$ is then represented parametrically by Eq. (18). Equation (18) also defines a transformation of variables from $(\mathbf{k},t)$ to $(\boldsymbol{\alpha},t)$. Let $\hat{\mathbf{u}}'(\boldsymbol{\alpha},t)$ denote the function which assumes the values of $\hat{\mathbf{u}}(\mathbf{k},t)$ at points on the characteristic passing through $\boldsymbol{\alpha}$ at $t = 0$. Then, $\hat{\mathbf{u}}'(\boldsymbol{\alpha},t)$ is defined by

$$\hat{\mathbf{u}}'(\alpha,t) = \hat{\mathbf{u}}(e^{-t\Gamma^T} \cdot \boldsymbol{\alpha},t) \, . \tag{19}$$

Along the characteristics (18), $\hat{\mathbf{u}}'$ obeys

$$\frac{\partial \hat{\mathbf{u}}'}{\partial t} = -\Gamma \cdot \hat{\mathbf{u}}' + \mathbf{B}(t) \cdot \hat{\mathbf{u}}' - \nu k^2(t) \hat{\mathbf{u}}' \, , \tag{20}$$

$$\hat{\mathbf{u}}'(\boldsymbol{\alpha},0) = \hat{\mathbf{u}}^{\circ}(\alpha) \, . \tag{21}$$

Here, $k^2(t) = \mathbf{k}(t) \cdot \mathbf{k}(t)$, with $\mathbf{k}(t)$ given by Eq. (18), and the tensor $\mathbf{B}(t)$ is

$$\mathbf{B}(t) = \frac{2}{k^2(t)}\mathbf{k}(t)\mathbf{k}(t)\cdot\Gamma \ . \tag{22}$$

For a fixed value of α, Eq. (20) represents a system of linear ordinary differential equations with initial condition (21). This linear system then governs the behavior of $\hat{\mathbf{u}}(\mathbf{k},t)$ along a characteristic. The solution of (20) is given by

$$\hat{\mathbf{u}}'(\alpha,t) = \Phi(\alpha,t)\cdot\hat{\mathbf{u}}^\circ(\alpha) \ , \tag{23}$$

where $\Phi(\alpha,t)$ denotes the fundamental matrix solution for the linear system (20). For fixed α, this fundamental matrix satisfies the equations

$$\frac{\partial}{\partial t}\Phi = -\Gamma\cdot\Phi + \mathbf{B}(t)\cdot\Phi - \nu k^2(t)\Phi \ ,$$

$$\Phi(\alpha,0) = \mathbf{I} \ . \tag{24}$$

Substituting the result

$$\alpha = e^{t\Gamma^T}\cdot\mathbf{k}$$

into (23), we obtain

$$\hat{\mathbf{u}}'(e^{t\Gamma^T}\cdot\mathbf{k},t) = \Phi(e^{t\Gamma^T}\cdot\mathbf{k},t)\cdot\hat{\mathbf{u}}^\circ(e^{t\Gamma^T}\cdot\mathbf{k}) \ .$$

Hence, in view of Eq. (19), it follows that

$$\hat{\mathbf{u}}(\mathbf{k},t) = \Phi(e^{t\Gamma^T}\cdot\mathbf{k},t)\cdot\hat{\mathbf{u}}^\circ(e^{t\Gamma^T}\cdot\mathbf{k}) \tag{25}$$

gives the solution of (15) and (13).

The inverse Fourier transform of $\hat{\mathbf{u}}(\mathbf{k},t)$ then yields the general solution for the velocity disturbance

$$\mathbf{u}(\mathbf{x},t) = \frac{1}{(2\pi)^3}\int \exp(-i\mathbf{k}\cdot\mathbf{x})\Phi(e^{t\Gamma^T}\cdot\mathbf{k},t)\cdot\hat{\mathbf{u}}^\circ(e^{t\Gamma^T}\cdot\mathbf{k})d\mathbf{k} \quad . \tag{26}$$

We can simplify this solution somewhat by changing the variable of integration from $\mathbf{k}$ to $\alpha = e^{t\Gamma^T}\cdot\mathbf{k}$. The Jacobian for this transformation is unity and we obtain the following form of the general solution

$$\mathbf{u}(\mathbf{x},t) = \frac{1}{(2\pi)^3}\int \exp[-i(e^{-t\Gamma^T}\cdot\alpha)\cdot\mathbf{x}]\Phi(\alpha,t)\cdot\hat{\mathbf{u}}^\circ(\alpha)d\alpha \quad . \tag{27}$$

V. Consideration of Fundamental Modes

In order to judge the stability of the flow from the general velocity disturbance solution (27), we must give consideration to a specific form of the initial disturbance $\mathbf{u}^\circ(\mathbf{x})$. The usual approach is to consider an initial disturbance which is a periodic function of spatial position. The solution of the velocity disturbance equation corresponding to this periodic initial disturbance is called a fundamental mode.

Let the initial disturbance be given by

$$\mathbf{u}^\circ(\mathbf{x}) = \exp(-i\alpha\cdot\mathbf{x})\mathbf{v}^\circ \quad , \tag{28}$$

where $\mathbf{v}^\circ$ is a constant vector, and the wave vector $\alpha = (\alpha_1,\alpha_2,\alpha_3)$ has real components. The fundamental mode solution is given by

$$\mathbf{u}(\mathbf{x},t) = \exp[-i(e^{-t\Gamma^T}\cdot\alpha)\cdot\mathbf{x}]\Phi(\alpha,t)\cdot\mathbf{v}^\circ \quad . \tag{29}$$

The general solution (27) obviously expresses the velocity disturbance with an arbitrary initial value $\mathbf{u}^\circ(\mathbf{x})$ as a superposition of these fundamental modes.

The stability of the basic flow with respect to a spatially periodic initial disturbance (28) is then determined by the asymptotic behavior as $t\to\infty$ of the fundamental mode solution (29). The term $\exp[-i(e^{-t\Gamma^T}\cdot\alpha)\cdot\mathbf{x}]$ stays bounded as $t\to\infty$. Hence, the growth or decay of the disturbance depends only on the behavior of $\Phi(\alpha,t)\cdot\mathbf{v}^\circ$ which for a fixed value of α is a solution of the linear system

$$\frac{d\mathbf{y}}{dt} = -\Gamma\cdot\mathbf{y} + \mathbf{B}(t)\cdot\mathbf{y} - \nu k^2(t)\mathbf{y} \ , \tag{30}$$

satisfying the initial condition

$$\mathbf{y}(o) = \mathbf{v}^o \ . \tag{31}$$

Here, $\mathbf{k}(t)$ and $\mathbf{B}(t)$ are defined by (18) and (22),respectively. It is not possible to obtain a simple expression for the solution of (30). Instead, we shall analyze the system asymptotically in order to determine the effect of the parameters α, E, ν, and λ on the behavior of solutions as $t\to\infty$.

We begin by deriving a differential inequality for the Euclidean norm of a solution of (30). Forming the inner product of Eq. (30) with $\mathbf{y}$ and introducing the Euclidean norm $||\mathbf{y}|| = (\mathbf{y}\cdot\mathbf{y})^{1/2}$, we obtain

$$||\mathbf{y}||\frac{d}{dt}||\mathbf{y}|| = (-\Gamma\cdot\mathbf{y})\cdot\mathbf{y} + (\mathbf{B}(t)\cdot\mathbf{y})\cdot\mathbf{y} - \nu k^2(t)||\mathbf{y}||^2 \ , \tag{32}$$

An application of the Cauchy-Schwarz inequality gives upper bounds for the first two terms on the right-hand side of Eq. (32). This leads to the differential inequality

$$\frac{d}{dt}||\mathbf{y}|| \le [3||\Gamma|| - \nu k^2(t)]||\mathbf{y}|| \ , \tag{33}$$

where $||\Gamma||$ denotes the spectral norm of Γ and is defined by

$$||\Gamma|| = \sup\left\{ \frac{||\Gamma\cdot\mathbf{x}||}{||\mathbf{x}||} : \quad \mathbf{x}\in\mathbf{R}^3 \ , \quad ||\mathbf{x}|| \neq 0 \right\} \ . \tag{34}$$

It can be shown that $||\Gamma||$ must also equal the square root of the largest eigenvalue of $\Gamma^T\Gamma$. Using (2) we find that for $0 \le \lambda \le 1$

$$||\Gamma|| = E \ . \tag{35}$$

Thus one obtains

$$\|\mathbf{y}(t)\| \le \|\mathbf{y}(o)\|\exp(3Et)\exp\left[-\nu \int_o^t k^2(\tau)d\tau\right] , \tag{36}$$

where

$$k^2(t) = \|e^{-t\Gamma^T}\cdot\boldsymbol{\alpha}\|^2 .$$

We shall determine the form of $k^2(t)$ separately for the cases $\lambda=0$ in which Γ^T has a multiple eigenvalue and $0 < \lambda \le 1$ in which Γ^T has distinct eigenvalues. The inequality (36) can then be used in each case to reveal conditions under which the solutions of (30) decay to zero as $t\to\infty$.

A. The Case $\lambda = 0$

For simple shear flow, $\lambda = 0$, a Cartesian coordinate system can be chosen such that

$$[\Gamma] = \begin{pmatrix} 0 & E & 0 \\ 0 & 0 & 0 \\ 0 & 0 & 0 \end{pmatrix} . \tag{37}$$

The fundamental matrix $e^{-t\Gamma^T}$ in this case is given by

$$e^{-t\Gamma^T} = \begin{pmatrix} 1 & 0 & 0 \\ -Et & 1 & 0 \\ 0 & 0 & 1 \end{pmatrix} . \tag{38}$$

The Cartesian components of $\mathbf{k}(t) = e^{-t\Gamma^T}\cdot\boldsymbol{\alpha}$ are then found to be

$$k_1(t) = \alpha_1, \quad k_2(t) = \alpha_2 - Et\alpha_1, \quad k_3(t) = \alpha_3, \tag{39}$$

and it follows that

$$\exp\left[-\nu \int_o^t k^2(\tau)d\tau\right] =$$

$$\exp[-\nu(\alpha_1^2 + \alpha_2^2 + \alpha_3^2)t]\exp(\nu E\alpha_1\alpha_2 t^2)\exp\left(-\frac{\nu E^2}{3}\alpha_1^2 t^3\right) . \tag{40}$$

Substituting (40) into the inequality (36), we obtain

$$\|\mathbf{y}(t)\| \le \|\mathbf{y}(o)\|\exp\{[3E-\nu(\alpha_1^2+\alpha_2^2+\alpha_3^2)]t\}\exp(\nu E\alpha_1\alpha_2 t^2)\exp\left[-\frac{\nu E^2}{3}\alpha_1^2 t^3\right] \quad (41)$$

From (41) we can conclude that $\|\mathbf{y}(t)\| \to 0$ as $t\to\infty$ if either of the following conditions are satisfied

$$\alpha_1 \neq 0 \ , \quad (42a)$$

or

$$\alpha_1 = 0 \ , \alpha_2^2+\alpha_3^2 > \frac{3E}{\nu} \ . \quad (42b)$$

If $\alpha_1 = 0$ and $\alpha_2^2+\alpha_3^2 < \frac{3E}{\nu}$, then the right-hand side of (41) is unbounded as $t\to\infty$. Whether or not $\|\mathbf{y}(t)\|$ is unbounded cannot be determined in this case, however.

B. The Case $0 < \lambda \le 1$

In this case we consider the form of Γ given by Eq. (2). The eigenvalues of $-\Gamma^T$ are $E\sqrt{\lambda}$, 0, and $-E\sqrt{\lambda}$, and the fundamental matrix $e^{-t\Gamma^T}$ is found to assume the following form

$$e^{-t\Gamma^T} =$$

$$\frac{1}{4\sqrt{\lambda}}\begin{bmatrix} -(1-\sqrt{\lambda})^2 e^{E\sqrt{\lambda}t} + (1+\sqrt{\lambda})^2 e^{-E\sqrt{\lambda}t} & (1-\lambda)(e^{E\sqrt{\lambda}t} - e^{-E\sqrt{\lambda}t}) & 0 \\ -(1-\lambda)(e^{E\sqrt{\lambda}t} - e^{-E\sqrt{\lambda}t}) & (1+\sqrt{\lambda})^2 e^{E\sqrt{\lambda}t} - (1-\sqrt{\lambda})^2 e^{-E\sqrt{\lambda}t} & 0 \\ 0 & 0 & 4\sqrt{\lambda} \end{bmatrix} \quad (43)$$

The Cartesian components of $\mathbf{k}(t) = e^{-t\Gamma^T}\cdot\boldsymbol{\alpha}$ are then given by

$$k_1(t) = \frac{1-\sqrt{\lambda}}{4\sqrt{\lambda}}(\mathbf{q}_1\cdot\boldsymbol{\alpha})e^{E\sqrt{\lambda}t} + \frac{1+\sqrt{\lambda}}{4\sqrt{\lambda}}(\mathbf{q}_2\cdot\boldsymbol{\alpha})e^{-E\sqrt{\lambda}t} \ , \quad (44a)$$

$$k_2(t) = \frac{1+\sqrt{\lambda}}{4\sqrt{\lambda}}(\mathbf{q}_1\cdot\boldsymbol{\alpha})e^{E\sqrt{\lambda}t} + \frac{1-\sqrt{\lambda}}{4\sqrt{\lambda}}(\mathbf{q}_2\cdot\boldsymbol{\alpha})e^{-E\sqrt{\lambda}t} \ , \quad (44b)$$

$$k_3(t) = \alpha_3 \ , \tag{44c}$$

where

$$\mathbf{q}_1 = (-1 + \sqrt{\lambda},\ 1 + \sqrt{\lambda},\ 0) \ \text{ and } \ \mathbf{q}_2 = (1 + \sqrt{\lambda},\ -1 + \sqrt{\lambda},\ 0) \ . \tag{45}$$

It then follows that

$$k^2(t) = \frac{1+\lambda}{8\lambda}(\mathbf{q}_1\cdot\boldsymbol{\alpha})^2 e^{2E\sqrt{\lambda}t} + \frac{1+\lambda}{8\lambda}(\mathbf{q}_2\cdot\boldsymbol{\alpha})^2 e^{-2E\sqrt{\lambda}t} + \alpha_3^2$$

$$+ \frac{1-\lambda}{4\lambda}(\mathbf{q}_1\cdot\boldsymbol{\alpha})(\mathbf{q}_2\cdot\boldsymbol{\alpha}) \ , \tag{46}$$

and

$$\|\mathbf{y}(t)\| \le \|\mathbf{y}(o)\| \exp[(3E - \nu\alpha_3^2)t] \exp\left\{-\frac{\nu}{E}\,\frac{1+\lambda}{16\lambda\sqrt{\lambda}}(\mathbf{q}_1\cdot\boldsymbol{\alpha})^2 e^{2E\sqrt{\lambda}t}\right\}$$

$$\times \exp\left\{\frac{\nu}{E}\,\frac{1+\lambda}{16\lambda\sqrt{\lambda}}(\mathbf{q}_2\cdot\boldsymbol{\alpha})^2 e^{-2E\sqrt{\lambda}t}\right\} \exp\left\{-\frac{\nu(1-\lambda)}{4\lambda}(\mathbf{q}_1\cdot\boldsymbol{\alpha})(\mathbf{q}_2\cdot\boldsymbol{\alpha})t\right\}$$

$$\times \exp\left\{\frac{\nu}{E}\,\frac{1+\lambda}{16\lambda\sqrt{\lambda}}[(\mathbf{q}_1\cdot\boldsymbol{\alpha})^2 - (\mathbf{q}_2\cdot\boldsymbol{\alpha})^2]\right\} \ . \tag{47}$$

From (47) we can conclude that $\|\mathbf{y}(t)\| \to 0$ as $t\to\infty$ under either of the following conditions

$$(\mathbf{q}_1\cdot\boldsymbol{\alpha}) = (-1 + \sqrt{\lambda})\alpha_1 + (1 + \sqrt{\lambda})\alpha_2 \neq 0 \ , \tag{48a}$$

or

$$(\mathbf{q}_1\cdot\boldsymbol{\alpha}) = 0 \ \text{ and } \ \alpha_3 > \left[\frac{3E}{\nu}\right]^{1/2} \ . \tag{48b}$$

The asymptotic behavior of $\mathbf{y}(t)$ cannot be determined from (47) if $\mathbf{q}_1\cdot\boldsymbol{\alpha} = 0$ and $\alpha_3 < (3E/\nu)^{1/2}$.

It remains now to determine the asymptotic behavior of solutions of (30) for

the cases

$$\lambda = 0,\ \alpha_1 = 0,\ \alpha_2^2 + \alpha_3^2 < \frac{3E}{\nu}\ , \tag{49a}$$

and

$$0 < \lambda \leq 1,\ (-1 + \sqrt{\lambda})\alpha_1 + \ (1 + \sqrt{\lambda})\alpha_2 = 0,\ \alpha_3 < \left[\frac{3E}{\nu}\right]^{1/2}\ . \tag{49b}$$

where stability could not be demonstrated by the preceding analysis. For these cases we consider a direct solution $\mathbf{y}(t)$ of the linear system (30). Let a function $\mathbf{z}(t)$ be defined by

$$\mathbf{y}(t) = \exp\left[-\nu \int_0^t k^2(\tau)d\tau\right]\mathbf{z}(t)\ . \tag{50}$$

Then $\mathbf{z}(t)$ satisfies the linear system

$$\frac{d\mathbf{z}}{dt} = -\Gamma\cdot\mathbf{z} + \mathbf{B}(t)\cdot\mathbf{z}\ . \tag{51}$$

The solutions of (30) are then obtained from the solutions of (51) using (50). We first consider case (49a).

C. The Case $\lambda = 0$ and $\alpha_1 = 0$

The components of Γ in this case are given by (37). From this it is found that

$$k_1(t) = 0,\ \ k_2(t) = \alpha_2,\ k_3(t) = \alpha_3\ .$$

We then find that $\mathbf{B}(t) = \mathbf{0}$, and thus $\mathbf{z}$ obeys

$$\frac{d\mathbf{z}}{dt} = -\Gamma\cdot\mathbf{z}\ ,$$

for which solutions are given by

$$\mathbf{z}(t) = e^{-t\Gamma}\cdot\mathbf{c} \ .$$

Here, $\mathbf{c}$ is a constant vector specifying the initial condition $\mathbf{c} = \mathbf{z}(0) = \mathbf{y}(0)$ and $e^{-t\Gamma}$ is the fundamental matrix solution

$$e^{-t\Gamma} = \begin{pmatrix} 1 & -Et & 0 \\ 0 & 1 & 0 \\ 0 & 0 & 1 \end{pmatrix} .$$

Since $\alpha_1 = 0$, Eq. (40) yields

$$\exp\left[-\nu \int_0^t k^2(\tau)d\tau \right] = e^{-\nu(\alpha_2^2 + \alpha_3^2)t} \ .$$

It then follows from Eq. (50) that all solutions of (30) in this case are of the form

$$\mathbf{y}(t) = e^{-\nu(\alpha_2^2 + \alpha_3^2)t} \begin{pmatrix} 1 & -Et & 0 \\ 0 & 1 & 0 \\ 0 & 0 & 1 \end{pmatrix} \cdot \mathbf{y}(0) \ . \qquad (52)$$

If $\alpha_2^2 + \alpha_3^2 \neq 0$, the solution decays to zero exponentially as $t\to\infty$. On the other hand, if $\alpha_1 = \alpha_2 = \alpha_3 = 0$, the "rigid-motion" disturbance simply convects with the base flow and grows linearly in time just as an element of fluid in the base flow would.

D. The Case $0 < \lambda \leq 1$ and $(-1 + \sqrt{\lambda})\alpha_1 + (1 + \sqrt{\lambda})\alpha_2 = 0$

We consider in this case the Cartesian coordinate system for which Γ is represented by Eq. (2). Under these conditions Eqs. (44a,b,c) give the Cartesian components of $\mathbf{k}(t)$ as

$$k_1(t) = \frac{1 + \sqrt{\lambda}}{4\sqrt{\lambda}} (\mathbf{q}_2\cdot\boldsymbol{\alpha})e^{-E\sqrt{\lambda}t} \ ,$$

$$k_2(t) = \frac{1-\sqrt{\lambda}}{4\sqrt{\lambda}}(\mathbf{q}_2\cdot\boldsymbol{\alpha})e^{-E\sqrt{\lambda}t},$$

$$k_3(t) = \alpha_3 ,$$

where $\mathbf{q}_2 = (1+\sqrt{\lambda}, -1+\sqrt{\lambda}, 0)$. If we substitute these expressions for $k_1(t)$, $k_2(t)$ and $k_3(t)$ into Eq. (22), we find that the components of $\mathbf{B}(t)$ are either zero or in the form

$$b_{ij}(t) = \frac{(constant)e^{-p_{ij}E\sqrt{\lambda}t}}{(\alpha_3)^2 + \frac{1+\lambda}{8\lambda}(\mathbf{q}_2\cdot\boldsymbol{\alpha})^2 e^{-2E\sqrt{\lambda}t}}, \quad (i,j = 1,2,3) \tag{53}$$

where $p_{ij} = 1$ or 2.

Since $\mathbf{B}(t) \neq 0$, it is not possible to find a simple analytic form of the solution of (51). We can, however, determine the asymptotic behavior of solutions as $t\to\infty$ with the aid of the following theorem due to Levinson.[18]

Theorem (Levinson).

Consider the linear system of differential equations

$$\frac{d\mathbf{z}}{dt} = \mathbf{A}\cdot\mathbf{z} + \mathbf{B}(t)\cdot\mathbf{z} ,$$

where (1) $\mathbf{A}$ is a constant nxn matrix with distinct eigenvalues $\mu_1, \mu_2, \ldots, \mu_n$; (2) $\mathbf{B}(t)$ is an nxn matrix for which the elements, $b_{ij}(t)$ satisfy

$$\int_0^\infty |b_{ij}(t)|\,dt < \infty \quad (i,j = 1,2,\ldots,n) .$$

Then for large t there exist n linearly independent solutions $\mathbf{z}^{(1)}, \mathbf{z}^{(2)}, \ldots, \mathbf{z}^{(n)}$ such that as $t\to\infty$

$$\mathbf{z}^{(k)}(t) = e^{\mu_k t}[\mathbf{w}^{(k)} + o(1)] \quad (k = 1,2,\ldots,n) , \tag{54}$$

where $\mathbf{w}^{(k)}$ is an eigenvector of $\mathbf{A}$ corresponding to the eigenvalue μ_k.

Thus, under the conditions stated in the theorem, the solutions of the full, variable coefficient system of equations behave asymptotically like solutions of the constant coefficient system

$$\frac{d\mathbf{z}}{dt} = \mathbf{A}\cdot\mathbf{z} .$$

For the case which we are now considering, the conditions of the theorem are satisfied. The elements of $\mathbf{B}(t)$ as given by (53) satisfy the integrability condition, and the matrix $\mathbf{A} = -\Gamma$ has the distinct eigenvalues $\mu_1 = E\sqrt{\lambda}$, $\mu_2 = 0$, and $\mu_3 = -E\sqrt{\lambda}$. Now, the general solution of Eq. (51) can be expressed as a linear combination of solutions in the form of (54). In view of Eq. (50), the general solution of the linear system can be expressed for large t as

$$\mathbf{y}(t) = \exp\left[-\nu \int_0^t k^2(\tau)d\tau \right] \sum_{k=1}^{3} c_k e^{\mu_k t}[\mathbf{w}^{(k)} + o(1)] , \qquad (55)$$

where the c_k are arbitrary constants and the $\mathbf{w}^{(k)}$ are eigenvectors of Γ corresponding to the eigenvalues $\mu_1 = E\sqrt{\lambda}$, $\mu_2 = 0$, and $\mu_3 = -E\sqrt{\lambda}$. Integrating (46) from 0 to t for this case where $\mathbf{q}_1\cdot\boldsymbol{\alpha} = 0$, we find

$$\exp\left[-\nu \int_0^t k^2(\tau)d\tau \right] = \exp\left[-\nu\alpha_3^2 t\right]\exp\left[-\frac{\nu}{E}\,\frac{1+\lambda}{16\lambda\sqrt{\lambda}}\,(\mathbf{q}_2\cdot\boldsymbol{\alpha})^2(1 - e^{-2E\sqrt{\lambda}t})\right] .$$

Hence, it follows that as $t\to\infty$

$$\|\mathbf{y}(t)\| = 0\{\exp[(E\sqrt{\lambda} - \nu\alpha_3^2)t]\} .$$

We conclude that if $0 < \lambda \le 1$ and $\mathbf{q}_1\cdot\boldsymbol{\alpha} = 0$, then $\|\mathbf{y}(t)\| \to 0$, if

$$\alpha_3 > \left(\frac{E\sqrt{\lambda}}{\nu}\right)^{1/2} ,$$

whereas $\|\mathbf{y}(t)\| \to \infty$, if

$$\alpha_3 < \left(\frac{E\sqrt{\lambda}}{\nu}\right)^{1/2} .$$

The effect of the parameters $\boldsymbol{\alpha}$, E, ν, and λ on the asymptotic behavior of solutions of (30) as $t\to\infty$ has been completely established. This in turn determines the asymptotic behavior of all fundamental mode velocity disturbances. We can consequently draw the following conclusions regarding the behavior of spatially periodic initial disturbances on two-dimensional linear flows.

In the case of simple shear flow ($\lambda = 0$), all spatially periodic initial disturbances (28) with wave vectors $\alpha \neq \mathbf{0}$ decay to zero as $t\to\infty$ for all positive values of E and ν. A disturbance with $\boldsymbol{\alpha} = \mathbf{0}$ will grow linearly in time for reasons cited earlier.

For "strong" flows where $0 < \lambda \leq 1$, all spatially periodic initial disturbances which satisfy $(-1 + \sqrt{\lambda})\alpha_1 + (1 + \sqrt{\lambda})\alpha_2 \neq 0$ decay to zero as $t\to\infty$ for all positive values of E and ν. If the disturbance wavenumbers α_1 and α_2 satisfy $(-1+\sqrt{\lambda})\alpha_1 + (1 + \sqrt{\lambda})\alpha_2 = 0$, on the other hand, then the disturbance will decay to zero if $\alpha_3 > (E\sqrt{\lambda}/\nu)^{1/2}$ and grow exponentially in time if $\alpha_3 < (E\sqrt{\lambda}/\nu)^{1/2}$. The necessary condition $(-1+\sqrt{\lambda})\alpha_1 + (1 + \sqrt{\lambda})\alpha_2 = 0$ for instability of a periodic initial disturbance has a simple physical interpretation. As shown in Fig. 2, the inlet streamline for a strong flow has a slope of $(\sqrt{\lambda} + 1)/(\sqrt{\lambda} - 1)$. The condition $(-1 + \sqrt{\lambda})\alpha_1 + (1 + \sqrt{\lambda})\alpha_2 = 0$ is met when the initial disturbance has lines of constant phase in the (x_1,x_2)-plane parallel to the inlet streamline. In other words, the initial disturbance is periodic in a direction normal to the inlet streamline.

VI. Exact Solution of Linearized Vorticity Disturbance Equation for $\lambda = 1$

It is possible to obtain an exact analytical solution of the linearized vorticity disturbance equation for the special case of pure extensional flow ($\lambda = 1$). Although the more general analysis of the preceding section includes this special case, the exact analytical solution proves to be useful in elucidating the

physical mechanism for instability.

We again consider the disturbance of a steady two-dimensional linear flow at some initial time t=0, as we did in Sec. III. Let $\boldsymbol{\omega}(\mathbf{x},t) = \nabla \times \mathbf{u}(\mathbf{x},t)$ and $\boldsymbol{\omega}^o(\mathbf{x}) = \nabla \times \mathbf{u}^o(\mathbf{x})$ denote the vorticity disturbance and its initial value, respectively. The linearized vorticity disturbance equation reads

$$\frac{\partial \boldsymbol{\omega}}{\partial t} + \mathbf{U}\cdot\nabla\boldsymbol{\omega} + \mathbf{u}\cdot\nabla\boldsymbol{\Omega} = \boldsymbol{\omega}\cdot\nabla\mathbf{U} + \boldsymbol{\Omega}\cdot\nabla\mathbf{u} + \nu\nabla^2\boldsymbol{\omega} \quad . \tag{56}$$

Here, $\boldsymbol{\Omega}(\mathbf{x}) = \nabla \times \mathbf{U}(\mathbf{x})$ is the basic vorticity with Cartesian components given by (5). For pure extensional flow ($\lambda = 1$), the basic vorticity field vanishes. Using this fact and substituting for the basic velocity field in (56), we obtain

$$\frac{\partial \boldsymbol{\omega}}{\partial t} + (\Gamma\cdot\mathbf{x})\cdot\nabla\boldsymbol{\omega} = \Gamma\cdot\boldsymbol{\omega} + \nu\nabla^2\boldsymbol{\omega} \quad . \tag{57}$$

This equation is to be solved for all $\mathbf{x} \in \mathbf{R}^3$ and $t \geq 0$, subject to the initial condition

$$\boldsymbol{\omega}(\mathbf{x},0) = \boldsymbol{\omega}^o(\mathbf{x}) \quad . \tag{58}$$

The solution can be obtained as in Sec. IV by application of an exponential Fourier transform. The Fourier transform of $\boldsymbol{\omega}(\mathbf{x},t)$ can be shown to be

$$\hat{\boldsymbol{\omega}}(\mathbf{k},t) = \exp\left[-\nu \int_0^t \|e^{(t-\tau)\Gamma^T}\cdot\mathbf{k}\|^2 d\tau\right] e^{t\Gamma}\cdot\hat{\boldsymbol{\omega}}^o(e^{t\Gamma^T}\cdot\mathbf{k}) \, .$$

This transform can be inverted with the aid of the convolution theorem to yield the following general solution for the vorticity disturbance

$$\boldsymbol{\omega}(\mathbf{x},t) = \frac{1}{(4\pi\nu)^{3/2}[\det\mathbf{A}(t)]^{1/2}} \int \exp\left[-\frac{1}{4\nu}\,\boldsymbol{\xi}\cdot\mathbf{A}^{-1}(t)\cdot\boldsymbol{\xi}\right] e^{t\Gamma}\cdot\boldsymbol{\omega}^o(e^{-t\Gamma}\cdot\mathbf{x} - \boldsymbol{\xi})\,d\boldsymbol{\xi} \quad , \tag{59}$$

where

$$\mathbf{A}(t) = \int_0^t e^{-\tau\Gamma}\cdot e^{-\tau\Gamma^T} d\tau \, . \tag{60}$$

We shall again resort to the consideration of spatially periodic initial vorticity disturbances in order to assess the stability of the flow. Let the initial vorticity disturbance be given by

$$\boldsymbol{\omega}^{\circ}(\mathbf{x}) = \exp(-i\boldsymbol{\alpha}\cdot\mathbf{x})\boldsymbol{\omega}^{\circ} \ , \tag{61}$$

where $\boldsymbol{\alpha}$ has real wavenumbers α_1, α_2, and α_3 as components and $\boldsymbol{\omega}^{\circ}$ is a constant vector. Substituting (61) into (59) and carrying out the integration, we obtain the fundamental mode disturbance

$$\boldsymbol{\omega}(\mathbf{x},t) = \exp[-i(e^{-t\Gamma^T}\cdot\boldsymbol{\alpha})\cdot\mathbf{x}]\exp\left[-\nu \int_0^t \|e^{-\tau\Gamma^T}\cdot\boldsymbol{\alpha}\|^2 d\tau\right] e^{t\Gamma}\cdot\boldsymbol{\omega}^{\circ} \ . \tag{62}$$

This solution applies to the case of pure extensional flow for which Γ has the representation

$$[\Gamma] = \begin{bmatrix} E & 0 & 0 \\ 0 & -E & 0 \\ 0 & 0 & 0 \end{bmatrix} ,$$

and

$$e^{t\Gamma} = \begin{bmatrix} e^{Et} & 0 & 0 \\ 0 & e^{-Et} & 0 \\ 0 & 0 & 1 \end{bmatrix} .$$

Thus, the fundamental mode solution (62) reduces to

$$\boldsymbol{\omega}(\mathbf{x},t) = \exp[-i(e^{-Et}\alpha_1 x_1 + e^{Et}\alpha_2 x_2 + \alpha_3 x_3)]\exp\left[\frac{-\nu}{2E}\alpha_1^2(1 - e^{-2Et})\right]$$

$$\times \exp\left[\frac{-\nu}{2E}\alpha_2^2(e^{2Et} - 1)\right]\exp(-\nu\alpha_3^2 t)(\omega_1^{\circ}e^{Et}, \omega_2^{\circ}e^{-Et}, \omega_3^{\circ}) \ . \tag{63}$$

From Eq. (63) we see that if $\alpha_2 \neq 0$, all components of $\boldsymbol{\omega}(\mathbf{x},t)$ decay to zero as

$t\to\infty$. If $\alpha_2 = 0$ and $\alpha_3 > (E/\nu)^{1/2}$, then all components of $\boldsymbol{\omega}(\mathbf{x},t)$ again decay to zero as $t\to\infty$. However, if $\alpha_2 = 0$ and $\alpha_3 < (E/\nu)^{1/2}$, then the component $\omega_1(\mathbf{x},t)$ must grow exponentially as $t\to\infty$. This result complies with the instability criterion found for fundamental mode velocity disturbances in Sec. V.

VII. Discussion

The results of the linear stability analysis predict that unbounded two-dimensional linear flows in the strong flow regime ($0 < \lambda \leq 1$) are unconditionally unstable. For any assignment of positive values to E and ν, a spatially periodic initial disturbance with wavenumbers α_1, α_2, and α_3 satisfying

$$(-1 + \sqrt{\lambda})\alpha_1 + (1 + \sqrt{\lambda})\alpha_2 = 0 ,$$

$$\alpha_3 < (E\sqrt{\lambda}/\nu)^{1/2},$$

must grow in time as $\exp[(E\sqrt{\lambda} - \nu\alpha_3^2)t]$. It was shown that such an unstable disturbance is initially invariant in a direction parallel to the inlet streamline in the plane of the basic flow.

Consideration of the vorticity disturbance Eq. (57) and its solution (63), both valid for pure extensional flow ($\lambda = 1$), yields a simple qualitative interpretation of the mechanism for instability. The vorticity component ω_1 along the principal axis of extensional strain increases at an exponential rate due to vortex line stretching, represented by the term $\Gamma\cdot\boldsymbol{\omega}$ in (57). However, this growth process competes against the stabilizing influence of vorticity diffusion, and the rate of diffusion in the x_1- or x_2-directions is modified in time due to the advection of vorticity represented by $(\Gamma\cdot\mathbf{x})\cdot\nabla\boldsymbol{\omega}$ in (57). The mechanism responsible for this advection effect is very simple. Because of the "stretching" or "extensional" nature of the basic flow, the effective wavenumber of the disturbance vorticity is altered by its advection in the flow. Thus, vorticity gradients either increase or

decrease in time and the stabilizing rate of vorticity diffusion is correspondingly increased or decreased. For this case of pure extensional flow, the principal axes of extension are parallel to the x_1- and x_2-axes, and the wavenumber of a disturbance which is periodic in x_1 decreases as $e^{-Et}\alpha_1$, while the wavenumber of a disturbance which is periodic in x_2 increases as $e^{Et}\alpha_2$. This effect of the basic flow on the magnitude of vorticity gradients is reflected in the complicated arguments of the exponential decay term

$$\exp\left[\frac{-\nu}{2E}\alpha_1^2(1-e^{-2Et})\right]\exp\left[\frac{-\nu}{2E}\alpha_2^2(e^{2Et}-1)\right]\exp(-\nu\alpha_3^2 t)$$

in solution (63). It is evident upon examination of (63) that the effect of diffusion, enhanced by the advective increase of vorticity gradients along the inlet streamline direction, will always dominate the simple exponential rate of vorticity growth due to vortex line stretching if $\alpha_2 \neq 0$. Only periodic initial vorticity disturbances which are aperiodic in the direction of the inlet streamline (in this case the x_2-direction) so that $\alpha_2 = 0$ can grow in time. Among these disturbances, only the disturbances with sufficiently small wavenumber $\alpha_3 < (E/\nu)^{1/2}$ are unstable. In these cases the growth rate of disturbance vorticity due to vortex line stretching by the basic flow exceeds the rate of decay from viscous diffusion in the x_3-direction normal to the basic flow plane.

The qualitative description of the mechanism for instability can be extended to the two-dimensional linear flows with $0 < \lambda < 1$ with only slight modification. These flows differ from pure extensional flow in that the inlet and outlet streamlines are no longer aligned with the principal axes of strain for the basic flow. Vortex line stretching along the principal axis of extensional strain again provides the source of instability. This effect cannot overcome the stabilizing effect of convection-enhanced diffusion if a periodic initial disturbance is not aperiodic in the direction of the inlet streamline. Any periodicity along the inlet

streamline leads to a faster-than-exponential rate of decay due to the "mixing" of positive and negative vorticity by diffusion. Periodic initial disturbances which do not vary along the inlet streamline can be unstable if the wavenumber in the direction normal to the basic flow plane is sufficiently small. In this case the stabilizing influence of diffusion in the direction of the inlet streamline is absent and the disturbance vorticity growth rate $e^{E\sqrt{\lambda}t}$ exceeds the diffusive decay rate $e^{-\nu a_S^2 t}$. For simple shear flow ($\lambda = 0$), vorticity disturbances can grow only linearly with time as a result of the weaker vortex line stretching. Viscous diffusion of disturbance vorticity still results in an exponential rate of decay for periodic initial disturbances. Hence, simple shear flow is stable with respect to all such disturbances.

Acknowledgment: This work was supported in part by a grant from the Fluid Mechanics Program of the National Science Foundation.

References

1. T. B. Benjamin, Proc. R. Soc. London Ser. A **359**, 1 (1978); and T. B. Benjamin, Proc. R. Soc. London Ser. A **359**, 27 (1978).

2. T. B. Benjamin and T. Mullin, Proc. R. Soc. London Ser. A **377**, 221 (1981).

3. T. B. Benjamin and T. Mullin, J. Fluid Mech. **121**, 219 (1982).

4. G. I. Taylor, Proc. R. Soc. London Ser. A **146**, 501 (1934).

5. F. D. Rumscheidt and S. G. Mason, J. Colloid Sci. **16**, 210 (1961).

6. H. P. Grace, Chem. Eng. Commun. **14**, 225 (1982).

7. R. W. Flumerfelt, Ind. Eng. Chem. Fundam. **11**, 312 (1972).

8. D. P. Pope and A. Keller, Colloid Poly. Sci. **255**, 633 (1977).

9. G. G. Fuller and L. G. Leal, Rheol. Acta **19**, 580 (1980).

10. L. Hopf, Ann. Phys. (4) **44**, 1 (1914).

11. A. P. Gallagher and A. McD. Mercer, J. Fluid Mech. **13**, 91 (1962).

12. W. H. Reid, Stud. Appl. Math. **61**, 83 (1979).

13. J. R. A. Pearson, J. Fluid Mech. **5**, 274 (1959).

14. G. Marrucci and G. Astarita, AIChE J. **13**, 931 (1967).

15. R. I. Tanner and R. R. Huilgol, Rheol. Acta **14**, 959 (1975).

16. R. I. Tanner, AIChE J. **22**, 910 (1976).

17. W. L. Olbricht, J. M. Rallison and L. G. Leal, J. Non-Newt. Fluid Mech. **10**, 291 (1982).

18. N. Levinson, Duke Math J. **15**, 111 (1948).

Figure Captions

Figure 1. Streamlines for two-dimensional linear flows. (a) $\lambda = 1$, (b) $\lambda = 0.5$, (c) $\lambda = 0$, (d) $\lambda = -0.5$, (e) $\lambda = -1$.

Figure 2. Streamlines for a strong flow ($\lambda = 0.5$). L_i: inlet streamline (slope = $(\sqrt{\lambda} + 1)/(\sqrt{\lambda} - 1)$). L_o: outlet streamline (slope = $(\sqrt{\lambda} - 1)/(\sqrt{\lambda} + 1)$).

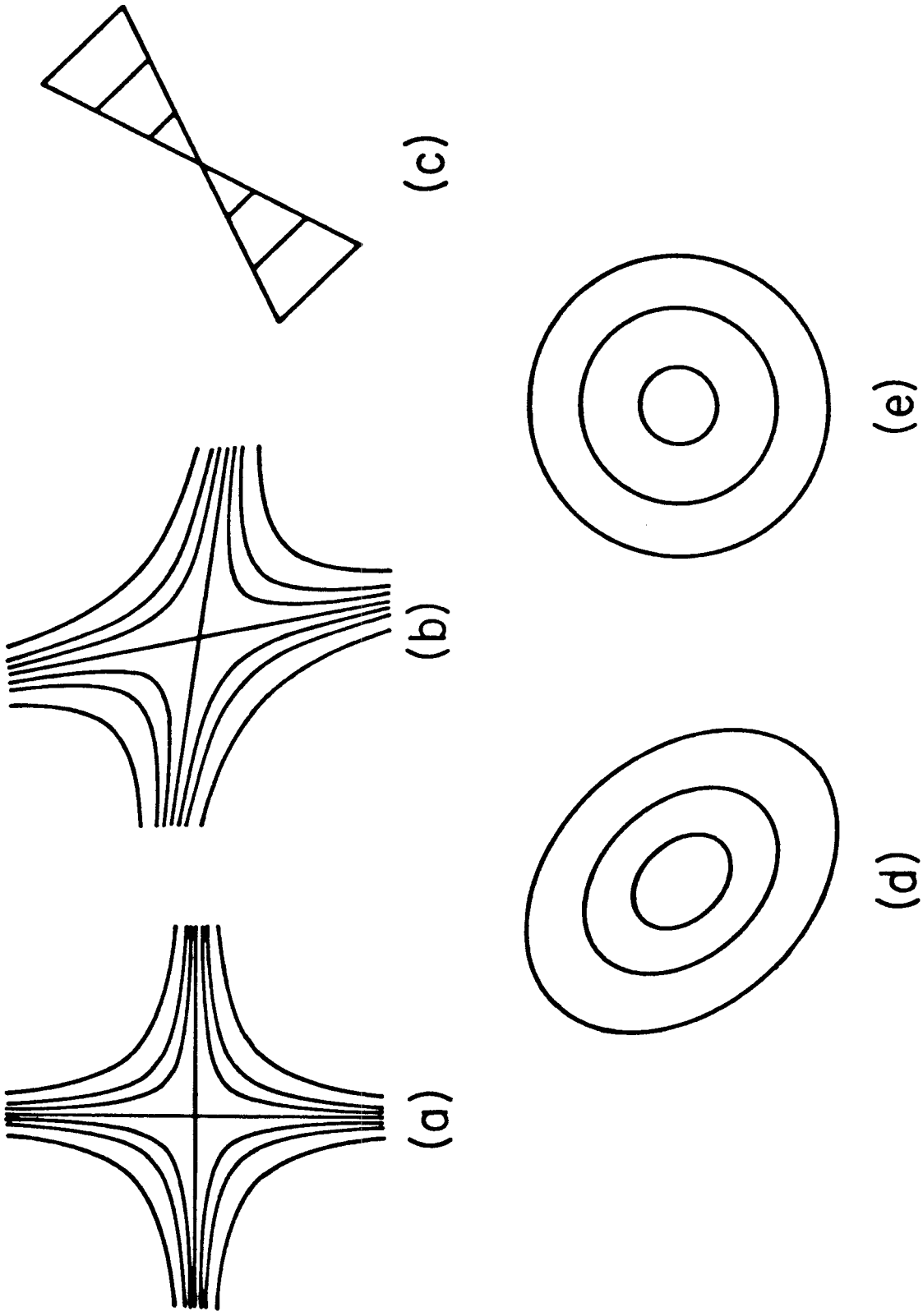

Figure 1

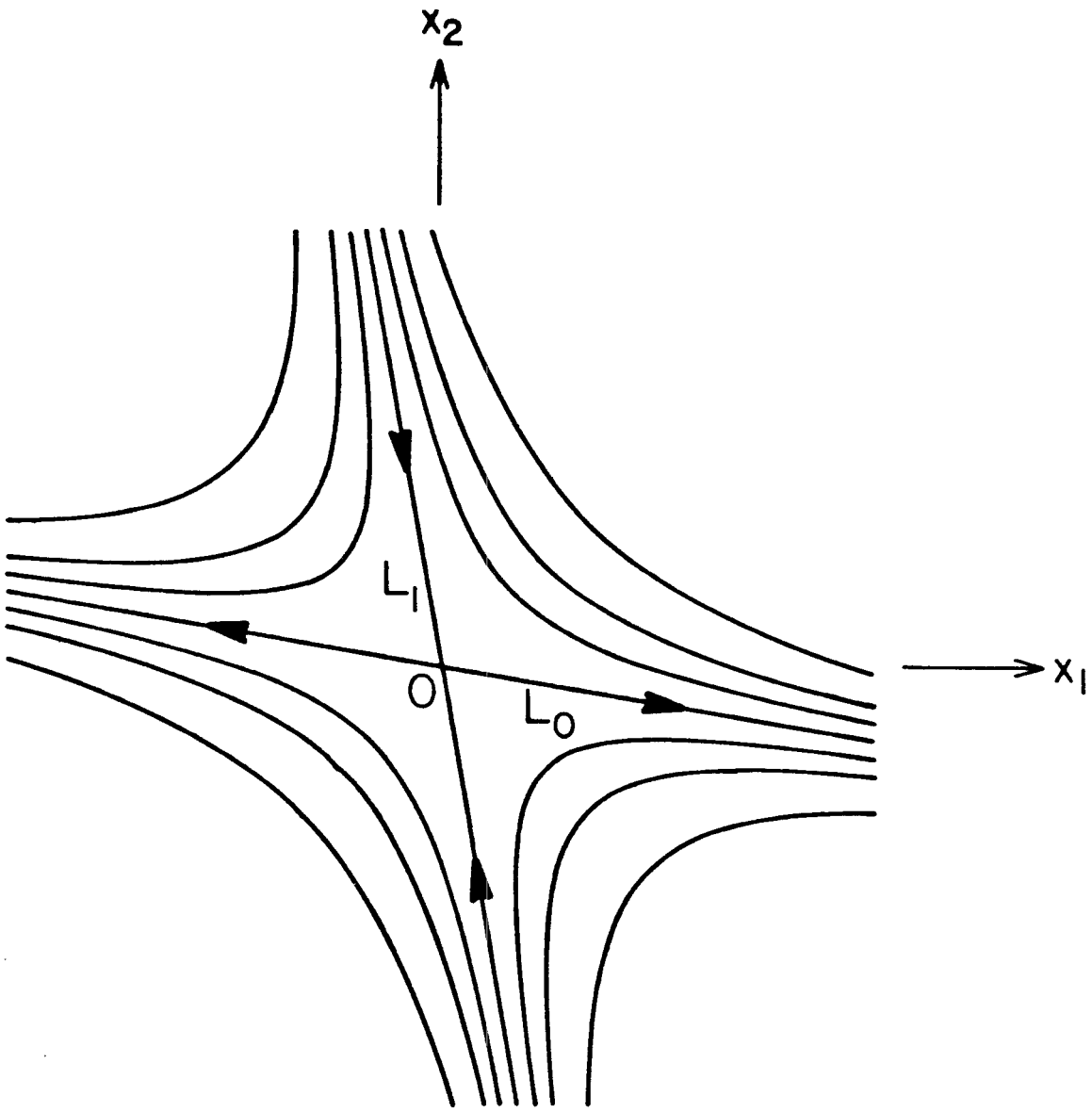

Figure 2

CHAPTER II

THE STABILITY OF TWO-DIMENSIONAL LINEAR FLOWS OF AN OLDROYD-TYPE FLUID

The text of Chapter II consists of an article which has been accepted for publication in the *Journal of Non-Newtonian Fluid Mechanics*.

The Stability of Two-Dimensional Linear Flows of an Oldroyd-Type Fluid

by

R. R. Lagnado, N. Phan-Thien†, and L. G. Leal

Department of Chemical Engineering
California Institute of Technology
Pasadena, California 91125

---

† Permanent address: Mechanical Engineering Department, Sydney University, N. S. W. 2006, Australia.

Summary

A linear stability analysis is made for an Oldroyd-type fluid undergoing steady two-dimensional flows in which the velocity field is a linear function of position throughout an unbounded region. This class of basic flows is characterized by a parameter λ which ranges from $\lambda = 0$ for simple shear flow to $\lambda = 1$ for pure extensional flow. The time derivatives in the constitutive equation can be varied continuously from co-rotational to co-deformational as a parameter β varies from 0 to 1. The linearized disturbance equations are analyzed to determine the asymptotic behavior as time $t \to \infty$ of a spatially periodic initial disturbance. It is found that unbounded flows in the range $0 < \lambda \leq 1$ are unconditionally unstable with respect to periodic initial disturbances which have lines of constant phase parallel to the inlet streamline in the plane of the basic flow. When the Weissenberg number is sufficiently small, only disturbances with sufficiently small wavenumber α_3 in the direction normal to the basic flow plane are unstable. However, for certain values of β, critical Weissenberg numbers can be found above which flows are unstable for all values of the wavenumber α_3.

1. Introduction

Many important industrial processes involve steady flows of polymeric liquids which exhibit complex non-Newtonian rheological behavior. Production rates in these processes are often limited by the onset of flow instabilities. Two well-known examples of this phenomenon are film casting and fiber spinning, where a periodic variation in fiber diameter or film thickness is observed when a critical take-up speed is exceeded [1]. Numerous attempts have been made to understand polymer processing instabilities via theoretical stability analyses for model viscoelastic fluids in simple flow geometries [1,2]. However, the majority of these studies have mimicked earlier work on the stability of Newtonian fluids in considering only unidirectional shear flows, such as Couette flow and plane Poiseuille flow. While shear flow may provide a useful approximation for some processes such as flow in a screw extruder, a number of important problems including film casting and fiber spinning involve extensional flow in which the velocity varies with position in its own coordinate direction. Efforts to understand the stability of extensional flows have so far been limited to Newtonian fluids. In an earlier paper, we considered the linear stability of a class of two-dimensional, homogeneous extensional flows in an unbounded domain. The only other work, so far as we are aware, has been *ad hoc* approximate analyses for actual processing flows, again for Newtonian fluids. Pearson and Matovich [3] examined the stability of the fiber spinning flow and Yeow [4] considered the film casting process.

In the present paper we extend our earlier work on the stability of Newtonian fluids in extensional flow [5], to consider the linear stability of a model non-Newtonian fluid that is undergoing one of the class of steady, two-dimensional linear flows in an unbounded domain. The complete class of two-dimensional linear flows can be characterized by only two parameters [6]. These are a shear

rate E and a parameter λ which ranges from $\lambda = -1$ for a purely rotational flow to $\lambda = 1$ for pure extensional flow, with the intermediate value $\lambda = 0$ corresponding to simple shear flow where the strength of the rotational and straining parts of the flow are equal. In the present work, we consider only values of λ in the range $0 \leq \lambda \leq 1$, for which the magnitude of the strain-rate exceeds the vorticity. The same flows were considered in our earlier analysis for Newtonian fluids [5]. The rheological behavior of the fluid is modeled using a version of the Oldroyd [7] constitutive equation, which is set up so that the form of the time derivatives can be altered between the two extremes of co-rotational and co-deformational by variation of one model parameter.

The motivation for our present study comes from three sources: first, we hope to gain some understanding of the effects of fluid elasticity on the stability of extensional flows; second, we hope to shed some light on the behavior of the Oldroyd-Maxwell model in flows with an extensional character where many unsuccessful attempts have been made to obtain numerical solutions of the equations of motion; third, we intend to provide a basis for comparison between predictions for the Oldroyd model and the behavior of real viscoelastic fluids in so-called two- and four-roll milling flows.

The problem with numerical solutions for (model) viscoelastic fluids is, by now, well known to most workers in rheology and non-Newtonian fluid mechanics. It is quite simply that in all published numerical studies, a relatively low limit on the Weissenberg number appears [$Wi \sim O(1)$] above which the numerical algorithms fail to converge [8]. The precise value of this limit depends on such factors as the constitutive model, the flow geometry, and the mesh size for the numerical scheme. We note, however, that the Oldroyd-Maxwell class of constitutive models, involving time derivatives ranging from co-rotational to co-deformational, have been by far the most prevalent among the variety of

constitutive models that have appeared in these numerical studies. This fact lends relevance to the Oldroyd-type model with adjustable time derivatives that we have chosen for the present investigation.

A good approximation to the two-dimensional linear flows considered here is generated by two- and four-roll mills [9]. Among the many important uses of these devices are experimental studies of flow-induced changes in the conformation of macromolecules in solution [10,11]. Such experimental studies, which involve viscoelastic fluids, are limited by the onset of instabilities in two- and four-roll mills at fairly small roller speeds. However, no thorough theoretical or experimental investigation of the stability of viscoelastic fluid flow in these devices has been made. In part, this is because of the complexity of the basic flows. Although the class of linear flows considered here is approximately realized in the central region between rollers, there is a weaker, complicated flow in the region outside the rollers. Furthermore, even in the central region, the real flow is not exactly two-dimensional, nor is it unbounded due to the presence of the rollers and the finite extent of the device in the third direction. In spite of these complications, it appears that the present analysis of the stability of an unbounded, linear, two-dimensional flow should provide an initial step toward understanding the stability of the real, two- and four-roll milling flows. As a complement to the present work, we are currently studying the stability of flows in the two- and four-roll mills experimentally for both Newtonian and non-Newtonian fluids. To some extent, it should be possible to separate the geometric limitations of applying an unbounded flow analysis from the equally unknown limitations of the constitutive model for this type of flow, by first comparing the predictions of our earlier analysis for Newtonian fluids with observations for Newtonian fluids, and then making the same comparison for the non-Newtonian case.

2. The Constitutive Equation

We consider an Oldroyd-type viscoelastic fluid model for which the extra-stress tensor τ is related to the rate-of-strain tensor $\mathbf{e} = \frac{1}{2}[\nabla\mathbf{u} + (\nabla\mathbf{u})^T]$ by the constitutive equation

$$\tau + \theta_1\left[\frac{D\tau}{Dt} - \beta(\mathbf{e}\cdot\tau + \tau\cdot\mathbf{e})\right] = 2\eta_0\mathbf{e} + 2\eta_0\theta_2\left[\frac{D\mathbf{e}}{Dt} - 2\beta(\mathbf{e}\cdot\mathbf{e})\right]. \tag{1}$$

Here, θ_1 is the relaxation time, θ_2 is the retardation time, and η_0 is the zero-shear viscosity. The quantities in square brackets represent time derivatives of the extra-stress τ and the rate-of-strain $\mathbf{e}$. The form of these time derivatives depends upon the parameter β which assumes values in the range $0 \le \beta \le 1$. When $\beta = 0$ the co-rotational time derivative appears, which is defined for an arbitrary tensor $\mathbf{B}$ as

$$\frac{D\mathbf{B}}{Dt} = \frac{\partial\mathbf{B}}{\partial t} + \mathbf{u}\cdot\nabla\mathbf{B} - \mathbf{w}\cdot\mathbf{B} + \mathbf{B}\cdot\mathbf{w},$$

where $\mathbf{w} = \frac{1}{2}[\nabla\mathbf{u} - (\nabla\mathbf{u})^T]$ is the vorticity tensor, and the constitutive equation reduces to the so-called co-rotational Jeffreys model. This model exhibits shear-thinning in simple shear flow, but a constant extensional viscosity. When $\beta = 1$, on the other hand, the co-deformational (Oldroyd) time derivative is attained, and (1) is the so-called Oldroyd-B model. This model exhibits a constant shear viscosity, but is strain-thickening in extensional flows.

The rheological behavior of an actual viscoelastic fluid will, in general, be best described from a qualitative point of view by some intermediate value of β ($0 < \beta < 1$), where an "intermediate" time derivative appears. Such "intermediate" time derivatives occur in constitutive models proposed both for polymer solutions of high concentration on the basis of networks with non-affine deformation [12,13], and for dilute solutions and suspensions on the basis of

theoretically derived constitutive equations [13,14].

It is well known that certain restrictions are necessary on the values of the constants which appear in the constitutive Eq. (1). These restrictions are discussed at length by Bird et al. [15] for the general Oldroyd 8-constant model. For the constitutive equation considered here, we require

$$\eta_0 > 0 \,, \tag{2}$$

and either

$$0 \le \frac{\theta_2}{\theta_1} \le 1 \quad \text{if} \quad \beta = 1 \,, \tag{3}$$

or

$$\frac{1}{9} \le \frac{\theta_2}{\theta_1} \le 1 \quad \text{if} \quad 0 \le \beta < 1 \,.$$

Further details regarding the constitutive Eq. (1) and its suitability as a model for the rheological behavior of viscoelastic fluids are discussed by Zana [16] and Tiefenbruck [17].

3. The Basic Velocity and Stress Fields

We consider, as the undisturbed velocity field, any of the class of unbounded, two-dimensional, linear flows

$$\mathbf{U} = \Gamma \cdot \mathbf{x} \,, \tag{4}$$

where

$$[\Gamma] = \frac{E}{2} \begin{bmatrix} 1+\lambda & 1-\lambda & 0 \\ -(1-\lambda) & -(1+\lambda) & 0 \\ 0 & 0 & 0 \end{bmatrix} , \tag{5}$$

and $\mathbf{x}$ is a general position vector. Here, $E \ge 0$ is a constant shear rate which represents the magnitude of the local velocity gradient, and λ is a constant

parameter whose value specifies the flow type, ranging from pure rotation for $\lambda = -1$ to pure strain for $\lambda = +1$. Figure 1 shows streamlines corresponding to several values of λ. The same class of flows was considered in our earlier paper on the stability of Newtonian fluids, and many other general features are discussed there. As in [5], we restrict our present considerations to "strong" flows for which $0 < \lambda \leq 1$, and (briefly) to simple shear flow where $\lambda = 0$. In the regime $0 < \lambda \leq 1$, the streamlines corresponding to (4) form a family of hyperbolas with two asymptotes which intersect at the stagnation point, having slopes $(\sqrt{\lambda} + 1)/(\sqrt{\lambda} - 1)$ and $(\sqrt{\lambda} - 1)/(\sqrt{\lambda} + 1)$, respectively. The first of these asymptotes will be referred to as the "inlet" streamline since flow is directed along it toward the stagnation point, while the other is referred to as the "outlet" streamline since the flow directed along it is away from the stagnation point. The streamlines for a typical strong flow are shown in Fig. 2.

In order to determine the undisturbed stresses, associated with the flow field (4) and (5), we substitute into the constitutive Eq. (1) and solve for the components of the extra-stress tensor **T**. The nonzero, steady Cartesian components of **T** are found to be

$$T_{11} = \frac{\eta_0 E\left(1 - \frac{\theta_2}{\theta_1}\right)(1+\lambda)[1 + E\theta_1\beta(1+\lambda)]}{1 - (E\theta_1)^2[\beta^2(1+\lambda)^2 - (1-\lambda)^2]} + \eta_0 E\frac{\theta_2}{\theta_1}(1+\lambda)\,, \tag{6a}$$

$$T_{22} = \frac{-\eta_0 E\left(1 - \frac{\theta_2}{\theta_1}\right)(1+\lambda)[1 - E\theta_1\beta(1+\lambda)]}{1 - (E\theta_1)^2[\beta^2(1+\lambda)^2 - (1-\lambda)^2]} - \eta_0 E\frac{\theta_2}{\theta_1}(1+\lambda)\,, \tag{6b}$$

$$T_{12} = T_{21} = \frac{-\eta_0 E\left(1 - \frac{\theta_2}{\theta_1}\right)E\theta_1(1-\lambda^2)}{1 - (E\theta_1)^2[\beta^2(1+\lambda)^2 - (1-\lambda)^2]}\,. \tag{6c}$$

The dimensionless product of the shear rate E and the relaxation time θ_1 defines the Weissenberg number for the basic flow, $Wi = E\theta_1$. It is evident, upon

examination of (6a)-(6c), that the stress components will become unbounded for a certain value of Wi,

$$Wi^* = [\beta^2(1+\lambda)^2 - (1-\lambda)^2]^{-1/2}, \tag{7}$$

provided

$$\beta^2(1+\lambda)^2 - (1-\lambda)^2 > 0. \tag{8}$$

On the other hand, when the constitutive equation and the basic flow are such that

$$\beta^2(1+\lambda)^2 - (1-\lambda)^2 \leq 0, \tag{9}$$

i.e.,

$$\beta \leq \frac{1-\lambda}{1+\lambda}.$$

then the stress components remain bounded for arbitrarily large values of Wi. In the case of simple shear flow ($\lambda = 0$), the stress components are clearly bounded for all Wi and for any β in the range $0 \leq \beta \leq 1$.

The critical Weissenberg number defined by (7) provides an upper limit on Wi above which the constitutive model (1) fails to predict physically realistic steady stress components for this basic flow. We interpret this to mean that the Oldroyd-type fluid considered here can realize steady, two-dimensional linear flow only under the conditions

$$0 \leq Wi < Wi^*, \quad \beta > (1-\lambda)/(1+\lambda), \tag{10a}$$

$$0 \leq Wi < \infty, \quad \beta \leq (1-\lambda)/(1+\lambda). \tag{10b}$$

In other words, the velocity field (4) does not exist as a valid solution to the equations of motion for this constitutive model when conditions (10a) and (10b) are violated. Consequently, when $\theta_2/\theta_1 \neq 1$, we confine our stability analysis to basic flows which satisfy conditions (10a) and (10b). When $\theta_2/\theta_1 = 1$, the

constitutive model reduces to that of a Newtonian fluid and restrictions (10a) and (10b) have no significance.

4. The Linearized Disturbance Equations

We present here the linearized equations which govern disturbances to the steady basic flow (4) for a fluid with constitutive model (1). In order to reduce the number of physical parameters, these disturbance equations are derived in dimensionless form, using as the characteristic time $t_c = E^{-1}$, the characteristic length $l_c = (\eta_0/\rho E)^{1/2}$, the characteristic velocity $U_c = (E\eta_0/\rho)^{1/2}$, and the characteristic pressure (stress) $p_c = \eta_0 E$.

For convenience, we let $\mathbf{U}(\mathbf{x})$ and $P(\mathbf{x})$ denote the velocity and pressure fields for the undisturbed flow, given by Eqs. (4) and (5). The corresponding extra-stress, strain-rate, and vorticity tensors are denoted as $\mathbf{T}(\mathbf{x})$, $\mathbf{E}(\mathbf{x})$, and $\mathbf{W}(\mathbf{x})$, respectively. Now let us suppose that this steady flow is disturbed slightly at some initial time $t = 0$. We denote the subsequent altered fields as

$$\mathbf{u}'(\mathbf{x},t) = \mathbf{U}(\mathbf{x}) + \mathbf{u}(\mathbf{x},t) ,$$

$$p'(\mathbf{x},t) = P(\mathbf{x}) + p(\mathbf{x},t) ,$$

$$\tau'(\mathbf{x},t) = \mathbf{T}(\mathbf{x}) + \tau(\mathbf{x},t) ,$$

$$\mathbf{e}'(\mathbf{x},t) = \mathbf{E}(\mathbf{x}) + \mathbf{e}(\mathbf{x},t) ,$$

and

$$\mathbf{w}'(\mathbf{x},t) = \mathbf{W}(\mathbf{x}) + \mathbf{w}(\mathbf{x},t) .$$

This altered flow must satisfy the equation of motion

$$\frac{\partial \mathbf{u}'}{\partial t} + \mathbf{u}'\cdot\nabla\mathbf{u}' = -\nabla p' + \nabla\cdot\tau' , \tag{11}$$

the continuity equation

$$\nabla\cdot\mathbf{u}' = 0 \,, \tag{12}$$

and the constitutive equation

$$\boldsymbol{\tau}' + \mathrm{Wi}\left[\frac{D\boldsymbol{\tau}'}{Dt} - \beta(\mathbf{e}'\cdot\boldsymbol{\tau}' + \boldsymbol{\tau}'\cdot\mathbf{e}')\right] = 2\mathbf{e}' + 2\varepsilon\mathrm{Wi}\left[\frac{D\mathbf{e}'}{Dt} - 2\beta(\mathbf{e}'\cdot\mathbf{e}')\right] . \tag{13}$$

The dimensionless parameters which appear in (13) are the Weissenberg number $\mathrm{Wi} = \mathrm{E}\theta_1$ and the ratio of the retardation and relaxation times $\varepsilon = \theta_2/\theta_1$, along with the previously defined parameter β.

The subsequent linear stability analysis is simplified by expressing Eqs. (11) and (13) in a modified form, which is obtained by simply decomposing the altered and basic stress tensors into viscous and viscoelastic parts:

$$\boldsymbol{\tau}' = 2\varepsilon\mathbf{e}' + \boldsymbol{\sigma}' \,, \tag{14a}$$

$$\mathbf{T} = 2\varepsilon\mathbf{E} + \boldsymbol{\Sigma} \,. \tag{14b}$$

Using the decomposition (14a), Eqs. (11) and (13) reduce to

$$\frac{\partial\mathbf{u}'}{\partial t} + \mathbf{u}'\cdot\nabla\mathbf{u}' = -\nabla p' + \varepsilon\nabla^2\mathbf{u}' + \nabla\cdot\boldsymbol{\sigma}' \,, \tag{15}$$

$$\boldsymbol{\sigma}' + \mathrm{Wi}\left[\frac{D\boldsymbol{\sigma}'}{Dt} - \beta(\mathbf{e}'\cdot\boldsymbol{\sigma}' + \boldsymbol{\sigma}'\cdot\mathbf{e}')\right] = 2(1-\varepsilon)\mathbf{e}' \,. \tag{16}$$

in which the time derivative of $\mathbf{e}'$ has been eliminated. We denote the difference between $\boldsymbol{\sigma}'$ and $\boldsymbol{\Sigma}$ as $\boldsymbol{\sigma}(\mathbf{x},t) = \boldsymbol{\sigma}'(\mathbf{x},t) - \boldsymbol{\Sigma}(\mathbf{x})$.

The linearized equations governing the disturbance variables $\mathbf{u}$, p, and $\boldsymbol{\sigma}$ are obtained from (12), (15), and (16) by subtracting the corresponding time-independent equations satisfied by the basic flow variables $\mathbf{U}$, P, and $\boldsymbol{\Sigma}$ and then neglecting terms which are nonlinear in any of the disturbance variables. Using (4), these dimensionless linearized disturbance equations can be written as

$$\frac{\partial \mathbf{u}}{\partial t} + (\Gamma\cdot\mathbf{x})\cdot\nabla\mathbf{u} + \Gamma\cdot\mathbf{u} = -\nabla p + \varepsilon\nabla^2\mathbf{u} + \nabla\cdot\boldsymbol{\sigma} \,, \tag{17}$$

$$\nabla\cdot\mathbf{u} = 0 \,, \tag{18}$$

$$\frac{\partial \boldsymbol{\sigma}}{\partial t} + (\Gamma\cdot\mathbf{x})\cdot\nabla\boldsymbol{\sigma} - \left(\frac{\beta+1}{2}\right)[\Gamma\cdot\boldsymbol{\sigma} + \boldsymbol{\sigma}\cdot\Gamma^T + \nabla\mathbf{u}\cdot\Sigma + \Sigma\cdot(\nabla\mathbf{u})^T]$$

$$-\left(\frac{\beta-1}{2}\right)[\Gamma^T\cdot\boldsymbol{\sigma} + \boldsymbol{\sigma}\cdot\Gamma + (\nabla\mathbf{u})^T\cdot\Sigma + \Sigma\cdot\nabla\mathbf{u}] + \frac{1}{Wi}\boldsymbol{\sigma} = \left(\frac{1-\varepsilon}{Wi}\right)[\nabla\mathbf{u} + (\nabla\mathbf{u})^T] \,. \tag{19}$$

The dimensionless components of Γ are given by (5) with E replaced by 1. The dimensionless components of the basic viscoelastic stress contribution Σ are obtained from (6a)-(6c) using (14b). The nonzero components of Σ are given by

$$\Sigma_{11} = \frac{(1-\varepsilon)(1+\lambda)[1 + Wi\beta(1+\lambda)]}{1 - Wi^2[\beta^2(1+\lambda)^2 - (1-\lambda)^2]} \tag{20a}$$

$$\Sigma_{22} = \frac{-(1-\varepsilon)(1+\lambda)[1 - Wi\beta(1+\lambda)]}{1 - Wi^2[\beta^2(1+\lambda)^2 - (1-\lambda)^2]} \tag{20b}$$

$$\Sigma_{12} = \Sigma_{21} = \frac{-(1-\varepsilon)Wi(1-\lambda^2)}{1 - Wi^2[\beta^2(1+\lambda)^2 - (1-\lambda)^2]} \,. \tag{20c}$$

In deriving the disturbance equations, (17)-(19), we have assumed that the basic flow is disturbed at some initial instant of time t = 0. This arbitrary initial disturbance in velocity and stress is specified by the initial conditions

$$\mathbf{u}(\mathbf{x},0) = \mathbf{u}^0(\mathbf{x}) \,, \tag{21a}$$

$$\boldsymbol{\sigma}(\mathbf{x},0) = \boldsymbol{\sigma}^0(\mathbf{x}) \,. \tag{21b}$$

These initial conditions may be prescribed arbitrarily within the limits of the following constraints. Both $\mathbf{u}^0(\mathbf{x})$ and $\boldsymbol{\sigma}^0(\mathbf{x})$ are assumed for physical reasons to be bounded for all $\mathbf{x} \in \mathbb{R}^3$. In addition, the disturbance velocity $\mathbf{u}^0(\mathbf{x})$ must be a solenoidal vector field since the fluid is incompressible. Furthermore, the initial disturbance velocity $\mathbf{u}^0(\mathbf{x})$ and the initial disturbance stress $\boldsymbol{\sigma}^0(\mathbf{x})$ must be related by the constitutive equation.

The stability of the basic flow with respect to infinitesimal disturbances is judged by determining the asymptotic behavior as $t \to \infty$ of the disturbance velocity field $\mathbf{u}(\mathbf{x},t)$, using Eqs. (17)-(19) subject to the initial conditions (21a) and (21b). A general solution of these equations is given in the following section. The fact that both $\mathbf{u}^0$ and $\boldsymbol{\sigma}^0$ must appear in this general solution, is a consequence of the fact that the constitutive equation cannot be inverted to obtain an explicit expression for $\boldsymbol{\sigma}$ in terms of $\mathbf{u}$. Thus, in spite of the fact that the stress could be eliminated, in principle, from the disturbance equations to obtain equations that involve $\mathbf{u}$ and p alone, this cannot be done in reality, and both $\mathbf{u}^0$ and $\boldsymbol{\sigma}^0$ thus appear in the general solution for $\mathbf{u}$. As we shall see, it is not necessary, insofar as the linear stability analysis is concerned, to spell out the details of the relationship between $\mathbf{u}^0$ and $\boldsymbol{\sigma}^0$.

5. General Solution of Linearized Disturbance Equations

Let us now consider the solution of the disturbance Eqs. (17)-(19) on an unbounded domain satisfying the arbitrary initial conditions (21a) and (21b). The fact that we seek solutions on an unbounded domain suggests the use of spatial Fourier transforms, defined according to

$$\hat{\mathbf{u}}(\mathbf{k},t) = \int \exp(i\mathbf{k}\cdot\mathbf{x})\mathbf{u}(\mathbf{x},t)d\mathbf{x}\,, \tag{22a}$$

$$\hat{p}(\mathbf{k},t) = \int \exp(i\mathbf{k}\cdot\mathbf{x})p(\mathbf{x},t)d\mathbf{x}\,, \tag{22b}$$

$$\hat{\boldsymbol{\sigma}}(\mathbf{k},t) = i\int \exp(i\mathbf{k}\cdot\mathbf{x})\boldsymbol{\sigma}(\mathbf{x},t)d\mathbf{x}\,, \tag{22c}$$

If we formally take the Fourier transform of Eqs. (17)-(19), (21a), and (21b), we obtain

$$\frac{\partial\hat{\mathbf{u}}}{\partial t} - (\Gamma^T\cdot\mathbf{k})\cdot\nabla_{\mathbf{k}}\hat{\mathbf{u}} + \Gamma\cdot\hat{\mathbf{u}} = i\hat{p}\mathbf{k} - \varepsilon k^2\hat{\mathbf{u}} - \hat{\boldsymbol{\sigma}}\cdot\mathbf{k}\,, \tag{23}$$

$$\mathbf{k}\cdot\hat{\mathbf{u}} = 0 \ , \tag{24}$$

$$\frac{\partial\hat{\sigma}}{\partial t} - (\Gamma^T\cdot\mathbf{k})\cdot\nabla_{\mathbf{k}}\hat{\sigma} - \left[\frac{\beta+1}{2}\right](\Gamma\cdot\hat{\sigma} + \hat{\sigma}\cdot\Gamma^T + \hat{\mathbf{u}}\mathbf{k}\cdot\Sigma + \Sigma\cdot\mathbf{k}\hat{\mathbf{u}}) \tag{25}$$

$$-\left[\frac{\beta-1}{2}\right](\Gamma^T\cdot\hat{\sigma} + \hat{\sigma}\cdot\Gamma + \mathbf{k}\hat{\mathbf{u}}\cdot\Sigma + \Sigma\cdot\hat{\mathbf{u}}\mathbf{k}) + \frac{1}{Wi}\hat{\sigma} = \left[\frac{1-\varepsilon}{Wi}\right](\hat{\mathbf{u}}\mathbf{k} + \mathbf{k}\hat{\mathbf{u}}) \ ,$$

$$\hat{\mathbf{u}}(\mathbf{k},0) = \hat{\mathbf{u}}^0(\mathbf{k}) \ , \tag{26}$$

$$\hat{\sigma}(\mathbf{k},0) = \hat{\sigma}^0(\mathbf{k}) \ . \tag{27}$$

Here, $\hat{\mathbf{u}}^0(\mathbf{k})$ denotes the Fourier transform of $\mathbf{u}^0(\mathbf{x})$, $\nabla_{\mathbf{k}}$ represents the gradient with respect to the wave vector $\mathbf{k}$, and $k^2 = \mathbf{k}\cdot\mathbf{k}$. Also, $\hat{\sigma}^0(\mathbf{k})$ is i times the Fourier transform of $\sigma^0(\mathbf{x})$.

The pressure term in (23) can be eliminated by first forming the inner product of Eq. (23) with $\mathbf{k}$ and using the condition (24) to obtain

$$i\hat{p}\mathbf{k} = \frac{2}{k^2}(\mathbf{k}\mathbf{k}\cdot\Gamma)\cdot\hat{\mathbf{u}} + \frac{1}{k^2}(\mathbf{k}\mathbf{k}\cdot\hat{\sigma})\cdot\mathbf{k} \ , \tag{28}$$

and then substituting (28) for the pressure term in Eq. (23). This substitution results in

$$\frac{\partial\hat{\mathbf{u}}}{\partial t} - (\Gamma^T\cdot\mathbf{k})\cdot\nabla_{\mathbf{k}}\hat{\mathbf{u}} + \Gamma\cdot\hat{\mathbf{u}} = -\varepsilon k^2\hat{\mathbf{u}} + \frac{2}{k^2}(\mathbf{k}\mathbf{k}\cdot\Gamma)\cdot\hat{\mathbf{u}} + \frac{1}{k^2}(\mathbf{k}\mathbf{k}\cdot\hat{\sigma})\cdot\mathbf{k} - \hat{\sigma}\cdot\mathbf{k} \ . \tag{29}$$

Equations (29) and (25) comprise a system of first-order linear partial differential equations for the components of $\hat{\mathbf{u}}(\mathbf{k},t)$ and $\hat{\sigma}(\mathbf{k},t)$, which are to be solved subject to the initial conditions (26) and (27). The solution can be obtained by means of the method of characteristics. The characteristics of (29) and (25) are determined by solving the following linear system and initial condition:

$$\frac{d\mathbf{k}}{dt} = -\Gamma^T\cdot\mathbf{k} \ , \tag{30}$$

$$\mathbf{k}(0) = \boldsymbol{\alpha} \ . \tag{31}$$

The solution

$$\mathbf{k}(t) = e^{-t\Gamma^T\cdot}\alpha \tag{32}$$

provides a parametric representation of the characteristic curve in $(\mathbf{k},t)$ space passing through the wave vector $\boldsymbol{\alpha}$ at $t = 0$. The functions $\hat{\mathbf{u}}'(\boldsymbol{\alpha},t)$ and $\hat{\boldsymbol{\sigma}}'(\boldsymbol{\alpha},t)$ defined by

$$\hat{\mathbf{u}}'(\boldsymbol{\alpha},t) \equiv \hat{\mathbf{u}}(e^{-t\Gamma^T\cdot}\boldsymbol{\alpha},t) \ , \tag{33}$$

$$\hat{\boldsymbol{\sigma}}'(\boldsymbol{\alpha},t) \equiv \hat{\boldsymbol{\sigma}}(e^{-t\Gamma^T\cdot}\alpha,t) \ , \tag{34}$$

assume the values of $\hat{\mathbf{u}}(\mathbf{k},t)$ and $\hat{\boldsymbol{\sigma}}(\mathbf{k},t)$, respectively, along the characteristic curve (32). Along the characteristic, which corresponds to some arbitrary fixed value of $\boldsymbol{\alpha}$, $\mathbf{u}$ and $\boldsymbol{\sigma}$ satisfy the first-order ordinary differential equations derived from (29) and (25):

$$\frac{\partial\hat{\mathbf{u}}'}{\partial t} = -\Gamma\cdot\hat{\mathbf{u}}' - \varepsilon k^2(t)\hat{\mathbf{u}}' + \frac{2}{k^2(t)}[\mathbf{k}(t)\mathbf{k}(t)\cdot\Gamma]\cdot\hat{\mathbf{u}}' + \frac{1}{k^2(t)}[\mathbf{k}(t)\mathbf{k}(t)\cdot\hat{\boldsymbol{\sigma}}']\cdot\mathbf{k}(t) - \hat{\boldsymbol{\sigma}}'\cdot\mathbf{k}(t) \ , \tag{35}$$

$$\frac{\partial\hat{\boldsymbol{\sigma}}'}{\partial t} = -\frac{1}{Wi}\hat{\boldsymbol{\sigma}}' + \left(\frac{\beta+1}{2}\right)[\Gamma\cdot\hat{\boldsymbol{\sigma}}' + \hat{\boldsymbol{\sigma}}'\cdot\Gamma^T + \hat{\mathbf{u}}'\mathbf{k}(t)\cdot\Sigma + \Sigma\cdot\mathbf{k}(t)\hat{\mathbf{u}}']$$

$$+\left(\frac{\beta-1}{2}\right)[\Gamma^T\cdot\hat{\boldsymbol{\sigma}}' + \hat{\boldsymbol{\sigma}}'\cdot\Gamma + \mathbf{k}(t)\hat{\mathbf{u}}'\cdot\Sigma + \Sigma\cdot\hat{\mathbf{u}}'\mathbf{k}(t)] + \left(\frac{1-\varepsilon}{Wi}\right)[\hat{\mathbf{u}}'\mathbf{k}(t) + \mathbf{k}(t)\hat{\mathbf{u}}'] \ , \tag{36}$$

where $\mathbf{k}(t)$ is given by (32), and $k^2(t) = \mathbf{k}(t)\cdot\mathbf{k}(t)$. The initial conditions corresponding to (26) and (27) are

$$\hat{\mathbf{u}}'(\boldsymbol{\alpha},0) = \hat{\mathbf{u}}^0(\boldsymbol{\alpha}) \ , \tag{37}$$

$$\hat{\boldsymbol{\sigma}}'(\boldsymbol{\alpha},0) = \hat{\boldsymbol{\sigma}}^0(\boldsymbol{\alpha}) \ , \tag{38}$$

The Fourier transforms $\hat{\mathbf{u}}(\mathbf{k},t)$ and $\hat{\boldsymbol{\sigma}}(\mathbf{k},t)$ can be recovered from the solution of (35)-(38) by means of the relations

$$\hat{\mathbf{u}}(\mathbf{k},t) = \hat{\mathbf{u}}'(e^{tr^T}\cdot\mathbf{k},t) \,, \tag{39}$$

$$\hat{\sigma}(\mathbf{k},t) = \hat{\sigma}'(e^{tr^T}\cdot\mathbf{k},t) \,, \tag{40}$$

which follow from (33) and (34)

Equations (35) and (36) correspond to a set of nine ordinary differential equations for the three components of $\hat{\mathbf{u}}'$ and the six independent components of $\hat{\sigma}'$. It is convenient for the purpose of representing this system to introduce the vector of independent disturbance components

$$\mathbf{y}(\mathbf{x},t) \equiv (u_1,u_2,u_3,\sigma_{11},\sigma_{12},\sigma_{13},\sigma_{22},\sigma_{23},\sigma_{33})^T \,,$$

and the corresponding vector of initial values

$$\mathbf{y}^0(\mathbf{x}) \equiv (u_1^0,u_2^0,u_3^0,\sigma_{11}^0,\sigma_{12}^0,\sigma_{13}^0,\sigma_{22}^0,\sigma_{23}^0,\sigma_{33}^0)^T \,.$$

Further, we let $\hat{\mathbf{y}}(\mathbf{k},t)$ and $\hat{\mathbf{y}}^0(\mathbf{k})$ denote the Fourier transforms of $\mathbf{y}$ and $\mathbf{y}^0$, respectively, and define the vector

$$\hat{\mathbf{y}}'(\alpha,t) \equiv (\hat{u}_1',\hat{u}_2',\hat{u}_3',\hat{\sigma}_{11}',\hat{\sigma}_{12}',\hat{\sigma}_{13}',\hat{\sigma}_{22}',\hat{\sigma}_{23}',\hat{\sigma}_{33}')^T \,,$$

containing the independent components of $\hat{\mathbf{u}}'$ and $\hat{\sigma}'$. It then follows from Eqs. (35)-(38) that the vector function $\hat{\mathbf{y}}'(\alpha,t)$ satisfies the linear system

$$\frac{\partial\hat{\mathbf{y}}'}{\partial t} = \mathbf{A}(t)\cdot\hat{\mathbf{y}}' \,, \tag{41}$$

and the initial condition

$$\hat{\mathbf{y}}'(\alpha,0) = \hat{\mathbf{y}}^0(\alpha) \,. \tag{42}$$

Here, $\mathbf{A}(t)$ is a 9x9 matrix whose components are listed in Appendix A.

The solution of (41) and (42) can be expressed as

$$\hat{\mathbf{y}}'(\alpha,t) = \Phi(\alpha,t)\cdot\hat{\mathbf{y}}^0(\alpha) \tag{43}$$

where $\Phi(\alpha,t)$ is the fundamental matrix solution for the linear system (41). In view of Eqs. (39) and (40), the Fourier transform $\hat{\mathbf{y}}$ is given by

$$\hat{\mathbf{y}}(\mathbf{k},t) = \hat{\mathbf{y}}'(e^{t\Gamma^T}\cdot\mathbf{k},t) = \Phi(e^{t\Gamma^T}\cdot\mathbf{k},t)\cdot\hat{\mathbf{y}}^0(e^{t\Gamma^T}\cdot\mathbf{k}) \ . \tag{44}$$

Taking the inverse Fourier transform of (44), we obtain

$$\mathbf{y}(\mathbf{x},t) = \frac{1}{(2\pi)^3}\int \exp(-i\mathbf{k}\cdot\mathbf{x})\Phi(e^{t\Gamma^T}\cdot\mathbf{k},t)\cdot\hat{\mathbf{y}}^0(e^{t\Gamma^T}\cdot\mathbf{k})d\mathbf{k} \ . \tag{45}$$

The form of this solution can be simplified by changing the variable of integration from $\mathbf{k}$ to $\boldsymbol{\xi} = e^{t\Gamma^T}\cdot\mathbf{k}$, yielding

$$\mathbf{y}(\mathbf{x},t) = \frac{1}{(2\pi)^3}\int \exp[-i(e^{-t\Gamma^T}\cdot\boldsymbol{\xi})\cdot\mathbf{x}]\Phi(\boldsymbol{\xi},t)\cdot\hat{\mathbf{y}}^0(\boldsymbol{\xi})d\boldsymbol{\xi} \ . \tag{46}$$

Equation (46) provides in final form a general solution for the components of the disturbance velocity $\mathbf{u}$ and disturbance stress $\boldsymbol{\sigma}$ in terms of the initial values $\mathbf{u}^0$ and $\boldsymbol{\sigma}^0$ and the fundamental matrix solution of the linear system (41).

6. Fundamental Mode Analysis

In order to assess the stability of the basic flow using the general disturbance solution (46), we must consider the initial disturbance vector $\mathbf{y}^0(\mathbf{x})$ in greater detail. We shall follow the usual approach of linear stability theory by representing the initial disturbance as a superposition of spatially periodic functions of the form

$$\mathbf{y}^0(\mathbf{x}) = \exp(-i\boldsymbol{\alpha}\cdot\mathbf{x})\mathbf{c}^0 \ , \tag{47}$$

where $\mathbf{c}^0$ is a constant vector, and the wave vector $\boldsymbol{\alpha}$ has real components α_1, α_2, and α_3. Taking the Fourier transform of (47) yields

$$\hat{\mathbf{y}}^0(\mathbf{k}) = (2\pi)^3\delta(\mathbf{k}-\boldsymbol{\alpha})\mathbf{c}^0 \ , \tag{48}$$

where δ denotes the Dirac delta function. Substituting (48) into the general solution (46), we obtain the fundamental mode solution

$$\mathbf{y}(\mathbf{x},t) = \exp[-i(e^{-t\Gamma^T}\cdot\boldsymbol{\alpha})\cdot\mathbf{x}]\Phi(\boldsymbol{\alpha},t)\cdot\mathbf{c}^0 \ . \tag{49}$$

A comparison of Eqs. (46) and (49) reveals that the general disturbance solution (46) is a superposition of fundamental modes of the form (49). Hence, stability criteria for the basic flow may be determined if the behavior of these fundamental mode disturbances is known asymptotically as $t \to \infty$ for each value of the wave vector $\boldsymbol{\alpha}$. Since the term $\exp[-i(e^{-tr^T}\cdot\boldsymbol{\alpha})\cdot\mathbf{x}]$ remains bounded as $t \to \infty$, we see from (49) that the growth or decay of the disturbance depends only on the behavior of $\Phi(\boldsymbol{\alpha},t)\cdot\mathbf{c}^0$ which is a solution of the linear system (41).

The elements of the coefficient matrix $\mathbf{A}(t)$ in (41) depend upon the values of the dimensionless parameters λ, Wi, ε, and β, along with the dimensionless components of the disturbance wave vector $\boldsymbol{\alpha}$. In addition, the elements of $\mathbf{A}(t)$ depend implicitly upon the characteristic length $l_c = (\eta_0/\rho E)^{1/2}$ used to nondimensionalize the components of $\boldsymbol{\alpha}$. Flow stability criteria will result from the determination of the effect of these parameters on the asymptotic behavior of solutions of the linear system (41).

7. Asymptotic Behavior of Linear System

Since the coefficient matrix $\mathbf{A}(t)$ in (41) is not constant, it is not possible to find a simple analytical solution of this linear system. It is possible under certain conditions, however, to determine the asymptotic behavior of solutions of (41) using the approach taken by Lagnado et al. [5] for the linear stability of a Newtonian fluid.

Employing similar manipulations to those described above, the Newtonian stability analysis was reduced to the problem of determining the asymptotic behavior as $t \to \infty$ of solutions of a linear system with a 3x3 nonconstant coefficient matrix. In that case, a differential inequality governing the Euclidean norm of a solution vector was first obtained. Sufficient conditions for stability were then obtained by solving this differential inequality for a decaying upper

bound on the solution norm. These conditions involved the components of the disturbance wave vector $\boldsymbol{\alpha} = (\alpha_1,\alpha_2,\alpha_3)$. The only case where asymptotic behavior could not be established in this way was

$$(-1 + \sqrt{\lambda})\alpha_1 + (1 + \sqrt{\lambda})\alpha_2 = 0 \tag{50}$$

Under condition (50) the coefficient matrix for the linear system was shown to assume the form $\mathbf{C} + \mathbf{B}(t)$, where $\mathbf{C}$ is a constant matrix and the elements of $\mathbf{B}(t)$ satisfy

$$\int_0^\infty |b_{ij}(t)|\,dt < \infty . \tag{51}$$

For these cases, the solutions of the full nonconstant coefficient system behave asymptotically for large time like solutions of the linear system with constant coefficient matrix $\mathbf{C}$ (cf. Levinson [18]). Thus the eigenvalues of $\mathbf{C}$ determine this asymptotic behavior.

In the present non-Newtonian stability analysis, the complicated form of the coefficient matrix $\mathbf{A}(t)$ in (41) prevents us from obtaining sufficient conditions for stability by means of a differential inequality. We can, however, repeat the analysis used in the Newtonian problem when condition (50) is satisfied. The ensuing conclusions regarding stability or instability of the non-Newtonian flow will, of course, only apply to the restricted class of initial disturbances characterized by condition (50). The elements of the coefficient matrix $\mathbf{A}(t)$, shown in Appendix A, depend upon the components of $\mathbf{k}(t) = e^{-t\Gamma^T}\cdot\boldsymbol{\alpha}$. The form of these components must be determined separately for the case of strong flows ($0 < \lambda \leq 1$) in which Γ^T has distinct eigenvalues and the case of simple shear flow ($\lambda = 0$) in which Γ^T has one multiple eigenvalue. For the sake of brevity we present the detailed analysis only for the strong flows in the remainder of this paper. The results for simple shear flow can be inferred from the limiting

behavior of the strong flow stability criteria in the limit as $\lambda \to 0$. The details of a parallel treatment for simple shear flow are given in Appendix C.

Strong Flows ($0 < \lambda \leq 1$)

In this case the dimensionless components of Γ are given by (5) with E replaced by 1. The eigenvalues of $-\Gamma^T$ are $\sqrt{\lambda}$, 0, and $-\sqrt{\lambda}$, and the fundamental matrix $e^{-t\Gamma^T}$ assumes the form

$$e^{-t\Gamma^T} = \frac{1}{4\sqrt{\lambda}} \begin{bmatrix} -(1-\sqrt{\lambda})^2 e^{\lambda^{1/2}t} + (1+\sqrt{\lambda})^2 e^{-\lambda^{1/2}t} & (1-\lambda)(e^{\lambda^{1/2}t} - e^{-\lambda^{1/2}t}) & 0 \\ -(1-\lambda)(e^{\lambda^{1/2}t} - e^{-\lambda^{1/2}t}) & (1+\sqrt{\lambda})^2 e^{\lambda^{1/2}t} - (1-\sqrt{\lambda})^2 e^{-\lambda^{1/2}t} & 0 \\ 0 & 0 & 4\sqrt{\lambda} \end{bmatrix} \tag{52}$$

for $0 < \lambda \leq 1$. The Cartesian components of $\mathbf{k}(t) = e^{-t\Gamma^T}\cdot\boldsymbol{\alpha}$ are then given by

$$k_1(t) = \frac{1-\sqrt{\lambda}}{4\sqrt{\lambda}}(\mathbf{q}_1\cdot\boldsymbol{\alpha})e^{\lambda^{1/2}t} + \frac{1+\sqrt{\lambda}}{4\sqrt{\lambda}}(\mathbf{q}_2\cdot\boldsymbol{\alpha})e^{-\lambda^{1/2}t}\,, \tag{53a}$$

$$k_2(t) = \frac{1+\sqrt{\lambda}}{4\sqrt{\lambda}}(\mathbf{q}_1\cdot\boldsymbol{\alpha})e^{\lambda^{1/2}t} + \frac{1-\sqrt{\lambda}}{4\sqrt{\lambda}}(\mathbf{q}_2\cdot\boldsymbol{\alpha})e^{-\lambda^{1/2}t}\,, \tag{53b}$$

$$k_3(t) = \alpha_3\,, \tag{53c}$$

where

$$\mathbf{q}_1 = (-1+\sqrt{\lambda},\ 1+\sqrt{\lambda},\ 0)\,, \tag{54a}$$

$$\mathbf{q}_2 = (1+\sqrt{\lambda},\ -1+\sqrt{\lambda},\ 0)\,. \tag{54b}$$

Note that the vectors $\mathbf{q}_1$ and $\mathbf{q}_2$ are directed along the "inlet" and "outlet" streamlines of the basic flow, respectively.

We consider only spatially periodic initial disturbances for which the wavenumbers α_1 and α_2 satisfy condition (50). This condition implies that

$$\mathbf{q}_1\cdot\boldsymbol{\alpha} = (-1+\sqrt{\lambda})\alpha_1 + (1+\sqrt{\lambda})\alpha_2 = 0\,,$$

and it follows that the components of $\mathbf{k}(t)$ simplify to

$$k_1(t) = \frac{1 + \sqrt{\lambda}}{4\sqrt{\lambda}} (\mathbf{q}_2 \cdot \boldsymbol{\alpha}) e^{-\lambda^{1/2} t} , \tag{55a}$$

$$k_2(t) = \frac{1 - \sqrt{\lambda}}{4\sqrt{\lambda}} (\mathbf{q}_2 \cdot \boldsymbol{\alpha}) e^{-\lambda^{1/2} t} , \tag{55b}$$

$$k_3(t) = \alpha_3 . \tag{55c}$$

Using (55a)-(55c), we find that under condition (50) the coefficient matrix $\mathbf{A}(t)$ is of the form

$$\mathbf{A}(t) = \mathbf{A}^{(1)} + \mathbf{B}(t) . \tag{56}$$

Here, $\mathbf{A}^{(1)}$ is a constant matrix whose elements are listed in Appendix B, and the elements of $\mathbf{B}(t)$ are either zero or satisfy

$$b_{ij}(t) = 0(e^{-p_{ij}\lambda^{1/2} t}) , \quad (i,j = 1,2,3), \tag{57}$$

where $p_{ij} = 1$, 2, or 3. The elements of $\mathbf{B}(t)$ clearly satisfy the integrability condition (51). Hence, the eigenvalues of $\mathbf{A}^{(1)}$ determine the asymptotic behavior as $t \to \infty$ of solutions of the linear system (41). The components of $\mathbf{A}^{(1)}$ depend upon the parameters λ, β, ε, Wi, and α_3, and the eigenvalues are therefore functions of these parameters. If all eigenvalues have negative real parts, then all solutions of (41) decay to zero. If, on the other hand, at least one eigenvalue has a positive real part, then there exist solutions of (41) which grow exponentially in time and the system is unstable for that combination of parameters.

The eigenvalues of $\mathbf{A}^{(1)}$ are the nine roots of the characteristic polynomial $\det(\mathbf{A}^{(1)} - \mu\mathbf{I})$. This polynomial can be partially factored to permit the immediate determination of five eigenvalues

$$\mu_1 = -\varepsilon\alpha_3^2 , \tag{58a}$$

$$\mu_2 = \mu_3 = -\frac{1}{\mathrm{Wi}} , \tag{58b}$$

$$\mu_4 = -\frac{1}{\mathrm{Wi}} - [\beta^2(1+\lambda)^2 - (1-\lambda)^2]^{1/2}, \tag{58c}$$

$$\mu_5 = -\frac{1}{\mathrm{Wi}} + [\beta^2(1+\lambda)^2 - (1-\lambda)^2]^{1/2}. \tag{58d}$$

The remaining four eigenvalues μ_6, μ_7, μ_8, and μ_9 are the roots of the quartic equation

$$\det \begin{bmatrix} -\varepsilon\alpha_3^2 - \left[\frac{1+\lambda}{2}\right] - \mu & -\left[\frac{1-\lambda}{2}\right] & -\alpha_3 & 0 \\ \left[\frac{1-\lambda}{2}\right] & -\varepsilon\alpha_3^2 + \left[\frac{1+\lambda}{2}\right] - \mu & 0 & -\alpha_3 \\ \left[\frac{1-\varepsilon}{\mathrm{Wi}}\right]\alpha_3 + \left[\frac{\beta-1}{2}\right]\Sigma_{11}\alpha_3 & \left[\frac{\beta-1}{2}\right]\Sigma_{12}\alpha_3 & -\frac{1}{\mathrm{Wi}} + \beta\left[\frac{1+\lambda}{2}\right] - \mu & \left[\frac{1-\lambda}{2}\right] \\ \left[\frac{\beta-1}{2}\right]\Sigma_{12}\alpha_3 & \left[\frac{1-\varepsilon}{\mathrm{Wi}}\right]\alpha_3 + \left[\frac{\beta-1}{2}\right]\Sigma_{22}\alpha_3 & -\left[\frac{1-\lambda}{2}\right] & \frac{-1}{\mathrm{Wi}} - \beta\left[\frac{1+\lambda}{2}\right] - \mu \end{bmatrix} = 0 \tag{59}$$

When $\lambda = 1$, the left-hand side of (59) can be factored as the product of two quadratic polynomials and the eigenvalues are easily found to be

$$\begin{Bmatrix}\mu_6 \\ \mu_7\end{Bmatrix} = -\frac{1}{2}(\varepsilon\alpha_3^2 + \frac{1}{\mathrm{Wi}} + 1 - \beta)$$

$$\pm\left\{\frac{1}{4}(\varepsilon\alpha_3^2 + \frac{1}{\mathrm{Wi}} + 1 - \beta)^2 - (1 + \varepsilon\alpha_3^2)(\frac{1}{\mathrm{Wi}} - \beta) - \left[\frac{1-\varepsilon}{\mathrm{Wi}}\right]\alpha_3^2 - \left[\frac{\beta-1}{2}\right]\Sigma_{11}\alpha_3^2\right\}^{1/2} \tag{60a}$$

$$\begin{Bmatrix}\mu_8 \\ \mu_9\end{Bmatrix} = -\frac{1}{2}(\varepsilon\alpha_3^2 + \frac{1}{\mathrm{Wi}} - 1 + \beta)$$

$$\pm\left\{\frac{1}{4}(\varepsilon\alpha_3^2 + \frac{1}{\mathrm{Wi}} - 1 + \beta)^2 - (-1 + \varepsilon\alpha_3^2)(\frac{1}{\mathrm{Wi}} + \beta) - \left[\frac{1-\varepsilon}{\mathrm{Wi}}\right]\alpha_3^2 - \left[\frac{\beta-1}{2}\right]\Sigma_{22}\alpha_3^2\right\}^{1/2} \tag{60b}$$

For $0 < \lambda < 1$, the polynomial in (59) cannot be factored conveniently and analytical expressions for the eigenvalues could be obtained only by the extremely complicated task of solving the quartic equation algebraically. As a consequence, we choose instead to determine the instability conditions for $0 < \lambda < 1$ by computing the eigenvalues numerically as the physical parameters are systematically varied.

8. Results

We determine and discuss here the conditions under which the strong two-dimensional linear flows are unstable with respect to disturbances satisfying condition (50) on wavenumbers α_1 and α_2. These instability conditions are illustrated by plotting neutral stability curves in the first quadrant of the (Wi,α_3^2)-plane for fixed values of the parameters λ, β, and ε. Such neutral stability curves separate regions of instability where at least one eigenvalue of $\mathbf{A}^{(1)}$ has a positive real part from regions of stability where all eigenvalues of $\mathbf{A}^{(1)}$ have negative real parts.

For convenience in making comparisons, we first summarize the results of the Newtonian stability analysis given by Lagnado et al. [5]. In this earlier study it was found that the strong, two-dimensional linear flows are unstable only for disturbances which satisfy condition (50) and for which

$$\alpha_3^2 = \frac{\nu \tilde{\alpha}_3^2}{E} < \sqrt{\lambda}$$

Here, $\tilde{\alpha}_3$ denotes the dimensional wavenumber in the direction normal to the plane of the basic flow, and ν is the Newtonian kinematic viscosity. Thus, only disturbances with small values of α_3 are unstable for a Newtonian fluid.

Proceeding with the present analysis, analytical expressions for the eigenvalues μ_1, μ_2, μ_3, μ_4, and μ_5 are provided by (58a)-(58d) for all flows in the range

$0 < \lambda \leq 1$. An inspection of these expressions reveals that the real parts of μ_1, μ_2, μ_3, and μ_4 are always negative since we must have $Wi \geq 0$ and $\varepsilon \geq 0$. Furthermore, the real part of μ_5 is always negative for all values of λ, Wi, and β which comply with restrictions (10a) and (10b). The real part of μ_5 is positive only when $\beta > (1-\lambda)/(1+\lambda)$ and $Wi > [\beta^2(1+\lambda)^2 - (1-\lambda)^2]^{-1/2}$. Under these conditions the Weissenberg number exceeds the critical value Wi^* at which the basic stress components become infinite. It is interesting to note that the "nonexistence" of the assumed basic flow as a solution for this Oldroyd-type constitutive equation is also reflected by an "apparent" instability for all values of the disturbance wavenumber α_3.

We proceed now with the determination of conditions for flow instability by examining the remaining eigenvalues μ_6, μ_7, μ_8, and μ_9 for values of the parameters which satisfy restrictions (10a) and (10b). Since the real parts of four separate eigenvalues determine these instability conditions, the corresponding neutral stability curves assume a piecewise smooth appearance.

Let us first consider the case $\lambda = 1$ corresponding to pure extensional flow. In this case, the remaining eigenvalues of $\mathbf{A}^{(1)}$ are given exactly by (60a) and (60b). With some effort, instability criteria for pure extensional flow can be derived from (60a) and (60b) as a set of algebraic relations that indicate when at least one eigenvalue has a positive real part. The resulting instability criteria are best illustrated by plotting neutral stability curves for several values of the parameters β and ε. These instability criteria are, of course, valid only over the range of Weissenberg numbers specified by restrictions (10a) and (10b) which, in the case of pure extensional flow ($\lambda = 1$), reduce to

$$0 \leq Wi < Wi^* = \frac{1}{2\beta} \quad \text{for} \quad 0 < \beta \leq 1 \quad \text{and} \quad \varepsilon \neq 1 ,$$

$$0 \leq \mathrm{Wi} < \infty \quad \text{for} \quad \beta = 0 \quad \text{or} \quad \varepsilon = 1 .$$

We first examine pure extensional flow for the limiting case $\beta = 1$ where co-deformational derivatives appear in the constitutive equation. For $\beta = 1$ and $\varepsilon \neq 1$, the assumed basic flow is valid only for $0 \leq \mathrm{Wi} < \mathrm{Wi}^* = 1/2$. The neutral stability curve is given by

$$\alpha_3^2 = \frac{1 + \mathrm{Wi}}{1 + \varepsilon \mathrm{Wi}} ,$$

and the flow is unstable for small wavenumbers satisfying

$$\alpha_3^2 < \frac{1 + \mathrm{Wi}}{1 + \varepsilon \mathrm{Wi}} .$$

Figure 3 shows this neutral stability curve plotted for several values of the parameter ε. The Newtonian criterion for instability of pure extensional flow is $\alpha_3^2 < 1$. This result is reproduced in the present theory both for $\mathrm{Wi} = 0$ and for $\varepsilon = 1$ for which the constitutive equation reduces to the Newtonian form. Fluid elasticity is seen to be destabilizing when $\beta = 1$ in the sense that the range of unstable wavenumbers α_3 increases with increasing Weissenberg number. Increasing the retardation time (i.e., ε) has a stabilizing effect in that a smaller range of α_3 values are unstable for a given Wi. The widest range of unstable wavenumbers at any Wi occurs in the case $\varepsilon = 0$ corresponding to a co-deformational Maxwell model.

We next examine the stability of pure extensional flow for $\beta = 0$. In this case, the constitutive equation assumes the co-rotational Jeffreys form, and there is no limit on Wi for the existence of the undisturbed steady flow. The neutral stability curve for the particular case $\varepsilon = 0.2$ is shown in Fig. 4. These results for $\varepsilon = 0.2$ are qualitatively representative of the behavior for $\lambda = 1$ and $\beta = 0$ over the entire range of the retardation parameter, $1/9 \leq \varepsilon < 1$. The neutral stability curve consists of the union of three intersecting smooth curves labeled a, b, and

c in Fig. 4. When $0 \le \mathrm{Wi} \le 1/\sqrt{1-\varepsilon}$, the flow is unstable for

$$\alpha_3^2 < \frac{1}{1 + (1-\varepsilon)\mathrm{Wi}},$$

(i.e., below curve a in Fig. 4). Thus, only the small wavenumber disturbances lead to instability when the Weissenberg number is sufficiently small, and in this sense the small Wi results are similar to those shown earlier for the co-deformational model ($\beta = 1$). However, in this case ($\lambda = 1$, $\beta = 0$), the fluid elasticity actually stabilizes the flow since the range of unstable wavenumbers decreases relative to the Newtonian fluid limit as Wi increases from 0 to $1/\sqrt{1-\varepsilon}$. This result for small Wi is, however, just a "small" correction to the basic Newtonian mode of instability. Elasticity begins to exert a very strong destabilizing influence when Wi exceeds $1/\sqrt{1-\varepsilon}$. Indeed, for $\mathrm{Wi} > 1/\sqrt{1-\varepsilon}$ the range of unstable wavenumbers first increases, and then for $1/(1-\varepsilon) < \mathrm{Wi} \le 1/(1-\sqrt{\varepsilon})$ we find that both small wavenumber disturbances satisfying

$$\alpha_3^2 < \frac{1}{\varepsilon}\left(1 - \frac{1}{\mathrm{Wi}}\right),$$

(i.e., below curve b in Fig. 4), and large wavenumber disturbances satisfying

$$\alpha_3^2 > \frac{1}{(1-\varepsilon)\mathrm{Wi} - 1},$$

(i.e., above curve c in Fig. 4) result in instability. In Fig. 4, the dotted line labeled d indicates the asymptote $\mathrm{Wi} = 1/(1-\varepsilon)$ to curve c for $\alpha_3^2 \to \infty$. This asymptote is significant in that it marks the critical value of Wi beyond which large wavenumber disturbances are unstable. Finally, the flow is unstable for the entire range $0 \le \alpha_3 < \infty$ when $\mathrm{Wi} \ge 1/(1-\sqrt{\varepsilon})$. This result is particularly interesting since the constitutive equation predicts finite basic stress components for all Weissenberg numbers when $\beta = 0$.

In this case of the co-rotational model ($\beta = 0$), an increase in retardation time (i.e., ε) has a slightly destabilizing effect for small Weissenberg numbers. This behavior is manifested by the fact that the neutral stability curve $\alpha_3^2 = 1/[1 + (1 - \varepsilon)\mathrm{Wi}]$ gradually rises up to the horizontal line $\alpha_3^2 = 1$ as $\varepsilon \to 1$. For large Weissenberg numbers, however, an increase in retardation time is strongly stabilizing for this model. In particular, both the critical Weissenberg number where instability first occurs for all wavenumbers, and the Weissenberg number above which large wavenumber disturbances become unstable, increase as ε increases, the first as $1/(1-\sqrt{\varepsilon})$ and the latter as $1/(1-\varepsilon)$. Indeed, these values tend to infinity as $\varepsilon \to 1$. Of course, this latter result is to be expected since the constitutive model reverts to that of a Newtonian fluid for $\varepsilon = 1$, and no instability was found in that case for large wavenumbers.

Finally, we turn to the results for intermediate forms of the constitutive equation associated with values of β in the range $0 < \beta < 1$. The typical behavior is illustrated by Fig. 5 which shows the neutral stability curve for $\lambda = 1$, $\beta = 0.5$, and $\varepsilon = 0.2$. We see that pure extensional flow is unstable to disturbances with small wavenumbers satisfying

$$\alpha_3^2 < \frac{1 + \beta\mathrm{Wi}}{1 + \varepsilon\beta\mathrm{Wi} + [(1 - \beta)(1 - \varepsilon)\mathrm{Wi}/(1 + 2\beta\mathrm{Wi})]},$$

(i.e., below curve a in Fig. 5) for sufficiently small values of Wi. Furthermore, for

$$\mathrm{Wi} \geq \frac{(1 - \varepsilon + \beta + 2\varepsilon\beta) - [(1 - \varepsilon + \beta + 2\varepsilon\beta)^2 - 8\varepsilon\beta^2]^{1/2}}{4\varepsilon\beta^2},$$

large wavenumber disturbances with

$$\alpha_3^2 > \frac{1 - \beta\mathrm{Wi}}{-1 + \varepsilon\beta\mathrm{Wi} + [(1 - \beta)(1 - \varepsilon)\mathrm{Wi}/(1 - 2\beta\mathrm{Wi})]},$$

(i.e., above curve b in Fig. 5) also become unstable. The critical Weissenberg number marking the onset of large wavenumber instability is indicated in Fig. 5

by the asymptote c to curve b. The branches of the neutral stability curve corresponding to small and large wavenumber instability eventually intersect, and the full range of wavenumbers $0 \leq \alpha_3 < \infty$ are unstable for values of Wi beyond this point. As we have already noted, the basic flow does not exist for $Wi > Wi^* = 1/(2\beta)$. In the case $\beta = 0.5$, plotted in Fig. 5, this corresponds to $Wi > 1$. It is noteworthy that the critical Weissenberg number for instability to disturbances of all wavenumbers is smaller than this limiting value. The effect of increasing retardation time (i.e., ε) for intermediate β is illustrated by Fig. 6 which depicts the neutral stability curve for $\lambda = 1$, $\beta = 0.5$, and $\varepsilon = 0.8$. It is apparent that as $\varepsilon \to 1$, the critical Weissenberg number, above which both small and large wavenumber disturbances are unstable, asymptotically approaches the limiting value $Wi^* = 1/(2\beta)$ for existence of the undisturbed, steady flow. Again we see that increasing the retardation parameter ε has a stabilizing effect.

We are unable to provide analytical descriptions of instability conditions for the remaining strong linear flows in the range $0 < \lambda < 1$. However, the neutral stability curves for these flows may be obtained from numerical calculations of the eigenvalues of $\mathbf{A}^{(1)}$. We find that the effects of the parameters β and ε on the neutral stability curves remain qualitatively similar to the results cited above for $\lambda = 1$.

Figure 7 illustrates the case $\lambda = 0.7$ and $\beta = 1$, with neutral stability curves plotted for several values of ε. These curves are similar to their counterparts shown in Fig. 3 for the case $\lambda = 1$. Again only small wavenumber disturbances are unstable for values of Weissenberg number below Wi^*. There are two essential differences, though. First, the range of Weissenberg number over which the steady undisturbed flow exists is larger when $\lambda = 0.7$ than when $\lambda = 1$. Indeed, in the case of a co-deformational model ($\beta = 1$) this range is given for arbitrary λ and $\varepsilon \neq 1$ by

$$0 \le \mathrm{Wi} < \mathrm{Wi}^* = [(1+\lambda)^2 - (1-\lambda)^2]^{-1/2} .$$

The upper limit Wi^* for the existence of the basic flow clearly tends to ∞ as $\lambda \to 0$. Second, the range of unstable disturbance wavenumbers α_3 is smaller for $\lambda = 0.7$ than for $\lambda = 1$ at any fixed Wi and ε. In view of the Newtonian instability condition $\alpha_3^2 < \sqrt{\lambda}$, it is clear that the neutral stability curves in regions of small Wi must tend toward $\alpha_3^2 = 0$ as $\lambda \to 0$ for any value of ε (and β, as well).

The case of a co-rotational model ($\beta = 0$) and an intermediate flow ($\lambda = 0.7$) is illustrated in Fig. 8, with neutral stability curves plotted for $\varepsilon = 0.2$ and $\varepsilon = 0.4$. Again, these curves are qualitatively similar to the neutral stability curve shown in Fig. 4 for $\lambda = 1$ and $\beta = 0$. We note that the curves in Fig. 8 are both piecewise smooth unions of three intersecting curves as in Fig. 4. The curves in Fig. 8 appear smooth, but this is only because the separate pieces intersect at points where their slopes are nearly equal. An increase in the retardation parameter ε is again seen to exert a stabilizing influence in the case $\lambda = 0.7$ by increasing the critical Weissenberg number beyond which large wavenumber disturbances are unstable.

A decrease in the value of the parameter λ appears to stabilize the basic flow with respect to disturbances satisfying condition (50) for all forms of the constitutive equation. This tendency is clearly indicated in Fig. 9 which compares neutral stability curves for $\lambda = 1$, $\lambda = 0.7$, and $\lambda = 0.5$, all corresponding to the specific case $\beta = 0$ and $\varepsilon = 0.2$. In general, the range of unstable small wavenumbers occurring for small values of the Weissenberg number decreases as $\lambda \to 0$. Furthermore, the critical Weissenberg numbers marking either large wavenumber instability or the nonexistence of the basic flow grow larger as $\lambda \to 0$. This behavior suggests that unbounded simple shear flow ($\lambda = 0$) should be linearly stable with respect to periodic initial disturbances satisfying condi-

tion (50) for all forms of the Oldroyd-type constitutive model (1). The physical significance of condition (50) is revealed in the case of simple shear flow when the present coordinate system is transformed by rotating the x_1- and x_2-axes through a 45° angle about the x_3-axis. Under this transformation, the new x_1-axis corresponds to the streamwise direction for simple shear flow and condition (50) reduces for $\lambda = 0$ to $\alpha_1 = 0$. Thus, it must be emphasized that the conclusion of stability for simple shear flow of this Oldroyd-type fluid applies only to spatially periodic initial disturbances with vanishing streamwise wavenumber. Other types of disturbances may lead to instability. This possibility is likely in view of the results of a study by Gorodtsov and Leonov [19]. They found that bounded plane Couette flow of a co-deformational Maxwell fluid ($\beta = 1$ and $\varepsilon = 0$ in this case) is unstable at small Reynolds number and large Weissenberg number for periodic disturbances with large wavenumbers in the streamwise direction.

9. Concluding Remarks

The linear stability analysis for unbounded, two-dimensional linear flows of an Oldroyd-type fluid reveals that the strong flows ($0 < \lambda \leq 1$) are unconditionally unstable. This instability persists for all forms of the constitutive equation ranging from the co-rotational type to the co-deformational type. This result was obtained by considering only spatially periodic initial disturbances with wavenumbers α_1 and α_2 in the x_1- and x_2-directions, respectively, which satisfy condition (50), viz.

$$(-1 + \sqrt{\lambda})\alpha_1 + (1 + \sqrt{\lambda})\alpha_2 = 0 .$$

As shown in Fig. 2, the inlet streamline for a strong flow in the $(x_1,x_2)-$plane has a slope of $(\sqrt{\lambda} + 1)/(\sqrt{\lambda} - 1)$. The preceding condition on α_1 and α_2 implies that the initial disturbance has lines of constant phase in the $(x_1,x_2)-$plane parallel

to the inlet streamline, and, therefore, is invariant in the direction parallel to the inlet streamline. For small values of Wi, initial disturbances of this type grow unstably in time if the wavenumber α_3 in the direction normal to the plane of the basic flow is sufficiently small. This is qualitatively the same result as obtained for a Newtonian fluid by Lagnado et al. [5]. Instability occurs in a Newtonian fluid undergoing a strong linear flow only for disturbances which are invariant along the inlet streamline and which satisfy $\alpha_3^2 < \sqrt{\lambda}$. It was shown that under these conditions, vortex line stretching causes the disturbance vorticity to grow in time at an exponential rate which exceeds the rate of decay due to convection-enhanced diffusion. For the Oldroyd-type fluid considered in the present study, the moderate elasticity associated with small values of Wi is seen to exert a relatively slight modifying influence on the physical mechanism for instability described for the Newtonian fluid, but not to change it in a fundamental way. We have shown that increases of Wi can be either stabilizing or destabilizing for an Oldroyd-type fluid, depending upon the form of the time derivatives that appear in the constitutive equation. For the co-deformational model ($\beta = 1$) a small increase in the Weissenberg number increases the range of wavenumbers α_3 corresponding to unstable disturbances. However, the opposite effect is observed for the co-rotational model ($\beta = 0$). In any case, the effects are small for $Wi \ll 1$, and are not of any great significance.

As the Weissenberg number increases to values of order unity [i.e., $Wi \sim O(1)$], however, a radical departure from the Newtonian or near-Newtonian behavior is predicted to occur. In particular, the presence of elastic effects which are comparable in magnitude to viscous effects appears to significantly destabilize the class of strong linear flows. This destabilization is characterized by the appearance a new branch of critical Weissenberg numbers, above which disturbances both with small and large values of the wavenumber α_3 are unstable. In any

attempt to interpret this result, it is important to recall that some forms of the constitutive equation yield physically unrealistic basic stress components when the Weissenberg number exceeds a certain value (thus, basic flows corresponding to these Weissenberg numbers are not allowable). In particular, when $\beta > (1 - \lambda)/(1 + \lambda)$, for the Oldroyd-type constitutive equation considered here, there is a finite value of the Weissenberg number, Wi^*, given by Eq. (7), at which the basic stress components become infinite. In such cases the large wavenumber instability for $Wi \geq Wi^*$ may be connected to the fact that the steady basic flow is not allowed by the constitutive model. However, for the co-rotational model ($\beta = 0$) and intermediate models ($0 < \beta < 1$) we find that instability for both small and large values of the wavenumber α_3 occurs at Weissenberg numbers where the basic flow is allowed and the behavior of the constitutive model appears to be perfectly reasonable.

It is important to emphasize that our stability results apply only to disturbances which satisfy condition (50), and there remains the uncertainty of whether or not this condition represents the most unstable disturbance mode for an Oldroyd-type fluid as it did for a Newtonian fluid. This uncertainty does not alter the conclusion of unconditional flow instability, though, since this is guaranteed by the existence of at least one unstable disturbance mode corresponding to each set of values assumed by the physical parameters. However, there may exist disturbances to the non-Newtonian flow which fail to satisfy (50) but which are unstable over a wider range of α_3 values at small Weissenberg numbers.

The change in mechanism which accounts for the instability of unbounded two-dimensional linear flows to large wavenumber (α_3) disturbances beyond a critical Weissenberg number assumes added significance when one attempts to discuss these results in the context of real two- and four-roll mill flows. Any

attempt to connect the stability theory for unbounded linear flows with actual milling flow behavior must address the fact that a milling device is bounded in extent and the flow it produces is accurately represented by the linear flow field only over the central region of the flow domain. The restricted size of the device in the direction normal to the plane of the flow has two effects on the stability problem. First, it imposes a *lower* limit on the wavenumber α_3 and a corresponding upper limit on the wavelength of a disturbance mode which can be realized. Second, the allowable disturbances must vanish at the top and bottom of the device due to the no-slip condition. We do not attempt to account for this second effect in the present work, in part because we see no justification for trying to apply boundary conditions at the top and bottom, without simultaneously applying boundary conditions at the roller surfaces and this would make the analysis impossibly complex. If we simply consider the effect of a geometric wavenumber cutoff, it is evident that the analysis predicts that the flow for Wi = 0 or Wi small should be stable up to some critical Reynolds number. Indeed, the top and bottom walls restrict the dimensional disturbance wavenumber $\tilde{\alpha}_3$ in the direction of the roller axes according to

$$\frac{2\pi}{\tilde{\alpha}_3} \leq 2h$$

where h is the length of the rollers. The results of our present study have shown that the unbounded linear flow is unstable for an Oldroyd-type fluid at small Weissenberg number only when

$$\alpha_3^2 = \frac{\eta_0 \tilde{\alpha}_3^2}{\rho E} < c .$$

Here, c is a constant which depends upon λ and Wi and assumes the value $c = \sqrt{\lambda}$ in the Newtonian case. Assuming that the boundaries exert no effect other than disturbance wavenumber restriction, one would expect the milling flow to

be stable for small Reynolds number

$$\mathrm{Re} = \frac{\rho E h^2}{\eta_0} < \frac{\pi^2}{c},$$

and unstable, otherwise. For large values of Weissenberg number, on the other hand, the unbounded flow is unstable to disturbances with arbitrarily *large* wavenumbers α_3. Such small wavelength disturbances could never be excluded by the presence of boundaries, and one is led to the conjecture that at a sufficiently large Weissenberg number a two-dimensional linear flow would be unstable and unrealizable in any portion of a milling device at any Reynolds number. This conjecture presumes, of course, that the rheological behavior of the fluid is adequately modeled by the constitutive Eq. (1). Broadbent et al. [20] have observed instabilities and irregularities in calendering flows of viscoelastic fluids in a two-roll mill which would seem to lend support to our conjecture. They found, in particular, that flow patterns for viscoelastic solutions of polyacrylamide and polyox were considerably three-dimensional in contrast to the reasonably two-dimensional flow patterns exhibited by Newtonian glycerol at the same roller speeds and gap widths. However, further discussion of these points awaits the completion of a thorough experimental study of flow in a four-roll mill which we are currently undertaking.

The predicted existence of an instability for strong flows of the Oldroyd model fluid to disturbances of all wavenumber at a critical Weissenberg number of O(1) is also suggestive of a possible connection with the problem of nonconvergence in the numerical solution of viscoelastic flows beyond a critical Weissenberg number of O(1), though, of course, the flows attempted numerically are more complicated than those considered in the present stability analysis. One possible cause for the convergence breakdown is temporal instability due either to the existence of a physical instability for the particular constitutive model and

flow, or the nonexistence of steady flow solutions for Wi larger than some critical value [21]. While a temporal instability may account for convergence problems in time-dependent numerical calculations, it is not necessarily apparent that a steady solution could not be obtained by a time-independent numerical technique. The introduction of iterative methods would, however, be expected to lead to difficulties. Indeed, Tanner [22] has shown that an iterative finite-difference scheme applied to steady one-dimensional flow of a Maxwell fluid becomes unstable when the Weissenberg number based on mesh size exceeds a critical value of O(1). In such numerical stability analyses, equations governing numerical disturbances (due to round-off error) are obtained from the discretized form of the equations of motion. For the simplest problems, solutions to these disturbance equations can be obtained by consideration of disturbance Fourier modes, yielding conditions for the growth or decay of numerical disturbances with increasing iteration number. The numerical stability analysis is similar in many ways to the present temporal stability analysis for the continuum equations, especially when one identifies iteration number as a sort of "false" time. Thus, it is plausible that there exists a connection between the mechanisms causing numerical and temporal instabilities for a particular constitutive equation. The results of the present investigation indicate that there is a mechanism built into Oldroyd-type constitutive models which results in destabilization of two-dimensional linear flows with respect to large wavenumber disturbances for sufficiently large Weissenberg numbers. In any numerical experiment, the small wavenumber (long wavelength) numerical disturbances will be absent below a minimum wavenumber corresponding to the physical length scale of the flow. The large wavenumber (small wavelength) numerical disturbances will be present, however, up to a maximum wavenumber associated with the mesh spacing for the numerical scheme. Hence, the convergence breakdown

of numerical solutions for Oldroyd-type constitutive models may be another manifestation of the instability mechanism described here.

One interesting result which may corroborate the connection between our stability results and the numerical convergence problem is the stabilizing effect of retardation time. As our analysis indicates, an increase in the retardation parameter ε stabilizes the basic flow by increasing the critical value of Weissenberg number above which disturbances of all wavenumbers α_3 are unstable. A similar conclusion was reached by Phan-Thien [23] who studied the linear stability of creeping torsional flow of an Oldroyd-B fluid ($\beta = 0$ in this case). He found that the basic flow is unstable if the Weissenberg number, defined by the product of relaxation time θ_1 and the angular velocity of the top disk, exceeds the value $\pi/\sqrt{(1-\varepsilon)/(5-2\varepsilon)}$. The stabilizing influence of retardation time (i.e., increasing ε) is seen clearly. By way of comparison, Crochet and Keunings [24] have shown that the range of Weissenberg numbers over which a steady "die swell" solution can be calculated using a finite-element method is four times larger for an Oldroyd-B model including a retardation time than for the corresponding Maxwell model which is obtained by setting the retardation time equal to zero.

Acknowledgment

This work was supported in part by a grant from the Fluid Mechanics Program of the National Science Foundation.

Appendix A. The Matrix A(t)

The matrix **A**(t) is a 9x9 matrix the nonzero elements of which are

$$a_{11} = -\varepsilon k^2 - \Gamma_{11} + \frac{2}{k^2}(k_1^2\Gamma_{11} + k_1k_2\Gamma_{21}),$$

$$a_{12} = -\Gamma_{12} + \frac{2}{k^2}(k_1^2\Gamma_{12} + k_1k_2\Gamma_{22}),$$

$$a_{14} = k_1\left(\frac{k_1^2}{k^2} - 1\right),$$

$$a_{15} = k_2\left(\frac{2k_1^2}{k^2} - 1\right),$$

$$a_{16} = k_3\left(\frac{2k_1^2}{k^2} - 1\right),$$

$$a_{17} = \frac{k_1k_2^2}{k^2},$$

$$a_{18} = \frac{2k_1k_2k_3}{k^2},$$

$$a_{19} = \frac{k_1k_3^2}{k^2},$$

$$a_{21} = -\Gamma_{21} + \frac{2}{k^2}(k_2k_1\Gamma_{11} + k_2^2\Gamma_{21}),$$

$$a_{22} = -\varepsilon k^2 - \Gamma_{22} + \frac{2}{k^2}(k_2k_1\Gamma_{12} + k_2^2\Gamma_{22}),$$

$$a_{24} = \frac{k_1^2k_2}{k^2},$$

$$a_{25} = k_1\left(\frac{2k_2^2}{k^2} - 1\right),$$

$$a_{26} = \frac{2k_1k_2k_3}{k^2},$$

$$a_{27} = k_2\left(\frac{k_2^2}{k^2} - 1\right),$$

$$a_{28} = k_3\left(\frac{2k_2^2}{k^2} - 1\right),$$

$$a_{29} = \frac{k_2 k_3^2}{k^2},$$

$$a_{31} = \frac{2}{k^2}(k_3 k_1 \Gamma_{11} + k_3 k_2 \Gamma_{21}),$$

$$a_{32} = \frac{2}{k^2}(k_3 k_1 \Gamma_{12} + k_3 k_2 \Gamma_{22}),$$

$$a_{33} = -\varepsilon k^2,$$

$$a_{34} = \frac{k_1^2 k_3}{k^2},$$

$$a_{35} = \frac{2k_1 k_2 k_3}{k^2},$$

$$a_{36} = k_1\left(\frac{2k_3^2}{k^2} - 1\right),$$

$$a_{37} = \frac{k_2^2 k_3}{k^2},$$

$$a_{38} = k_2\left(\frac{2k_3^2}{k^2} - 1\right),$$

$$a_{39} = k_3\left(\frac{k_3^2}{k^2} - 1\right),$$

$$a_{41} = \left[\frac{2(1-\varepsilon)}{Wi}\right]k_1 + 2\beta\Sigma_{11}k_1 + (\beta + 1)\Sigma_{12}k_2,$$

$$a_{42} = (\beta - 1)\Sigma_{12}k_1,$$

$$a_{44} = -\frac{1}{Wi} + 2\beta\Gamma_{11},$$

$$a_{45} = 2\Gamma_{12},$$

$$a_{51} = \left[\frac{1-\varepsilon}{Wi}\right]k_2 + \left[\frac{\beta-1}{2}\right]\Sigma_{11}k_2 + \beta\Sigma_{12}k_1 + \left[\frac{\beta+1}{2}\right]\Sigma_{22}k_2,$$

$$a_{52} = \left[\frac{1-\varepsilon}{Wi}\right]k_1 + \left[\frac{\beta+1}{2}\right]\Sigma_{11}k_1 + \beta\Sigma_{12}k_2 + \left[\frac{\beta-1}{2}\right]\Sigma_{22}k_1,$$

$$a_{54} = \Gamma_{21},$$

$$a_{55} = -\frac{1}{Wi}$$

$$a_{57} = \Gamma_{12},$$

$$a_{61} = \left[\frac{1-\varepsilon}{Wi}\right]k_3 + \left[\frac{\beta-1}{2}\right]\Sigma_{11}k_3$$

$$a_{62} = \left[\frac{\beta-1}{2}\right]\Sigma_{12}k_3$$

$$a_{63} = \left[\frac{1-\varepsilon}{Wi}\right]k_1 + \left[\frac{\beta+1}{2}\right]\Sigma_{11}k_1 + \left[\frac{\beta+1}{2}\right]\Sigma_{12}k_2,$$

$$a_{66} = -\frac{1}{Wi} + \beta\Gamma_{11},$$

$$a_{68} = \Gamma_{12},$$

$$a_{71} = (\beta-1)\Sigma_{12}k_2,$$

$$a_{72} = \left[\frac{2(1-\varepsilon)}{Wi}\right]k_2 + (\beta+1)\Sigma_{12}k_1 + 2\beta\Sigma_{22}k_2,$$

$$a_{75} = 2\Gamma_{21},$$

$$a_{77} = -\frac{1}{Wi} + 2\beta\Gamma_{22},$$

$$a_{81} = \left[\frac{\beta-1}{2}\right]\Sigma_{12}k_3,$$

$$a_{82} = \left[\frac{1-\varepsilon}{Wi}\right]k_3 + \left[\frac{\beta-1}{2}\right]\Sigma_{22}k_3,$$

$$a_{83} = \left(\frac{1-\varepsilon}{Wi}\right)k_2 + \left(\frac{\beta+1}{2}\right)\Sigma_{12}k_1 + \left(\frac{\beta+1}{2}\right)\Sigma_{22}k_2,$$

$$a_{86} = \Gamma_{21},$$

$$a_{88} = -\frac{1}{Wi} + \beta\Gamma_{22},$$

$$a_{93} = \left[\frac{2(1-\varepsilon)}{Wi}\right]k_3,$$

$$a_{99} = -\frac{1}{Wi}.$$

Here, k_1, k_2, and k_3 are the components of $\mathbf{k}(t) = e^{-t\Gamma^T}\cdot\boldsymbol{\alpha}$, and $k^2 = k_1^2 + k_2^2 + k_3^2$. Also, Γ_{11}, Γ_{12}, Γ_{21}, and Γ_{22} are dimensionless components of Γ and are given by (5) with E replaced by 1. The components Σ_{11}, Σ_{12}, and Σ_{22} are given by (20a)-(20c).

Appendix B. The Matrix $\mathbf{A}^{(1)}$

The matrix $\mathbf{A}^{(1)}$ is a constant 9x9 matrix the nonzero elements of which are

$$a_{11} = -\varepsilon\alpha_3^2 - \frac{1}{2}(1+\lambda),$$

$$a_{12} = -\frac{1}{2}(1-\lambda),$$

$$a_{16} = -\alpha_3,$$

$$a_{21} = \frac{1}{2}(1-\lambda),$$

$$a_{22} = -\varepsilon\alpha_3^2 + \frac{1}{2}(1+\lambda),$$

$$a_{28} = -\alpha_3,$$

$$a_{33} = -\varepsilon\alpha_3^2,$$

$$a_{44} = -\frac{1}{Wi} + \beta(1+\lambda),$$

$$a_{45} = 1-\lambda,$$

$$a_{54} = -\frac{1}{2}(1-\lambda),$$

$$a_{55} = -\frac{1}{Wi},$$

$$a_{57} = \frac{1}{2}(1-\lambda),$$

$$a_{61} = \left(\frac{1-\varepsilon}{Wi}\right)\alpha_3 + \left(\frac{\beta-1}{2}\right)\Sigma_{11}\alpha_3$$

$$a_{62} = \left(\frac{\beta-1}{2}\right)\Sigma_{12}\alpha_3$$

$$a_{66} = -\frac{1}{Wi} + \frac{\beta}{2}(1+\lambda),$$

$$a_{68} = \frac{1}{2}(1-\lambda),$$

$$a_{75} = -(1-\lambda),$$

$$a_{77} = -\frac{1}{Wi} - \beta(1+\lambda),$$

$$a_{81} = \left[\frac{\beta-1}{2}\right]\Sigma_{12}\alpha_3,$$

$$a_{82} = \left[\frac{1-\varepsilon}{Wi}\right]\alpha_3 + \left[\frac{\beta-1}{2}\right]\Sigma_{22}\alpha_3,$$

$$a_{86} = -\frac{1}{2}(1-\lambda),$$

$$a_{88} = -\frac{1}{Wi} - \frac{\beta}{2}(1+\lambda),$$

$$a_{93} = \left[\frac{2(1-\varepsilon)}{Wi}\right]\alpha_3,$$

$$a_{99} = -\frac{1}{Wi},$$

where the components Σ_{11}, Σ_{12}, and Σ_{22} are given by (20a)-(20c).

Appendix C. Simple Shear Flow ($\lambda = 0$)

In the case of simple shear flow, the components of the basic velocity gradient tensor Γ are given by Eq. (5) with $\lambda = 0$. If we transform the coordinate system corresponding to (5) by rotating the x_1- and x_2-axes through a 45° angle about the x_3-axis, then the components of Γ assume the following simpler form when $\lambda = 0$:

$$[\Gamma] = E\begin{bmatrix} 0 & 1 & 0 \\ 0 & 0 & 0 \\ 0 & 0 & 0 \end{bmatrix} . \tag{C1}$$

The nonzero components of the basic stress tensor $\mathbf{T}$ (relative to this new coordinate system) are predicted for simple shear flow by the constitutive Eq. (1) to be

$$T_{11} = \frac{\eta_0 E^2(\theta_1 - \theta_2)(1 + \beta)}{1 + (E\theta_1)^2(1 - \beta^2)} , \tag{C2a}$$

$$T_{22} = \frac{-\eta_0 E^2(\theta_1 - \theta_2)(1 - \beta)}{1 + (E\theta_1)^2(1 - \beta^2)} , \tag{C2b}$$

$$T_{12} = T_{21} = \frac{\eta_0 E[1 + E^2\theta_1\theta_2(1 - \beta^2)]}{1 + (E\theta_1)^2(1 - \beta^2)} . \tag{C2c}$$

Note that these components remain bounded for all values of $Wi = E\theta_1$ for $0 \le \beta \le 1$. In dimensionless form, the nonzero components of the viscoelastic stress contribution Σ defined by (14b) are given by

$$\Sigma_{11} = \frac{(1 - \varepsilon)Wi(1 + \beta)}{1 + Wi^2(1 - \beta^2)} , \tag{C3a}$$

$$\Sigma_{22} = -\frac{(1 - \varepsilon)Wi(1 - \beta)}{1 + Wi^2(1 - \beta^2)} , \tag{C3b}$$

$$\Sigma_{12} = \Sigma_{21} = \frac{1 - \varepsilon}{1 + Wi^2(1 - \beta^2)} . \tag{C3c}$$

The fundamental matrix $e^{-t\Gamma^t}$ (dimensionless) assumes the form

$$e^{-t\mathbf{\Gamma}^T} = \begin{bmatrix} 1 & 0 & 0 \\ -t & 1 & 0 \\ 0 & 0 & 1 \end{bmatrix} . \tag{C4}$$

and the components of $\mathbf{k}(t) = e^{-t\mathbf{\Gamma}^T} \cdot \boldsymbol{\alpha}$ are given by

$$k_1(t) = \alpha_1, \quad k_2(t) = \alpha_2 - \alpha_1 t, \quad k_3(t) = \alpha_3, \tag{C5}$$

Stability criteria for simple shear flow can be determined by considering the asymptotic behavior of solutions of the linear system (41) when $\lambda = 0$. We can carry out this analysis only for spatially periodic initial disturbances satisfying condition (50). In the new coordinate system, this condition reduces (for $\lambda = 0$) to

$$\alpha_1 = 0 . \tag{C6}$$

Thus, we consider disturbances to simple shear flow only with vanishing streamwise wavenumber. In this case the components of $\mathbf{k}(t)$ are constants

$$k_1(t) = 0, \quad k_2(t) = \alpha_2, \quad k_3(t) = \alpha_3, \tag{C7}$$

and the coefficient matrix $\mathbf{A}(t)$ for the linear system (41) reduces to a constant matrix $\mathbf{C}$. The components of $\mathbf{C}$ may be obtained from the expressions for the components of $\mathbf{A}(t)$ listed in Appendix A by substituting the results (C1) (made dimensionless with E replaced by 1), (C3a)-(C3c), and (C7). Under condition (C6), the eigenvalues of $\mathbf{C}$ determine the asymptotic behavior of solutions of (41) as $t \to \infty$, since $\mathbf{C}$ is the constant coefficient matrix. These eigenvalues are the roots of the ninth-degree characteristic polynomial of $\mathbf{C}$. This polynomial has no readily apparent factored form, so stability criteria for simple shear flow would have to be determined by numerical computation of the eigenvalues of $\mathbf{C}$ for fixed values of the parameters β, Wi, ε, α_2, and α_3. It appears from our numerical computations that the eigenvalues of $\mathbf{C}$ always have negative real parts. Since it is impossible to check the eigenvalues for all admissible values of the parameters, numerical computation alone cannot guarantee that conditions do

not exist under which some eigenvalues have positive real parts. However, the results for strong flows ($0 < \lambda \leq 1$) in the limit as $\lambda \to 0$ strongly suggest that simple shear flow is linearly stable with respect to disturbances of the form (C6) under all conditions on the physical parameters.

References

1. C. J. S. Petrie and M. M. Denn, A.I.Ch.E. J., **22** (1976) 209.

2. J. R. A. Pearson, Ann. Rev. Fluid Mech., **8** (1976) 163.

3. J. R. A. Pearson and M. A. Matovich, Ind. Eng. Chem. Fund., **8** (1969) 605.

4. Y. L. Yeow, J. Fluid Mech., **66** (1974) 613.

5. R. R. Lagnado, N. Phan-Thien and L. G. Leal, Phys. Fluids, **27** (1984) 1094.

6. G. Marrucci and G. Astarita, A.I.Ch.E. J., **13** (1967) 931.

7. J. G. Oldroyd, Proc. Roy. Soc. London Ser. A, **245** (1958) 278.

8. M. J. Crochet and K. Walters, Ann. Rev. Fluid Mech., **15** (1983) 241.

9. G. G. Fuller and L. G. Leal, J. Polym. Sci. Polym. Phys. Ed., **19** (1981) 557.

10. D. P. Pope and A. Keller, Colloid Poly. Sci., **255** (1977) 633.

11. G. G. Fuller and L. G. Leal, Rheol. Acta, **19** (1980) 580.

12. N. Phan-Thien and R. I. Tanner, J. Non-Newt. Fluid Mech., **2** (1977) 353.

13. M. W. Johnson, Jr. and D. Segalman, J. Non-Newt. Fluid Mech., **2** (1977) 255.

14. E. J. Hinch and L. G. Leal, J. Fluid Mech., **52** (1972) 683.

15. R. B. Bird, R. C. Armstrong and O. Hassager, Dynamics of Polymeric Liquids, Vol. 1, John Wiley and Sons, New York, 1977.

16. E. Zana, PhD Thesis, California Institute of Technology (1975).

17. G. Tiefenbruck, PhD Thesis, California Institute of Technology (1980).

18. N. Levinson, Duke Math J., **15** (1948) 111.

19. V. A. Gorodtsov and A. I. Leonov, P. M. M., **31** (1967) 310.

20. J. M. Broadbent, D. C. Pountney and K. Walters, J. Non-Newt. Fluid Mech., **3** (1978) 359.

21. A. R. Davies, in: K. W. Morton and M. J. Baines (Eds.), Numerical Methods for Fluid Dynamics, Academic Press, New York, 1982, pp. 323-339.

22. R. I. Tanner, J. Non-Newt. Fluid Mech., **10** (1982) 169.

23. N. Phan-Thien, J. Non-Newt. Fluid Mech., **13** (1983) 325.

24. M. J. Crochet and R. Keunings, J. Non-Newt. Fluid Mech., **10** (1982) 339.

Figure Captions

Figure 1. Streamlines for two-dimensional linear flows. (a) $\lambda = 1$, (b) $\lambda = 0.5$, (c) $\lambda = 0$, (d) $\lambda = -0.5$, (e) $\lambda = -1$.

Figure 2. Streamlines for a strong flow ($\lambda = 0.5$). L_i: inlet streamline (slope = $(\sqrt{\lambda} + 1)/(\sqrt{\lambda} - 1)$). L_o: outlet streamline (slope = $(\sqrt{\lambda} - 1)/(\sqrt{\lambda} + 1)$).

Figure 3. Neutral stability curves for $\lambda = 1$, $\beta = 1$, and $\varepsilon = 0$, 0.2, 0.8, and 1.

Figure 4. Neutral stability curve for $\lambda = 1$, $\beta = 0$, and $\varepsilon = 0.2$.

Figure 5. Neutral stability curve for $\lambda = 1$, $\beta = 0.5$, and $\varepsilon = 0.2$.

Figure 6. Neutral stability curve for $\lambda = 1$, $\beta = 0.5$, and $\varepsilon = 0.8$.

Figure 7. Neutral stability curves for $\lambda = 0.7$, $\beta = 1$, and $\varepsilon = 0$, 0.2, 0.8, and 1.

Figure 8. Neutral stability curves for $\lambda = 0.7$, $\beta = 0$, and $\varepsilon = 0.2$ and 0.4.

Figure 9. Neutral stability curves for $\beta = 0$, $\varepsilon = 0.2$, and $\lambda = 1$, 0.7, and 0.5.

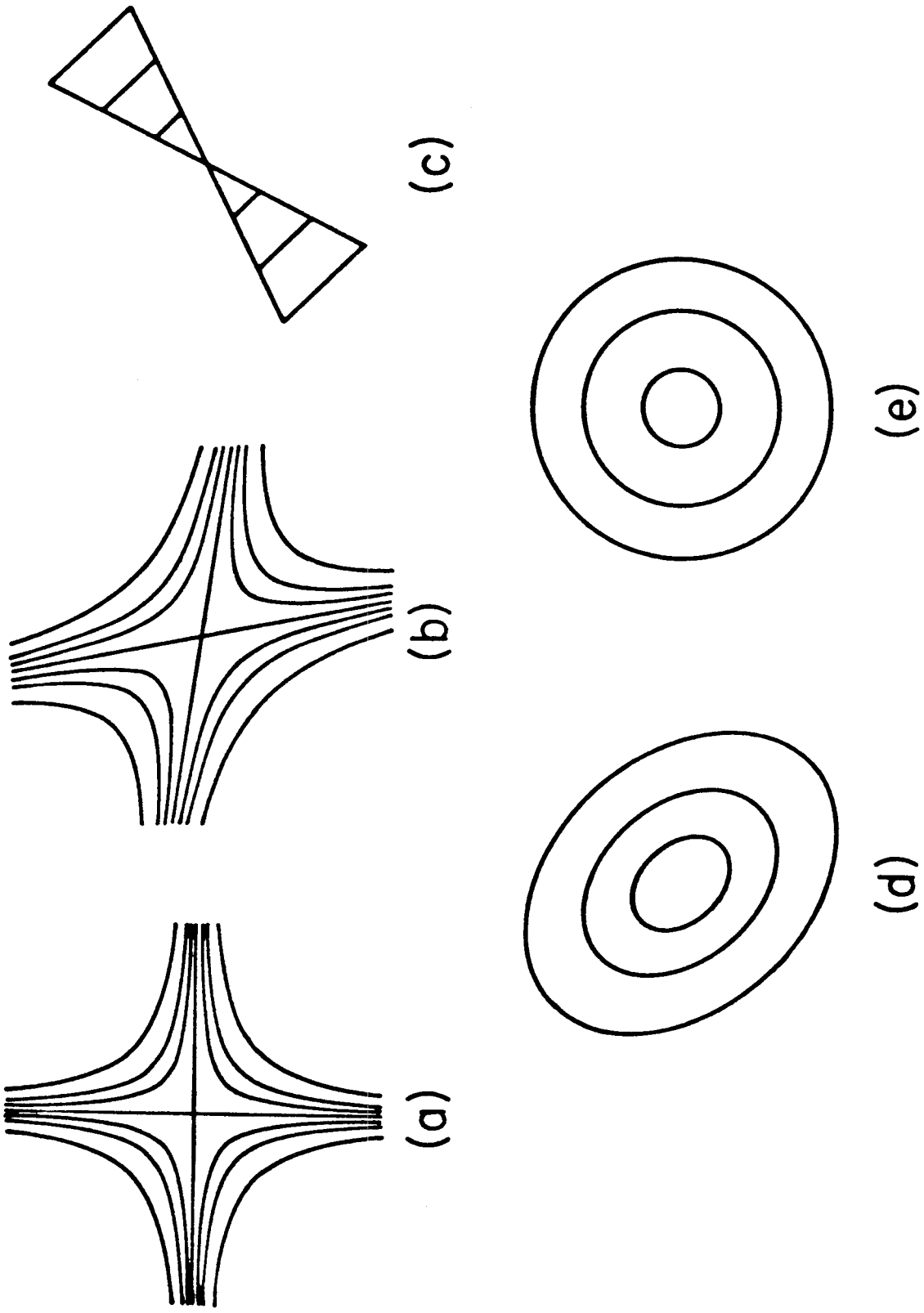

Figure 1

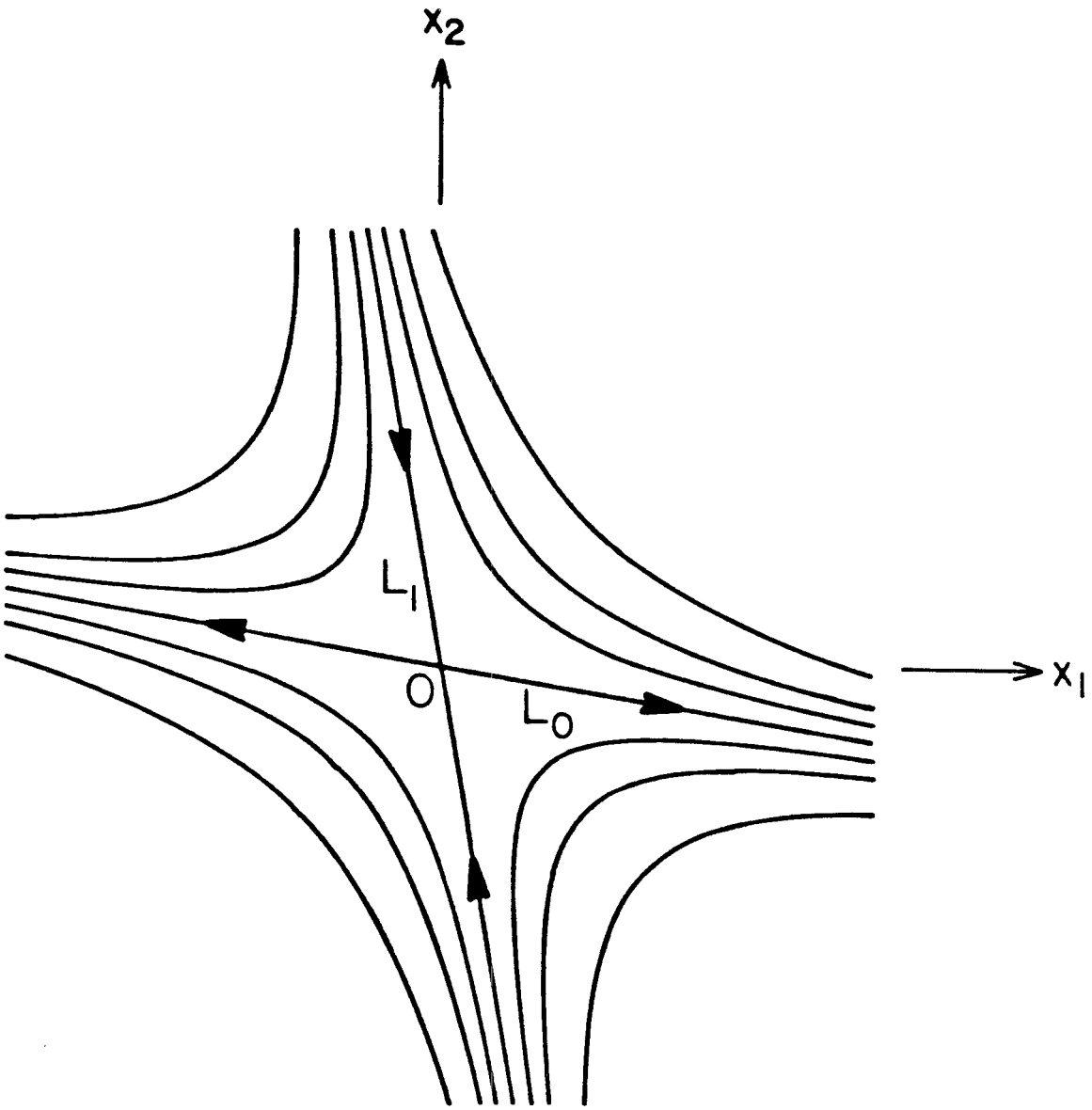

Figure 2

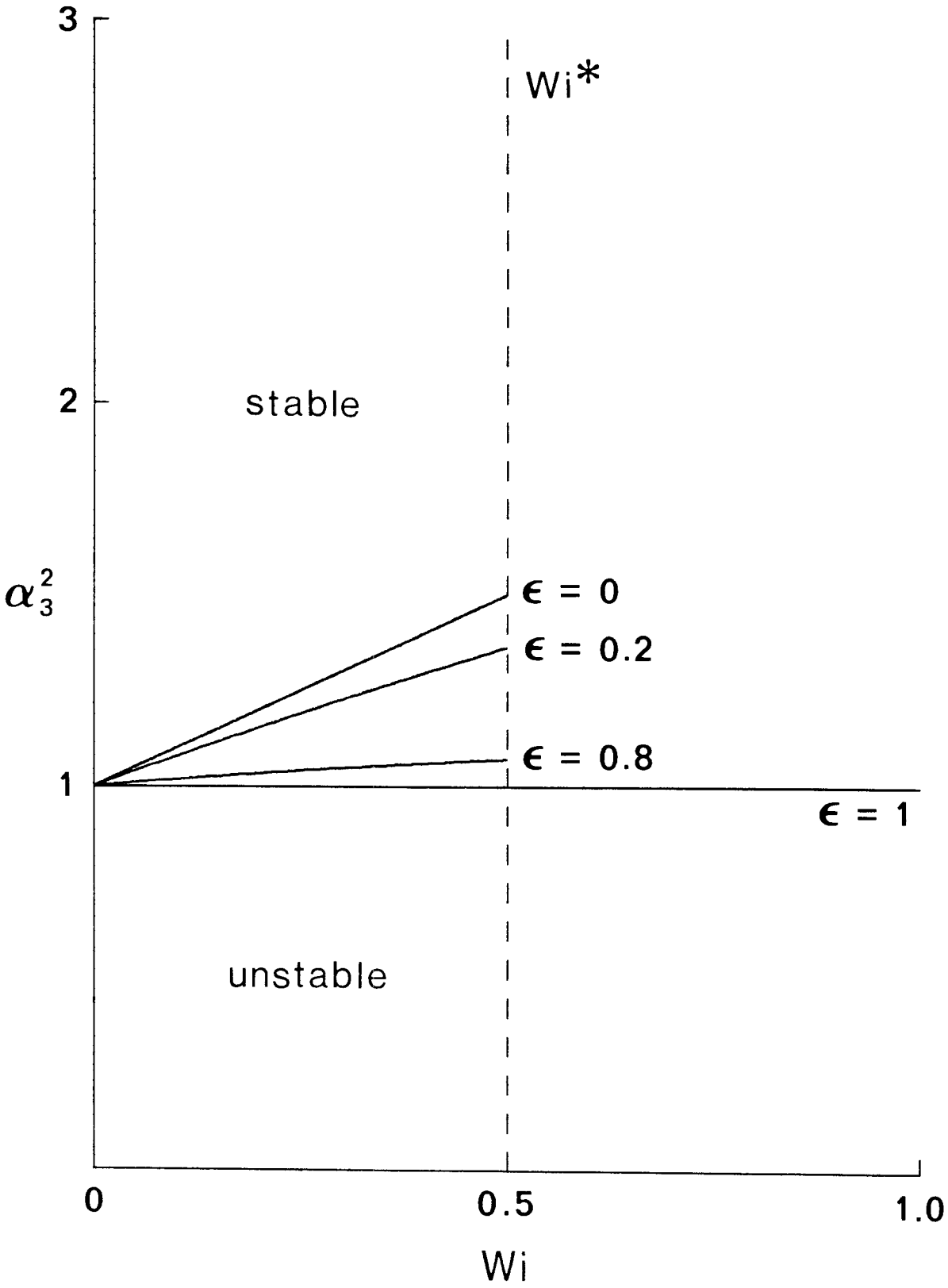
3
2
1
0
0.5
1.0
Wi
Wi*
stable
unstable
α_3^2
$\epsilon = 0$
$\epsilon = 0.2$
$\epsilon = 0.8$
$\epsilon = 1$

Figure 3

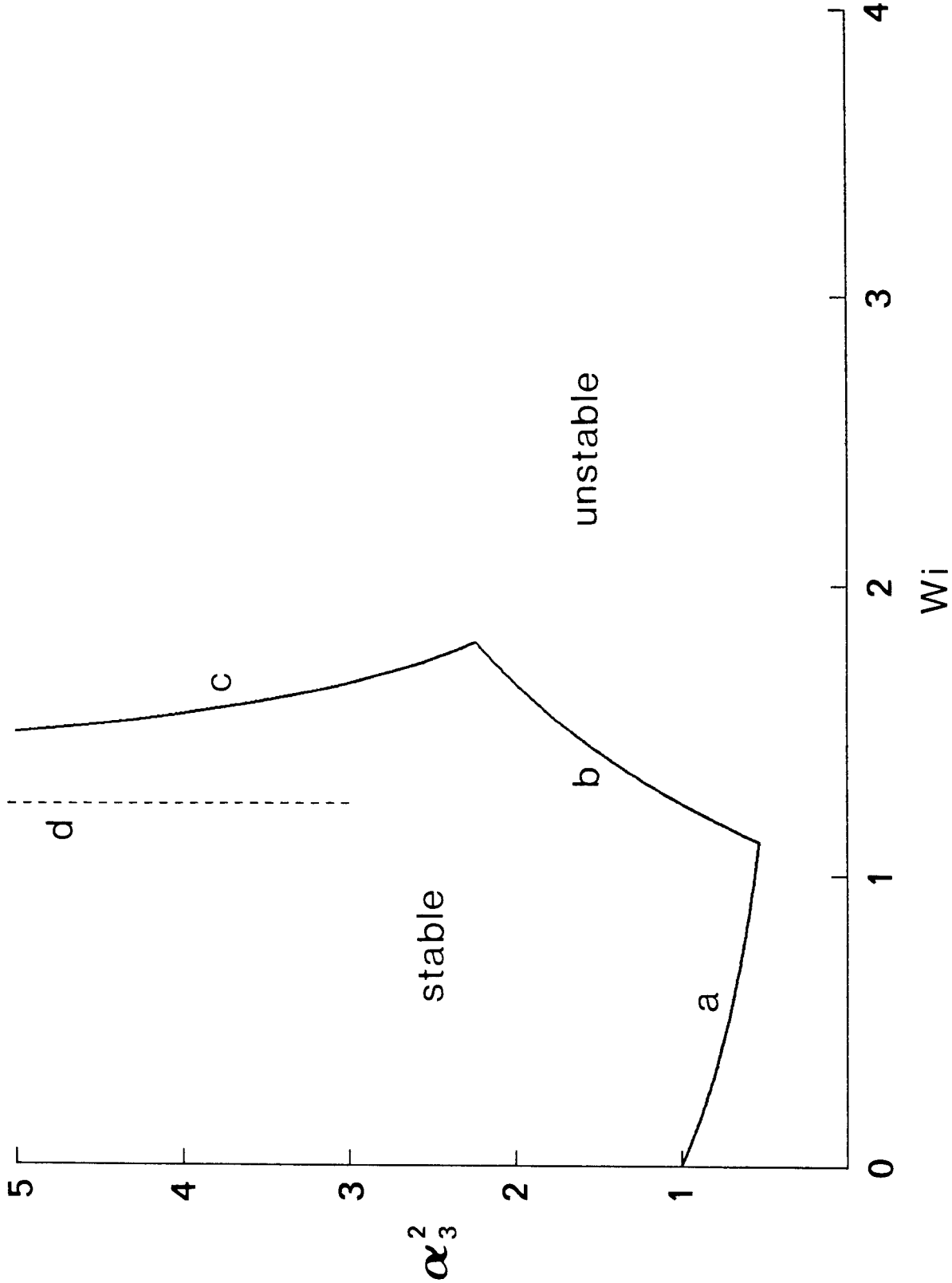

Figure 4

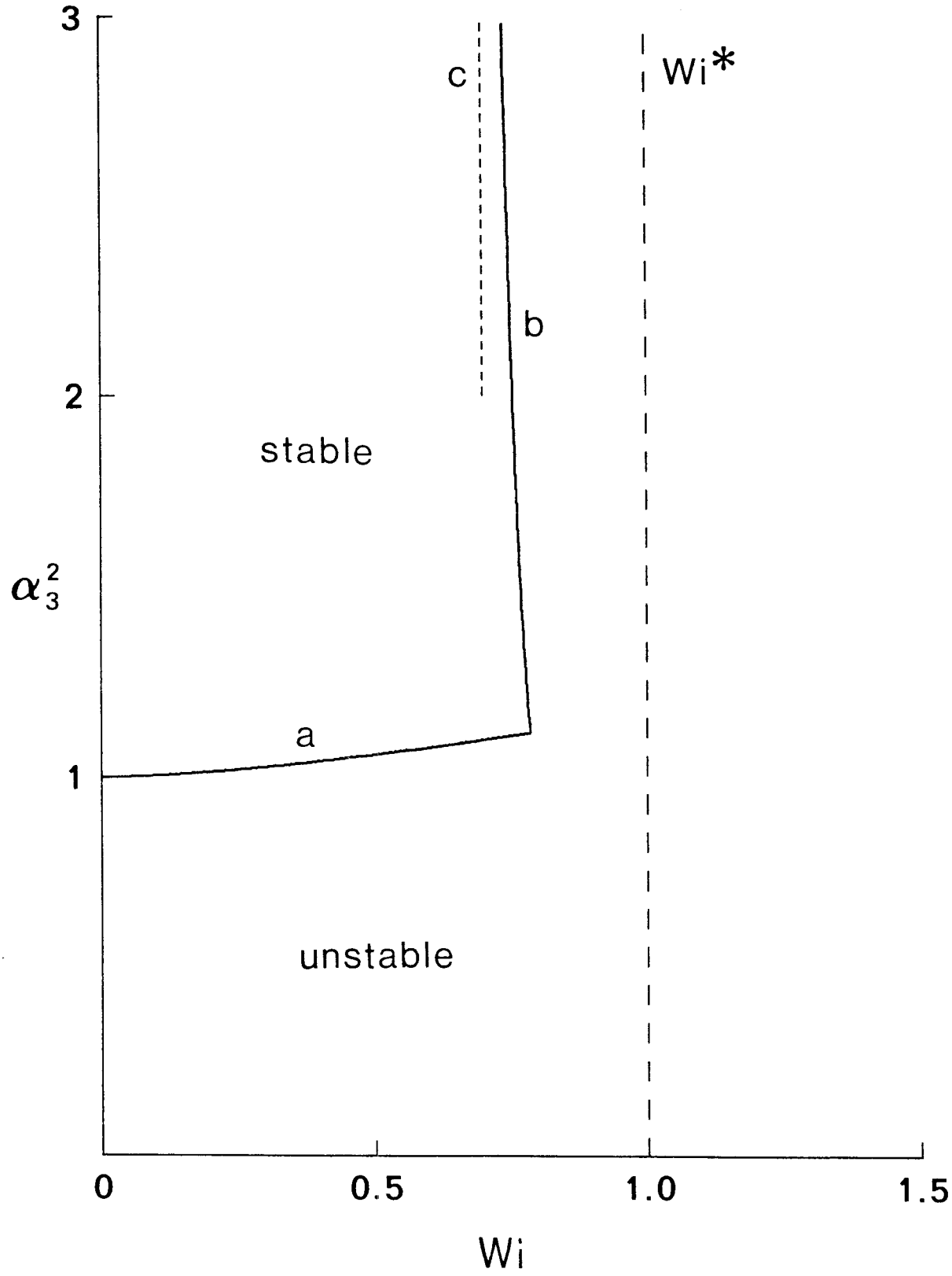

Figure 5

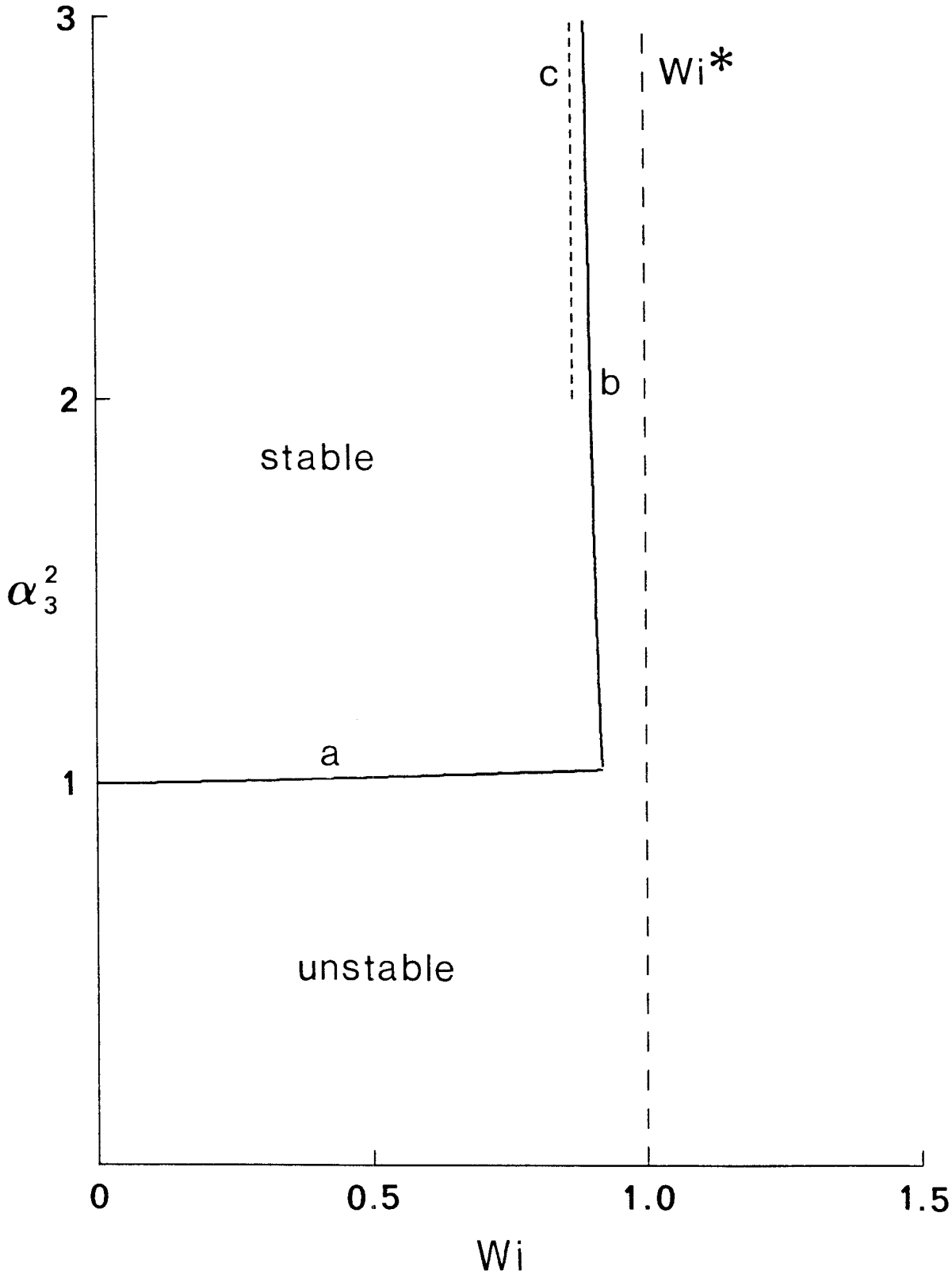

Figure 6

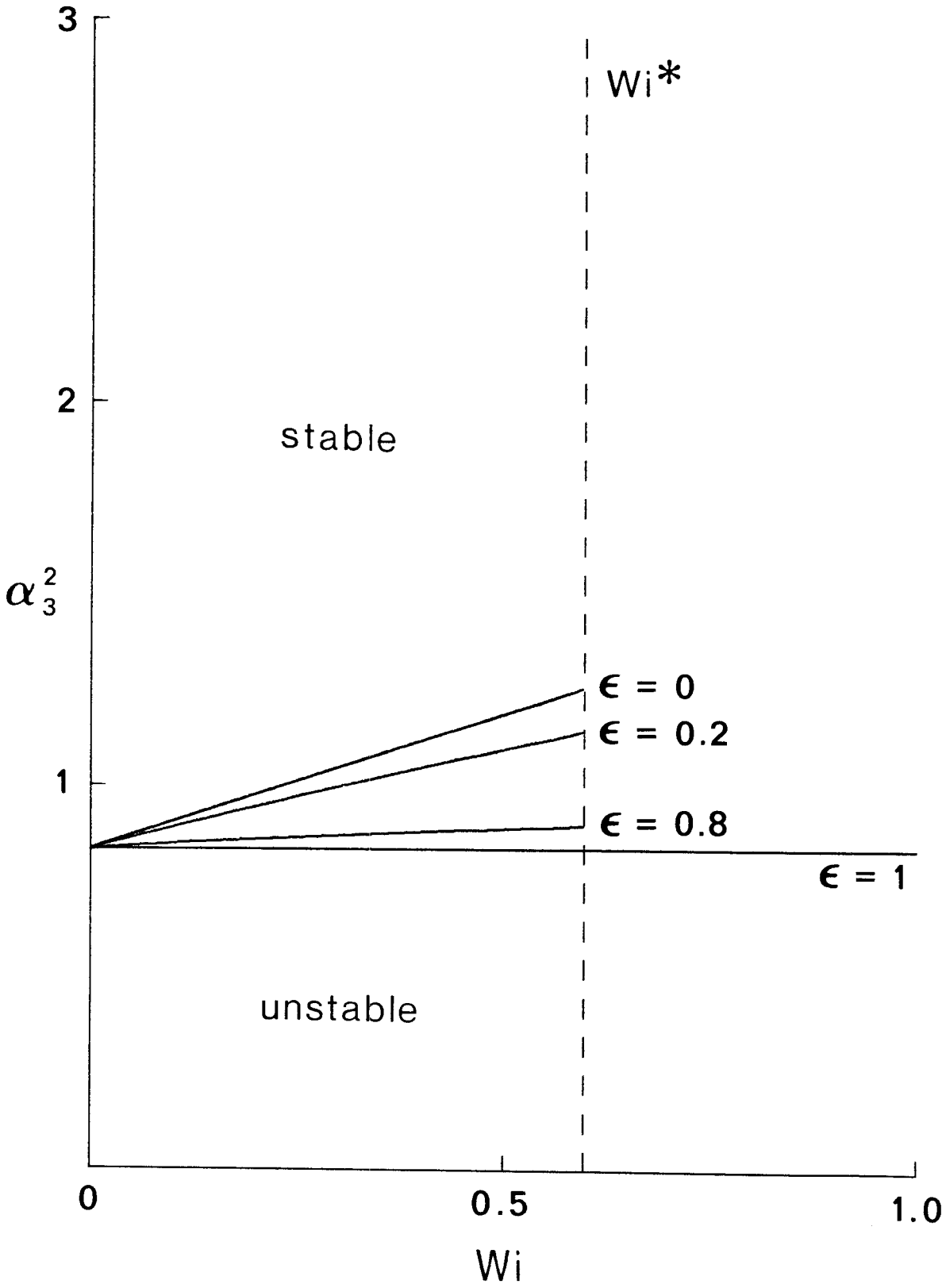
3
2
1
0
0.5
1.0
Wi
Wi*
stable
unstable
α_3^2
$\epsilon = 0$
$\epsilon = 0.2$
$\epsilon = 0.8$
$\epsilon = 1$

Figure 7

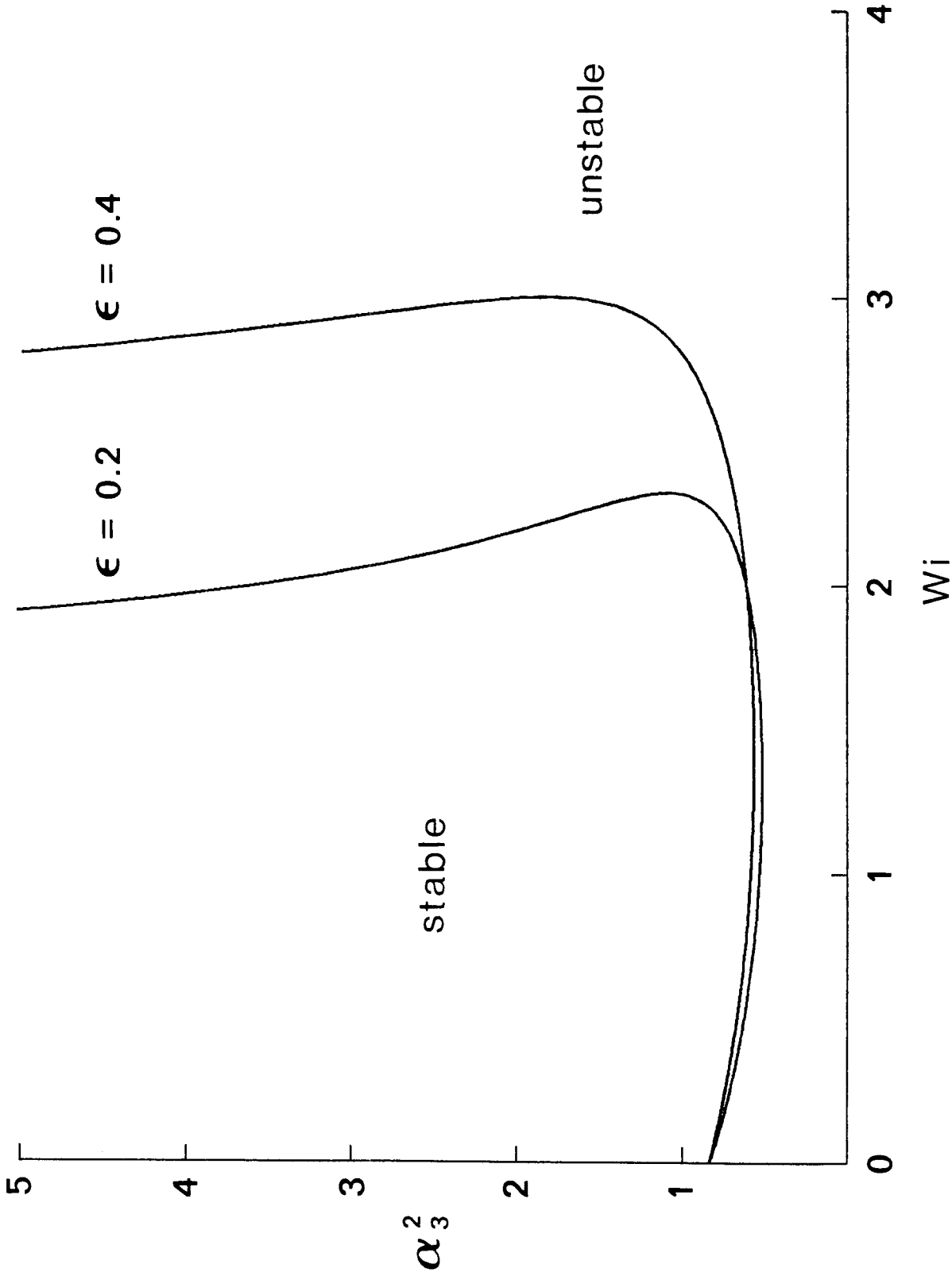

Figure 8

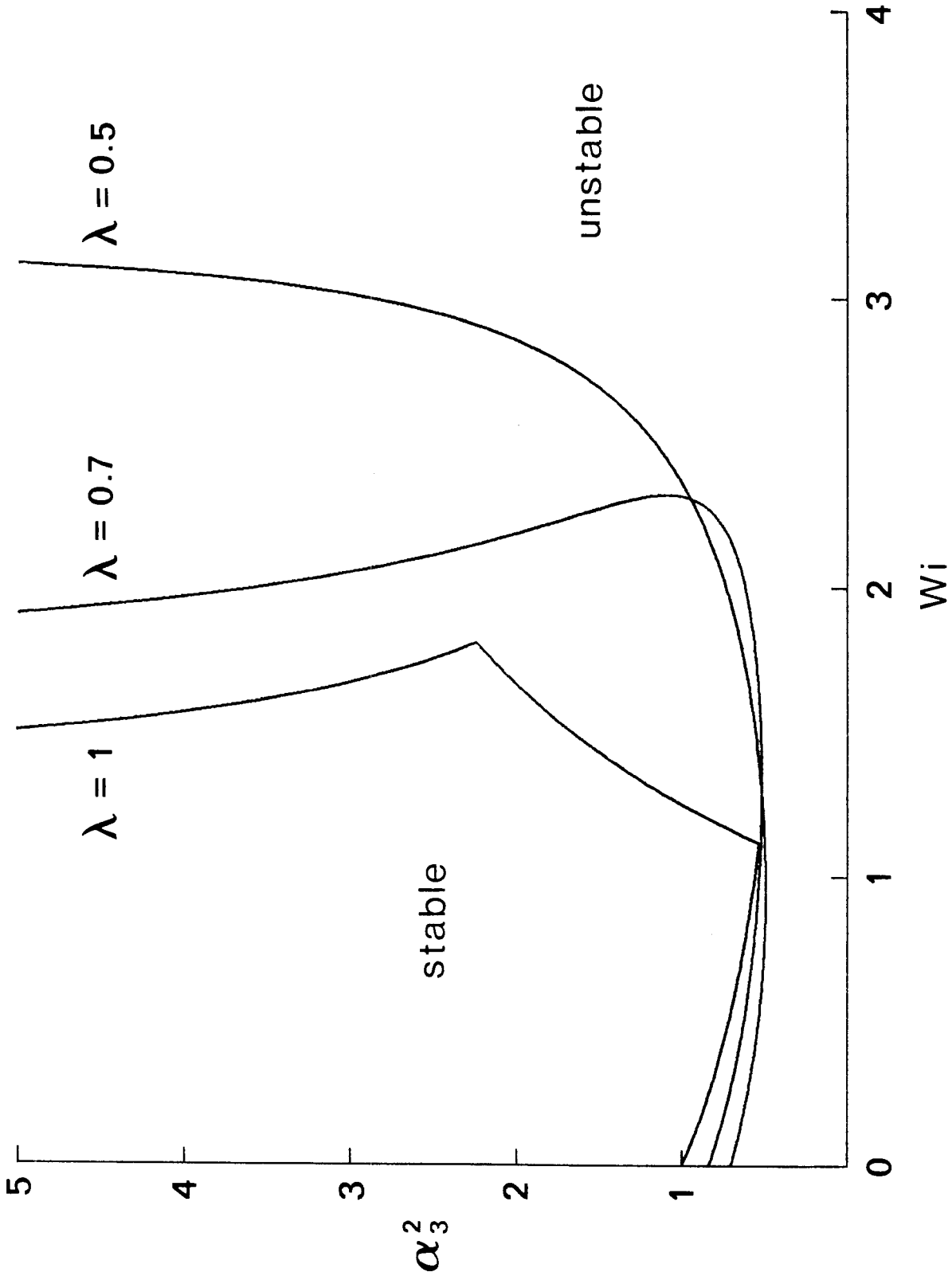

Figure 9

CHAPTER III

AN EXPERIMENTAL STUDY OF FLOW IN A FOUR-ROLL MILL

Abstract

An experimental study of the flow of a Newtonian fluid in a four-roll mill has been made by means of flow visualization and photography. The effect of increasing Reynolds number (i.e., roller speed) on the appearance of the flow field between the rollers is reported. Observations have been made using two four-roll mills with different ratios of roller length to gap width between adjacent rollers (namely, L/d = 3.39 and 12.73), in order to investigate the effect of the distance separating top and bottom bounding surfaces. In all experiments the rollers were made to rotate with equal angular speeds and in appropriate directions so as to simulate a pure extensional flow in the central region between the rollers. At sufficiently small Reynolds numbers, the flow in both devices is essentially two-dimensional throughout most of the region between the rollers, except near the top and bottom bounding surfaces where a three-dimensional flow involving four symmetrically positioned vortices appears. The vertical extent of this two-dimensional flow gradually diminishes and the vortices grow in size and strength as the Reynolds number is increased up to a quasi-critical range. An increase in Reynolds number through this quasi-critical range results in an abrupt transition to a steady three-dimensional flow throughout the *entire* region between the rollers. The three-dimensionality is significantly less pronounced in the device with L/d = 12.73, however. At sufficiently high Reynolds numbers beyond the quasi-critical range, the flow becomes unsteady in time and eventually turbulent.

I. Introduction

The four-roll mill was originally developed by G. I. Taylor[1] for an experimental study of the formation of emulsions. This study examined, in particular, the deformation and breakup of a fluid drop suspended in another fluid undergoing an extensional flow. Taylor invented the four-roll mill specifically for the purpose of generating an approximation to two-dimensional extensional flow (hyperbolic flow) in the suspending fluid. However, this device is considerably more important as an experimental tool in that it is capable of simulating a wide variety of two-dimensional flows of which the pure extensional flow considered by Taylor is one special case. As a consequence of this versatility, the four-roll mill has been used in numerous experimental investigations of such phenomena as drop deformation and breakup,[1-6] flow-induced changes in the conformation of macromolecules in solution (studied via birefringence measurements),[7-11] and shear-induced crystallization of polymers.[12]

The basic geometric configuration of a typical four-roll mill is illustrated in Figure 1. This device consists of four cylindrical rollers of diameter D, radius R, and length L which are contained in a box with internal dimensions W × W × H. The rollers are symmetrically positioned around the center of the box so that their central axes are parallel and pass through the corners of a square with sides of length S. The width of the gap between adjacent rollers is then given by d = S - D. Rotation of the four rollers produces flow in the fluid filling the container.

The aforementioned experimental applications of the four-roll mill rely on the assumption that the rollers can be suitably driven to produce any flow in the class of *linear* two-dimensional flows throughout a central region in the device. This class of flows may be represented by a velocity field **U** of the form

$$\mathbf{U} = \Gamma \cdot \mathbf{x} \ , \tag{1}$$

where $\mathbf{x}$ is a general position vector and Γ is a constant velocity gradient tensor with Cartesian components given by

$$[\Gamma] = \frac{E}{2} \begin{bmatrix} 1+\lambda & 1-\lambda & 0 \\ -(1-\lambda) & -(1+\lambda) & 0 \\ 0 & 0 & 0 \end{bmatrix} . \tag{2}$$

Here, $E \geq 0$ is the magnitude of the local velocity gradient, and λ is a flow-type parameter ranging from -1 to 1. The cases $\lambda = -1$, $\lambda = 0$, and $\lambda = 1$ correspond to pure rotational flow, simple shear flow, and pure extensional flow, respectively. Typical streamlines are shown in Figure 2, and further kinematical details are discussed by Fuller and Leal[10] and Lagnado et al.[13] We note here that all of the flows given by (1) and (2) possess a central stagnation point. For flows in the range $0 \leq \lambda \leq 1$ the streamlines are open and form a family of hyperbolas with asymptotes that are separated by an angle φ given by

$$\tan(\varphi/2) = \sqrt{\lambda} \ . \tag{3}$$

On the other hand, if $-1 \leq \lambda < 0$, then the streamlines are closed and form a family of ellipses with major axis length a and minor axis length b related to λ by

$$\frac{b}{a} = \sqrt{-\lambda} \ . \tag{4}$$

Giesekus[14] first demonstrated that a four-roll mill can be used to simulate two-dimensional linear flows. In order to produce these flows, the device must be operated so that each of the rollers in a diagonal pair (e.g., rollers 1 and 3 or rollers 2 and 4 in Figure 2) have the same angular speed and direction of rotation. If the ratio of the angular speeds of these diagonal pairs of rollers (i.e., $\omega_{1,3}/\omega_{2,4}$) is in the range from -1 to 1, then a stagnation point appears at the center of the region between the rollers, and the flow is approximately of the form given by (1) and (2) in a neighborhood of the stagnation point. In fact, the flow parameter λ is related to the angular speeds of the rollers by

$$\lambda = -\frac{\omega_{1,3}}{\omega_{2,4}} \tag{5}$$

Giesekus verified this fact by showing that equations (3) and (4) were satisfied with λ defined by (5) and corresponding values of φ, a, and b measured from photographs of actual streamlines produced in a four-roll mill.

It is obvious that the linear flow field given by (1) and (2) cannot represent the flow everywhere in a four-roll mill due to the presence of the rollers and the container surfaces where the no-slip condition must be satisfied. Furthermore, the flow in the space between the rollers can never be truly two-dimensional; a significant component of velocity in the vertical direction will be present in the vicinity of the top and bottom container surfaces. Thus, the actual flow in a four-roll mill may be described as the superposition of a *primary* flow given by (1) and (2) and a *secondary* flow which accounts for the effects induced by the boundary surfaces. Another problem encountered in experimental applications of the four-roll mill is the onset of flow instability which limits the range of roller speeds in which the two-dimensional linear flow field appears in at least a portion of the device. An increase in roller speed (and Reynolds number) eventually causes a transition from the two-dimensional linear flow in the space between the rollers to a steady three-dimensional flow and, ultimately, to a turbulent flow throughout the entire region. Although this occurrence has been reported by numerous investigators as an undesirable limitation on the scope of their experiments, no attempt has ever been made to characterize the process leading to this instability.

In the present paper, we report the results of a flow-visualization study of the four-roll mill which examines the effect of increasing roller speed (and Reynolds number) on the qualitative features of the flow in the space between the rollers. Observations were made using two four-roll mills with two different values of the ratio L/d (i.e., roller length over gap width between adjacent

rollers). In both devices the ratio of the distance between centers of adjacent rollers to roller diameter is S/D = 1.295. This ratio was selected to optimize the fit between the circular roller surfaces and hyperbolic streamlines associated with pure extensional flow ($\lambda = 1$) by minimizing the area between the curves. Bentley[5] discusses at length various design criteria for four-roll mills. These criteria prescribe values of S/D in the range from 1.172 to 1.414. Thus, the spacing of the rollers in the present study is typical of devices used in experimental applications. An important result of the present study is a description of the effect of increasing roller speed on the evolution of the secondary flow in the space between the rollers. In particular, we describe changes in the vertical extent of the region throughout which the secondary flow is negligible and the flow is essentially two-dimensional. We also elucidate the destabilization process which results in fully three-dimensional flow between the rollers.

The results of the present study provide some practical information which may be of use in the design of four-roll mills for experimental applications. However, our main purpose is to gain some understanding of the fundamental mechanism associated with the instability of extensional flows. This study is, in fact, intended to serve as an experimental complement to the theoretical investigation of the stability of two-dimensional linear flows by Lagnado et al.[13] This theoretical study consisted of a linear stability analysis for an *unbounded* Newtonian fluid undergoing two-dimensional linear flows in the range from simple shear flow ($\lambda = 0$) to pure extensional flow ($\lambda = 1$). We shall discuss our experimental observations of pure extensional flow in the four-roll mill in the context of the theoretical results and attempt to explain similarities and differences.

The present study is similar to many others in the area of hydrodynamic stability in that it involves the following question; given the results of a theoreti-

cal linear stability analysis for an unbounded or semibounded fluid undergoing a simple flow, how are these results connected to observations of an approximate realization of the same flow in a region of finite extent? This question of the role of boundaries on flow stability is an important problem of current interest to many investigators in the field of fluid mechanics. A good example of this general problem is provided by the many recent investigations of the stability of flow between two rotating concentric cylinders (i.e., a Couette device). A theoretical linear stability analysis of circular Couette flow between cylinders of infinite length was first undertaken by Taylor[15] and later refined in many other studies. In the simplest case, fluid fills the annular space between a stationary outer cylinder and an inner cylinder rotating with an adjustable, constant angular speed. The theory predicts that the circular Couette flow becomes unstable at a critical value of a suitably defined Reynolds number. Above this critical Reynolds number, the simple circular Couette flow exchanges stability with a more complicated flow involving steady toroidal vortices (i.e., so-called Taylor cells). In experimental studies of flow between concentric cylinders of *finite* extent, the presence of end boundaries causes a deviation from the predictions of the idealized theory for infinitely long cylinders. It is found that the Taylor cells do not appear suddenly at a critical Reynolds number, but they develop gradually as the Reynolds number is raised through a narrow, quasi-critical range. This quasi-critical range is, however, close to the critical Reynolds number predicted by the idealized theory. Experiments by Kusnetsov et al.[16] have shown that the Taylor cells do not develop uniformly throughout the annular space between the cylinders but spread inward from the top and bottom boundaries. Further studies of end effects on Couette flow have been conducted by Benjamin and coworkers.[17–21] These studies have demonstrated a large multiplicity in the stable steady flows which are realizable in a Couette device beyond the quasi-critical range of Reynolds number. The present study of the four-roll mill is, in a sense,

a first step as an extensional-flow analog of these investigations of flow stability in a Couette device.

II. Experimental Details

A. Apparatus: Four - Roll Mill

The experimental study was conducted using two separate four-roll mills. The geometric configuration and dimensions of these two devices are identical except for the length of the rollers and the depth of the enclosing containers. These differences allowed for an investigation of the effect of the distance between the top and bottom container surfaces on the three-dimensional character of the flow.

A schematic diagram of the shallower four-roll mill (hereafter referred to as FRM1) is shown in Figure 3. The four rollers in this device are contained in a box, the internal dimensions of which are $7 \times 7 \times 1.6$ in. The top and bottom of the container are 1/4 in. thick Pyrex plates, while the side walls are made of 1/2 in. thick Lucite. Each of the four rollers is a cylinder, 1.5 in. long by 1.5 in. diameter, made of anodized aluminum and fitted with a stainless steel axle. These axles run in bearings which are contained in housings cemented to the outer surface of the top plate of the container. The rollers are mounted so that their central axes are parallel and fixed in position at the corners of a square with sides of length 1.942 in. Clearances of 1/32 in. and 1/16 in. are present between the rollers and the inner surfaces of the top and bottom plates of the container, respectively.

The schematic diagram of the deeper four-roll mill (hereafter referred to as FRM2) appears in Figure 4. Only the side view is shown, since the top-view dimensions are identical to those of FRM1. For FRM2, the rollers are 5.625 in. long, and the enclosing container has internal dimensions of $7 \times 7 \times 6.1$ in. The

clearance between the rollers and the top of the container is 1/32 in. (as in FRM1), but the clearance between the rollers and the bottom of the container is 7/16 in. This added clearance allows the bottom of the container in FRM2 to be covered with a thin layer of mercury, if desired, in order to study the effect of a free bounding surface on the flow. The effect of a solid bottom surface with the same clearance as in FRM1 can also be studied by placing a 3/8 in. thick Lucite plate at the bottom of FRM2. The only other difference between the two devices is that the bottom of the container in FRM2 is made of 1/4 in. thick Lucite rather than Pyrex. All other details of the construction of FRM1 and FRM2 are identical.

In both four-roll mills, the rollers are driven by four independent variable-speed d.c. motors through clutch and gear assemblies. The clutches are operated electrically and can be engaged simultaneously in order to "instantaneously" initiate the flow. The speed of each motor is measured by an electromagnetic sensor which sends a signal to a digital tachometer. The motors are connected to electronic controllers which can maintain constant motor speeds to within one or two percent throughout the range from 200 to 2400 r.p.m. A gear reduction of 6:1 then produces roller angular speeds ranging from 3.5 to 42 rad/s (approximately).

B. Procedure: Flow Visualization and Photography

The test fluids used for the experiments were aqueous solutions of glycerol. For the purpose of flow visualization, a small quantity of tracer particles (IG101 Eccospheres, manufactured by Emerson & Cuming, Inc.) were suspended in the fluid. These particles are hollow glass spheres of approximately 100 μm mean diameter and 0.24 g/cm^3 mean density. By illuminating the fluid in flow, these highly reflective particles could produce trajectory streaks on a time exposure photograph. We assume that these trajectories accurately correspond to

streamlines for the flow with tracer particles absent but, otherwise, under identical conditions. This assumption is justified if the particles are sufficiently small, i.e., the particles follow true streamlines with increasing accuracy as the particle diameter decreases. A general rule for particle selction is that the particle size should be at least one order of magnitude smaller than the fine structure of the flow being investigated.[22] The tracer particles of 100 μm diameter easily satisfied this criterion in the experiments to be reported.

The fluid in the four-roll mill was illuminated by a planar beam of light with a thickness of 1/8 to 1/4 in. The beam was produced by shining the light from a 300 W projector bulb through a deep channel formed by two parallel aluminum plates held 1/8 in. apart. This method of illumination allowed streamlines in thin cross-sections of the flow domain to be viewed and photographed. Several different regions inside the four-roll mill were selected to be photographed in this manner in order to convey the most important features of the three-dimensional flow. These regions are described below with reference being made to the coordinate system and notation of Figure 1.

Region 1. $0 < x_1 < d$, $-d/2 < x_2 < d/2$, $-h/2 < x_3 < h/2$

This region is a vertical section in the space between the rollers parallel to the (x_2,x_3)–plane. Photographs were made with the camera lens aligned perpendicularly (i.e., in the negative x_1–direction) so that the *primary* flow was directed *towards* the camera.

Region 2. $-d/2 < x_1 < d/2$, $0 < x_2 < d$, $-h/2 < x_3 < h/2$

This region is a vertical section in the space between the rollers parallel to the (x_1,x_3)–plane. Photographs were made with the camera lens aligned perpendicularly (i.e., in the negative x_2–direction) so that the *primary* flow was directed *away* from the camera.

Region 3. $-d/2 < x_1 < d/2$, $-d/2 < x_2 < d/2$, $-b/2 < x_3 < b/2$

This region is a horizontal section at mid-height in the space between the rollers which is parallel to the (x_1,x_2)–plane (i.e., the plane of the primary flow). The thickness of this region is denoted by b, the light beam thickness. Photographs were made with the camera positioned above and the camera lens aligned perpendicularly (i.e., in the negative x_3–direction).

The photographs were made on Kodak Tri-X Pan film rated at 400 ASA using a Canon A-1 camera equipped with a FD 200mm f/4 Macro lens. The exposure time was usually set at one second, which was a sufficient length of time for the tracer particles to produce long, continuous streaks on the photographs. A variable power supply was used to adjust the intensity of the light so that the proper exposure could be obtained with an f-stop of 4.0. This f-stop was chosen to reduce the depth-of-field to about 1/4 in. around the mid-plane of the illuminated region on which the camera was focused.

The temperature of the fluid in the four-roll mill could be measured to within 0.01 °C using a thermistor which was encased in a brass thermometer well projecting through the filling tube of the container. During the course of an experiment, the fluid temperature was found to rise by as much as 5 to 10 °C due to viscous heat generation and the presence of the illuminating device. A temperature reading was made when each photograph was taken. The kinematic viscosities of the test fluids were measured with a Cannon-Fenske Routine viscometer over the range of temperatures encountered in the experiments (20 to 30 °C). For each fluid, the viscosity-temperature data were found to closely fit a relationship of the form

$$\ln \nu = A + \frac{B}{T} ,$$

where ν is the kinematic viscosity and T is the absolute temperature. The

parameters A and B were obtained by the method of least squares. The kinematic viscosity and the Reynolds number could then be calculated from the temperature and roller speed associated with the flow conditions in each photograph.

III. Observations

In the flow-visualization studies of the two four-roll mills, the rollers were made to rotate in the following manner. All of the rollers rotated with the same angular speed ω, and each of the rollers in one diagonal pair rotated in a clockwise direction while each of the rollers in the other diagonal pair rotated in a counterclockwise direction. This, of course, is the mode of operation required to produce pure extensional flow (see Figure 2, $\lambda = 1$). For a four-roll mill operated in this manner, the flow depends upon a single dynamical parameter, the Reynolds number, which we define as

$$\mathrm{Re} = \frac{\omega R d}{\nu} , \tag{6}$$

where R is the radius of the rollers, d is the gap width between adjacent rollers, and ν is the kinematic viscosity of the fluid. Our observations are presented as sequences of streamline photographs for increasing values of this Reynolds number.

A. FRM1 (L/d = 3.39)

We first describe the flows observed in the shallower four-roll mill FRM1. The test fluid used was a glycerol/water mixture with a concentration of approximately 90% glycerol by weight and a kinematic viscosity of 194.7 centistokes at 20.0 °C. A sequence of photographs showing streamlines near the horizontal mid-plane (i.e., Region 3) are shown in Figures 5 - 7. Portions of the rollers appear in the corners of the photographs. The upper left-hand and lower right-hand rollers were rotating in the clockwise direction while the upper

right-hand and lower left-hand rollers were rotating in the counterclockwise direction. Thus, the fluid was flowing into the region between the rollers from the gaps pictured at the top and bottom of each photograph, and it was flowing out through the gaps at the right and left. It is apparent from the photographs in Figures 5 and 6 that up to a Reynolds number of about 37, the flow in a thin region around the horizontal mid-plane appears to be an essentially two-dimensional pure extensional flow near the stagnation point between the rollers. The streamlines seem to show no detectable deviation from the hyperbolic shape in photographs 5(a)-(f) and 6(a). Of course, the streamline photographs alone are insufficient to confirm a *quantitative* agreement with the velocity field given by equations (1) and (2). However, an investigation of the homogeneity of the flow field produced in the same four-roll mill was conducted by Fuller et al.[23] In this study, homodyne light-scattering spectroscopy was employed to measure the velocity gradient profile on the horizontal mid-plane. These measurements were made for values of the Reynolds number up to 13.4 and showed that the velocity gradient is constant in a region around the stagnation point with dimensions approximately equal to the gap width between two adjacent rollers. This region corresponds roughly to the highly illuminated square area seen in the center of each photograph in Figures 5 - 7.

The sequence of photographs in Figure 6 shows that a fully three-dimensional flow eventually develops as the Reynolds number increases. The onset of a vertical component of velocity at the horizontal mid-plane occurs at a Reynolds number of about 37. This three-dimensional motion is just perceptible in Figure 6(b) at Re = 38.6 where streamlines appear to cross in the vicinity of the stagnation point. The subsequent photographs of Figure 6 and those of Figure 7 reveal that the three-dimensional flow becomes more pronounced as the Reynolds number increases beyond 40 and is characterized by a helical swirling motion of fluid as it passes out of the region between the rollers.

Indeed, a *steady* vortex develops which is aligned in the direction of the outflow axis (i.e., the x_1–axis). However, the streamlines near the roller surfaces and those along the inflow axis in the roller gaps shown at the top and bottom of each photograph remain essentially unchanged in appearance from the low Reynolds number photographs of Figure 5. Thus, the three-dimensional motion at the horizontal mid-plane is confined to a strip along the outflow axis.

The process leading to the development of the swirling flow is more clearly illustrated by side-view photographs of Regions 1 and 2. Figures 8 - 11 show the effect of increasing Reynolds number on the flow pattern in Region 1. These photographs depict a vertical cross-section of the flow in the space between the rollers as viewed along an outflow axis. The rollers appearing at the right and left in the photographs were rotating so that the primary flow was directed out of the plane of the photograph. At low Reynolds number (i.e., $Re < 5$) the flow is essentially two-dimensional throughout most of the region between the rollers except near the top and bottom container surfaces. Near these surfaces, a secondary flow with a non-zero vertical component of velocity is always present. Both the magnitude of the secondary flow and the vertical extent of the region where it is significant gradually increase as the Reynolds number grows larger. Correspondingly, the vertical extent of the region in which the flow is effectively two-dimensional decreases. The photographs in Figure 8 show streamlines for values of Reynolds number in the range from 16 to 37. These photographs clearly reveal the structure of the secondary flow as four symmetrically positioned vortices. The fluid motion in these vortices is a helical superposition of the primary flow, which follows hyperbolic paths in horizontal planes through the region between the rollers, and the secondary flow, which involves a circular motion in the vertical planes of Region 1. The fluid spirals in a clockwise direction in the upper right-hand and lower left-hand vortices. The spiraling motion is counterclockwise in the other two vortices. When the Reynolds number

attains a value of about 37, the four vortices completely fill the region between the rollers, and the flow is two-dimensional *only* on the horizontal mid-plane.

Up to Re = 37, the flow field remains symmetric with respect to the horizontal and vertical mid-planes (i.e., the (x_1,x_2)–, (x_2,x_3)–, and (x_1,x_3)–planes in Figure 1). The appearance of the flow field changes abruptly, however, as the Reynolds number is increased through a quasi-critical range, approximately given by $37 < Re < 41$. The sequence of photographs in Figure 10 provides a *striking* illustration of the transition which occurs in this quasi-critical range. At a Reynolds number of about 37, the flow field loses its symmetric appearance with respect to the horizontal mid-plane and the vertical mid-plane containing the outflow axis. This event is illustrated by Figures 10(a) and 10(b) and is accompanied by the incipience of a non-zero vertical component of velocity at each point on the horizontal mid-plane. Thus, the loss of symmetry in the vortex structure shown in Figure 10 coincides with the onset of three-dimensional motion seen in the top-view photographs of Figure 6. As the Reynolds number is increased further through the quasi-critical range, one of the upper votices gradually shifts in position towards the center of Region 1. As this vortex shifts, it assumes a highly eccentric elliptical shape and it displaces the diagonally opposed lower vortex. This displaced vortex diminishes in size and eventually retreats behind one of the rollers. Simultaneously, the remaining two vortices assume centered positions above and below the elliptical vortex.

For each value of the Reynolds number in (and beyond) the quasi-critical range two different steady flows may be realized. These two flows differ only in the orientation of the semi-major axis of the central elliptical vortex. In one type of flow this axis is inclined at an angle of +45° with respect to the vertical direction; in the other type of flow the angle of inclination is –45° from vertical. The first orientation (+45°) has already been shown in Figure 10 and is attained

when the upper right-hand vortex shifts to the center as the Reynolds number is increased through the quasi-critical range. The other possible orientation ($-45°$) results from a shift of the upper left-hand vortex with increasing Reynolds number. The particular orientation which is actually attained in an experiment depends upon the order in which the speeds of the rollers are raised to increase the Reynolds number. Aside from this multiplicity in vortex orientation, the steady flow patterns in the quasi-critical range depend uniquely on the Reynolds number. Thus, the same flow pattern will be observed at a given Reynolds number regardless of whether this Reynolds number is attained by gradual increase from below, gradual decrease from above, or instantaneous initiation of the flow.

As the Reynolds number is increased beyond the quasi-critical range up to about 50, the eccentricity of the central vortex decreases. This effect is illustrated by the sequence of photographs in Figure 11. These photographs also indicate that the central vortex expands slightly with increasing Reynolds number, thereby causing the upper and lower vortices to become flatter in appearance. The steady three-vortex pattern persists with no other changes in structure up to a Reynolds number of about 60. Beyond $Re = 60$, the flow becomes increasingly unsteady in time and eventually turbulent. However, the characterization of this process is beyond the scope of a flow-visualization study employing a still camera.

The photographic sequences in Figures 12 - 15 depict the evolution of the flow in Region 2 with increasing Reynolds number. These photographs correspond identically or closely in Reynolds number to the Region 1 photographs in Figures 8 - 11. Figures 12 - 15 show the flow in a vertical cross-section of the region between the rollers viewed along an inflow axis. This view is considerably less effective in conveying the features of the flow since the interest-

ing vortex structure is aligned with the outflow axis. Nevertheless, the photographs in Figures 12 and 13 give a good indication of the secondary-flow development near the top and bottom container surfaces with increasing Reynolds number. Also, the photographs in Figure 15 provide a lateral view of the central vortex which appears beyond the quasi-critical range $37 < Re < 41$.

B. FRM2 (L/d = 12.73)

Two different flow-visualization studies of the deeper four-roll mill FRM2 were conducted. In the first study, solid bounding surfaces were present above and below the rollers in FRM2, as they were in FRM1. The second study considered the effect of a slip boundary condition on the flow in the region between the rollers. This was accomplished by replacing the solid boundary beneath the rollers of FRM2 with a layer of mercury. Both studies were conducted using the same glycerol/water mixture (approximately 90% glycerol by weight) that was used in FRM1.

No-slip condition at top and bottom boundaries

For the first study, the 3/8 in. thick Lucite plate was placed on the bottom of FRM2 so that the clearance between the rollers and the top and bottom surfaces containing the fluid were the same as in FRM1. The photographs in Figures 16 - 17 show streamlines in Region 1 of FRM2 for values of the Reynolds number below 37. Only the bottom half of Region 1, extending from the bottom container surface to the horizontal mid-plane, was photographed because the view of the top half was obscured by the structure supporting the motors. However, the flow fields were observed to be symmetrical with respect to the horizontal mid-plane throughout this range of the Reynolds number. These photographs illustrate the development of the secondary flow near the top and bottom container boundaries. The four vortices appear to develop in a manner

identical to the process observed in FRM1 up to Re = 37. The four vortices in FRM2 are again symmetrically positioned and appear to grow in size at the same rate as the ones which form in FRM1. Even at Reynolds numbers near 37, a large portion of the region between the rollers in FRM2 is occupied by fluid which undergoes an essentially two-dimensional flow. This is in sharp contrast to the observation that the vortices completely filled the space between the rollers in FRM1 at Re = 37. The increased extent of the region of two-dimensional flow in FRM2 in contrast to FRM1 is an obvious consequence of the increased roller length in FRM2 and the fact that the boundary vortices grow at the same rate in both devices.

An abrupt transition in the vortex structure also occurs in FRM2 as the Reynolds number is increased through a quasi-critical range beyond Re = 37. The photographs of Figure 18 reveal that this transition is characterized by a loss of symmetry in the boundary vortices with respect to a vertical mid-plane (i.e., the (x_2,x_3)–plane). As the Reynolds number increases, one vortex grows and shifts in a lateral direction to displace the neighboring vortex. This process occurs simultaneously at both the top and bottom container boundaries. Furthermore, a vertical component of velocity begins to develop in the region bounded above and below by the vortices (where the flow was previously two-dimensional). However, in contrast to FRM1, this quasi-critical transition is *not* accompanied by the development of a distinctive swirling flow in the center of the region between the rollers. In fact, the precise nature of the three-dimensional motion which develops between the boundary vortices cannot be easily conveyed by the flow-visualization photographs.

Figure 19 shows a sequence of photographs for values of the Reynolds number past the quasi-critical range. The flow continues to be steady and distinguished by the asymmetric appearance of the boundary vortices up to a Rey-

nolds number of about 55. At this point, an unsteady motion commences which involves a periodic inward shedding of vortices from the top and bottom boundaries. The frequency of this vortex shedding increases with increasing Reynolds number. Eventually the vortex shedding assumes a chaotic quality, and the flow tends towards complete turbulence.

Slip condition at bottom boundary

The second series of observations of flow in FRM2 was made with the 3/8 in. thick Lucite plate removed from beneath the rollers and replaced by a 3/8 in. thick layer of mercury. In this way, the no-slip condition previously imposed at the bottom boundary of the region between the rollers was replaced by a weaker constraint requiring continuity of velocity and shear stress across the mercury interface.

The effect of the mercury interface on the evolution of secondary flow in FRM2 is illustrated by Figures 20-22. The photographs in these figures show streamlines in the bottom half of Region 1 of FRM2 above the mercury interface. As the Reynolds number is increased, the secondary flow develops above the mercury interface in a manner similar to that observed when the solid bottom boundary was present. Once again, two vortices appear at the bottom of Region 1. Beyond Re = 37 the vortices lose their symmetric appearance with respect to the vertical mid-plane (see Figure 22). The steady vortex patterns again persist up to a Reynolds number of about 55, above which the flow becomes unsteady as vortices are shed upward from the mercury interface.

Although the process of vortex growth above the mercury interface is qualitatively similar to the process observed above a solid boundary, the rate of growth in the presence of the mercury interface is significantly slower. This is clearly indicated by a comparison of Figure 16c and Figure 21c. The vortices appearing in Figure 21c above the mercury interface at Re = 20.5 are

approximately half the size of the vortices seen in Figure 16c above the solid surface and again at Re = 20.5. Thus, the development of the secondary flow in the region between the rollers is strongly influenced by the precise nature of the boundary conditions imposed at the top and bottom container surfaces.

IV. Discussion

This study has shown that flow in a four-roll mill can assume an extremely complicated, albeit interesting, three-dimensional character throughout the region between the rollers prior to the onset of turbulence. A secondary flow involving four symmetrically positioned vortices is always present near the top and bottom container boundaries. This secondary flow is enhanced as the Reynolds number increases up to a quasi-critical range. Through this quasi-critical range a rapid transition occurs which alters the symmetry and structure of the flow. The exact nature of this transition is dependent upon the ratio of roller length to gap width between adjacent rollers, L/d. This transition is accompanied by the incipience of three-dimensional motion throughout the entire region between the rollers. However, the three-dimensionality appears to be significantly less pronounced for larger values of L/d. In all cases, the quasi-critical range of Reynolds number is closely followed by a critical Reynolds number corresponding to the onset of unsteady flow.

The secondary flow near the top and bottom boundaries can extend a significant distance towards the horizontal mid-plane, even for fairly low values of the Reynolds number (i.e., Re = O(10)). Since the usual experimental purpose of the four-roll mill is to simulate *two-dimensional* linear flows, it is extremely important to take this secondary flow into account when designing an apparatus for a specific experimental purpose. Flow birefringence measurements, for example, are averaged over the entire depth of a four-roll mill. Thus, the secondary flow will cause deviations in the measured level of birefringence from the

level which would exist in a true two-dimensional linear flow. The obvious remedy suggested by this flow-visualization study is to make the ratio L/d as large as possible in order to maximize the extent of the region of two-dimensional flow at a given Reynolds number. This remedy has practical limitations, of course. Furthermore, there will probably exist an upper limit on the Reynolds number beyond which a good approximation to two-dimensional flow may never be realized, regardless of the magnitude of L/d.

These observations of flow in a four-roll mill provide a good example of an interesting fluid-mechanical phenomenon: the transition with increasing Reynolds number of a simple steady laminar flow to a more complicated steady laminar flow. In this case, the initial flow may be represented by a two-dimensional pure extensional velocity field throughout at least part of the flow domain. Thus, as a first step towards understanding the experimentally observed phenomenon we attempt to apply the linear stability theory for two-dimensional linear flows of an unbounded fluid obtained by Lagnado et al.[13] According to this theory, unbounded two-dimensional linear flows in the range $0 < \lambda \leq 1$ are unconditionally unstable. For any positive values of the basic flow shear rate E and the kinematic viscosity ν, there exist spatially periodic initial disturbances which grow exponentially in time. Such destabilizing disturbances have wave vectors $\alpha = (\alpha_1, \alpha_2, \alpha_3)$ whose components satisfy the following necessary and sufficient conditions for instability:

$$(-1 + \sqrt{\lambda})\alpha_1 + (1 + \sqrt{\lambda})\alpha_2 = 0 \ , \tag{7}$$

$$\alpha_3^2 < \frac{E\sqrt{\lambda}}{\nu} \ . \tag{8}$$

Equation (7) is satisfied by periodic disturbances having lines of constant phase in the plane of the basic flow that are parallel to the inlet streamline of the basic flow. Among such initial disturbances, only those with sufficiently small

values of the wavenumber α_3 in the direction normal to the plane of the basic flow are unstable. The linear stability theory also shows that for pure extensional flow ($\lambda = 1$) the growth of disturbances is accompanied by the growth of only one component of vorticity, namely, the component along the principal axis of extensional strain. In the case of pure extensional flow, the principal axis of extensional strain coincides with the outlet streamline and the outflow axis in the four-roll mill (i.e., the x_1–axis).

In order to apply this linear stability theory to a four-roll mill, some account must be made of the fact that the flow in a four-roll mill is bounded by solid surfaces. The boundaries have two effects on the stability problem. First, they induce a secondary flow, thereby rendering the basic flow of the linear stability analysis invalid outside of a central region in the flow domain. Second, they impose a restriction on the wavelengths of disturbances which can be realized within the finite extent of the flow device. The only effect which can be easily accounted for is the disturbance wavelength restriction imposed by the top and bottom container surfaces. Any velocity disturbance must vanish on these surfaces due to the no-slip condition. Thus, the disturbance wavenumber in the direction normal to the plane of the basic flow must be restricted according to

$$\frac{2\pi}{\alpha_3} \leq 2H , \tag{9}$$

where H is the distance between the top and bottom container surfaces. Hence, in view of the instability criterion (7), one would expect a pure extensional flow ($\lambda = 1$) to be stable in a four-roll mill under the condition

$$\frac{EH^2}{\nu} < \pi^2 , \tag{10}$$

and unstable, otherwise. This stability criterion neglects all boundary effects other than the wavenumber cut-off imposed by the top and bottom container

surfaces. The dimensionless group EH^2/ν in (10) is a Reynolds number based on the shear rate E of the basic flow. Fuller and Leal[10] have measured the shear rate for the linear flows generated in the horizontal mid-plane of FRM1. They found that this shear rate depends upon the angular speed ω of the fastest pair of rollers according to the linear relationship

$$E = 0.678\,\omega\,, \tag{11}$$

The same linear relationship should be valid for the flow in FRM2, since the horizontal dimensions of this device are identical to those of FRM1. Equation (11) and the dimensions of FRM1 and FRM2 may be used to determine instability criteria for the two four-roll mills, equivalent to (10), but involving the Reynolds number $Re = \omega Rd/\nu$. In this manner, we predict the instability of two-dimensional pure extensional flow under the following conditions:

$$Re > 1.89 \quad (in\ FRM1)\,,$$

$$Re > 0.30 \quad (in\ FRM2)\,.$$

Thus, the idealized theory predicts that an increase in the distance between the top and bottom container surfaces (i.e., an increase in L/d) should lower the critical Reynolds number for instability.

The idealized theory presented above differs from the experimental observations in two respects. First, the theory predicts that the two-dimensional pure extensional flow in a four-roll mill should become unstable at a fairly low value of the Reynolds number. However, no sharp transition was observed in either FRM1 or FRM2 at the respective predicted critical Reynolds numbers. The two-dimensional flow gradually evolved into a three-dimensional flow with increasing Reynolds number as a result of secondary-flow development. Furthermore, the observed flows showed no apparent decrease in stability corresponding to an

increase in L/d. Presumably, the boundary effects neglected in the idealized theory account for this discrepancy. In the case of Couette flow, the experimentally observed quasi-critical range of Reynolds number associated with the growth of Taylor vortices is in good quantitative agreement with the results of the linear stability theory for infinitely long cylinders. In this case, however, the linear stability theory includes the presence of the cylinder surfaces and only neglects the small top and bottom boundaries of the annular flow domain. In the present study of the four-roll mill, no attempt has been made to analyze the apparently considerable effect of roller surfaces and container side walls on the flow. A complete analysis of the flow in a four-roll mill would require numerical solution of the full Navier-Stokes equations. However, such an analysis appears to be intractable at present due to the extremely complex geometric features of the four-roll mill.

References

1. G. I. Taylor, Proc. R. Soc. London Ser. A **146**, 501 (1934).

2. F. D. Rumscheidt and S. G. Mason, J. Colloid Sci. **16**, 210 (1961).

3. H. P. Grace, Chem. Eng. Commun. **14**, 225 (1982).

4. S. Torza, R. G. Cox, and S. G. Mason, J. Colloid Interface Sci. **38**, 395 (1972).

5. B. J. Bentley, PhD Thesis, California Institute of Technology (1984).

6. J. D. Sherwood, J. Fluid Mech. **144**, 281 (1984).

7. D. G. Crowley, F. C. Frank, M. R. Mackley, and R. G. Stephenson, J. Polym. Sci. Polym. Phys. Ed. **14**, 111 (1976).

8. D. P. Pope and A. Keller, Colloid Polym. Sci. **255**, 633 (1977).

9. G. G. Fuller and L. G. Leal, Rheol. Acta **19**, 580 (1980).

10. G. G. Fuller and L. G. Leal, J. Polym. Sci. Polym. Phys. Ed. **19**, 557 (1980).

11. P. N. Dunlap, PhD Thesis, California Institute of Technology (1985).

12. S. Torza, J. Polym. Sci. Polym. Phys. Ed. **13**, 43 (1975).

13. R. R. Lagnado, N. Phan-Thien, and L. G. Leal, Phys. Fluids **27**, 1094 (1984).

14. H. Giesekus, Rheol. Acta **2**, 113 (1962).

15. G. I. Taylor, Philos. Trans. R. Soc. London Ser. A **223**, 289 (1923).

16. E. A. Kusnetsov, V. S. Lvov, Y. E. Nesterikhin, Y. E. Shmojlov, V. S. Sobolev, M. D. Spector, S. A. Timokhin, E. N. Utkin, and Y. G. Vasilenko, Inst. Automation and Electrometry, Siberian Branch, U.S.S.R. Acad. Sci., Preprint no. 58 (1977)

17. T. B. Benjamin, Proc. R. Soc. London Ser. A **359**, 1 (1978).

18. T. B. Benjamin, Proc. R. Soc. London Ser. A **359**, 27 (1978).

19. T. B. Benjamin and T. Mullin, Proc. R. Soc. London Ser. A **377**, 221 (1981).

20. T. Mullin, J. Fluid Mech. **121**, 207 (1982).

21. T. B. Benjamin and T. Mullin, J. Fluid Mech. **121**, 219 (1982).

22. W. Merzkirch, *Flow Visualization* (Academic, New York, 1974), p. 30.

23. G. G. Fuller, J. M. Rallison, R. L. Schmidt, and L. G. Leal, J. Fluid Mech. **100**, 555 (1980).

Figure Captions

Figure 1. Four-roll mill geometry. (a) top view, (b) side view.

Figure 2. Flow fields produced in a four-roll mill.

Figure 3. Diagram of apparatus FRM1. (a) top view, (b) side view.

Figure 4. Diagram of apparatus FRM2 (side view).

Figure 5. Streamlines in Region 3 of FRM1. (a) Re = 5.9, (b) Re = 11.8, (c) Re = 20.9, (d) Re = 23.9, (e) Re = 27.0, (f) Re = 34.9.

Figure 6. Streamlines in Region 3 of FRM1. (a) Re = 36.9, (b) Re = 38.6, (c) Re = 39.5, (d) Re = 40.1, (e) Re = 40.7, (f) Re = 41.1.

Figure 7. Streamlines in Region 3 of FRM1. (a) Re = 42.3, (b) Re = 44.8, (c) Re = 46.0, (d) Re = 50.7, (e) Re = 54.6, (f) Re = 56.5.

Figure 8. Streamlines in Region 1 of FRM1. (a) Re = 4.1, (b) Re = 5.6, (c) Re = 8.2, (d) Re = 10.8, (e) Re = 11.1, (f) Re = 13.5.

Figure 9. Streamlines in Region 1 of FRM1. (a) Re = 16.2, (b) Re = 18.7, (c) Re = 21.2, (d) Re = 26.2, (e) Re = 32.9, (f) Re = 36.2.

Figure 10. Streamlines in Region 1 of FRM1. (a) Re = 37.7, (b) Re = 38.1, (c) Re = 38.7, (d) Re = 39.2, (e) Re = 39.9, (f) Re = 41.4.

Figure 11. Streamlines in Region 1 of FRM1. (a) Re = 42.0, (b) Re = 42.6, (c) Re = 45.6, (d) Re = 48.3, (e) Re = 51.1, (f) Re = 54.2.

Figure 12. Streamlines in Region 2 of FRM1. (a) Re = 4.1, (b) Re = 5.6, (c) Re = 8.2, (d) Re = 10.8, (e) Re = 11.1, (f) Re = 13.5.

Figure 13. Streamlines in Region 2 of FRM1. (a) Re = 16.1, (b) Re = 18.7, (c) Re = 21.2, (d) Re = 26.2, (e) Re = 32.9, (f) Re = 36.4.

Figure 14. Streamlines in Region 2 of FRM1. (a) Re = 38.0, (b) Re = 38.1, (c) Re = 38.7, (d) Re = 39.9, (e) Re = 40.7.

Figure 15. Streamlines in Region 2 of FRM1. (a) Re = 42.0, (b) Re = 45.7, (c) Re = 48.0, (d) Re = 52.4, (e) Re = 54.7.

Figure 16. Streamlines in Region 1 of FRM2. (a) Re = 4.0, (b) Re = 10.1, (c) Re = 20.5.

Figure 17. Streamlines in Region 1 of FRM2. (a) Re = 24.8, (b) Re = 29.1, (c) Re = 36.0.

Figure 18. Streamlines in Region 1 of FRM2. (a) Re = 37.3, (b) Re = 39.4, (c) Re = 40.5.

Figure 19. Streamlines in Region 1 of FRM2. (a) Re = 42.8, (b) Re = 45.0, (c) Re = 47.0.

Figure 20. Streamlines in Region 1 of FRM2. (mercury layer present) (a) Re = 4.0, (b) Re = 10.1, (c) Re = 20.5.

Figure 21. Streamlines in Region 1 of FRM2. (mercury layer present) (a) Re = 24.8, (b) Re = 29.2, (c) Re = 36.0.

Figure 22. Streamlines in Region 1 of FRM2. (mercury layer present) (a) Re = 38.3, (b) Re = 40.6, (c) Re = 45.3.

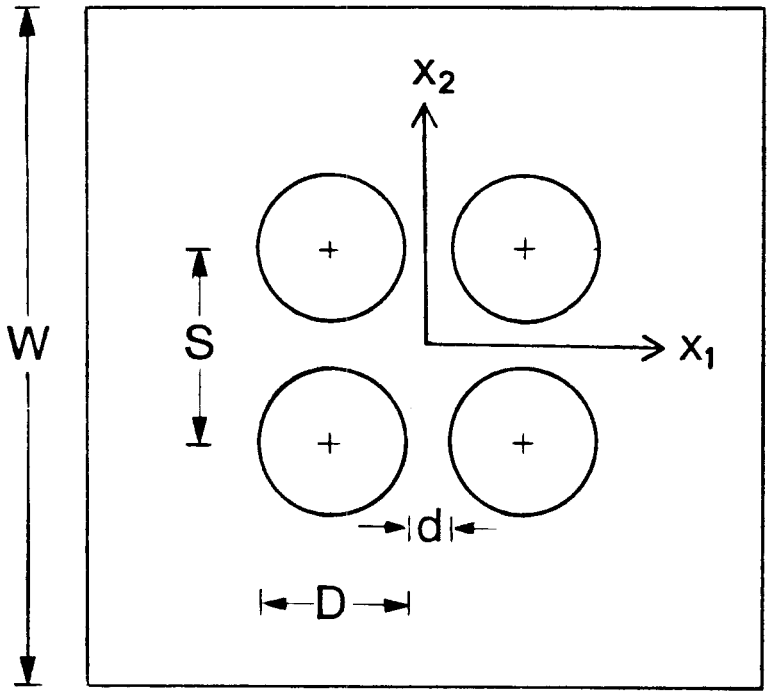

(a)

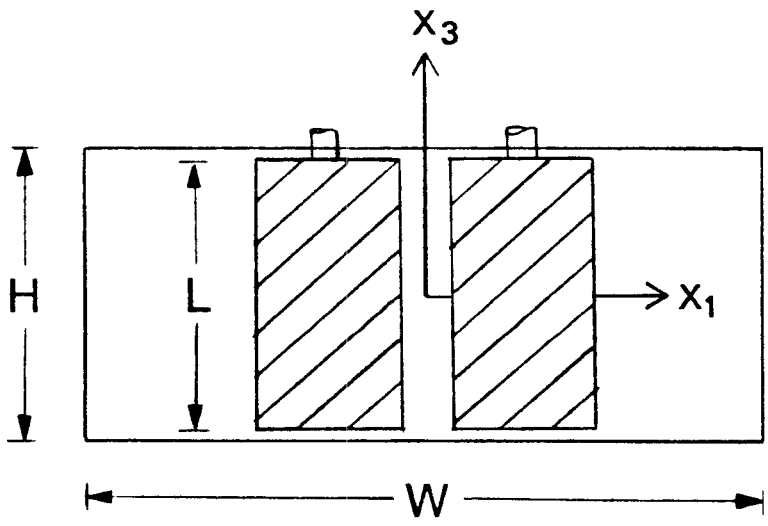

(b)

Figure 1

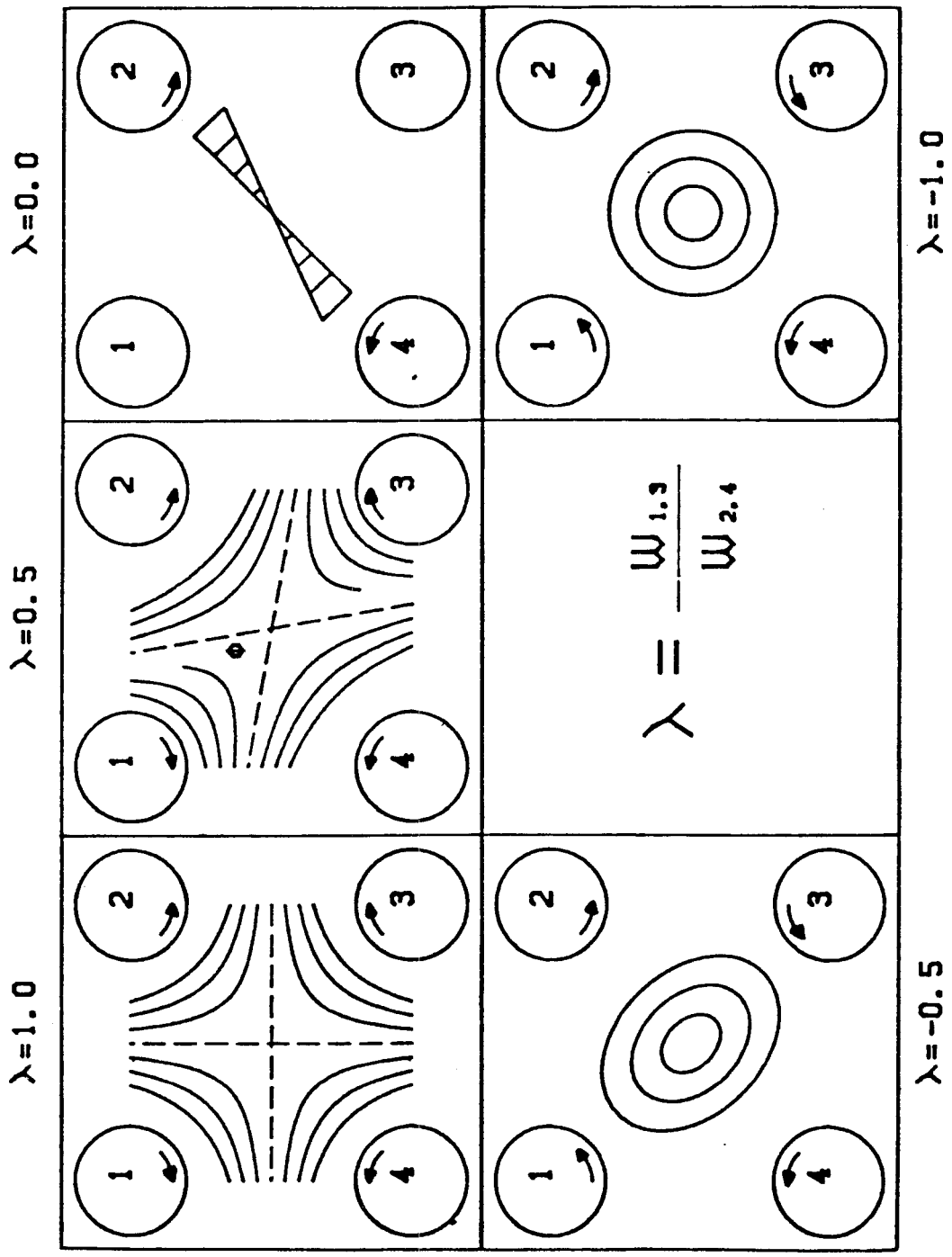

Figure 2

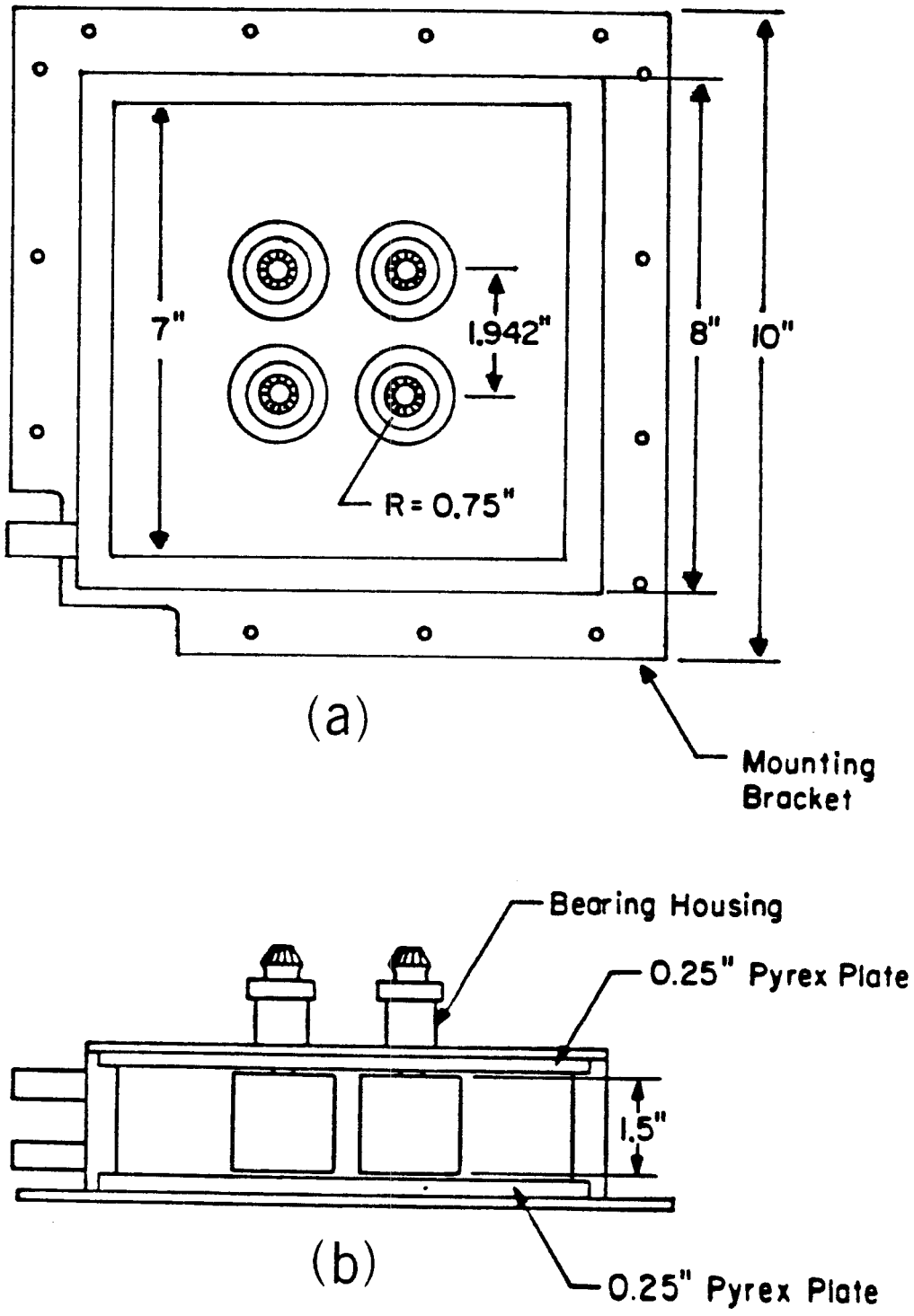
7"
1.942"
8"
10"
R = 0.75"
(a)
Mounting Bracket
Bearing Housing
0.25" Pyrex Plate
1.5"
(b)
0.25" Pyrex Plate

Figure 3

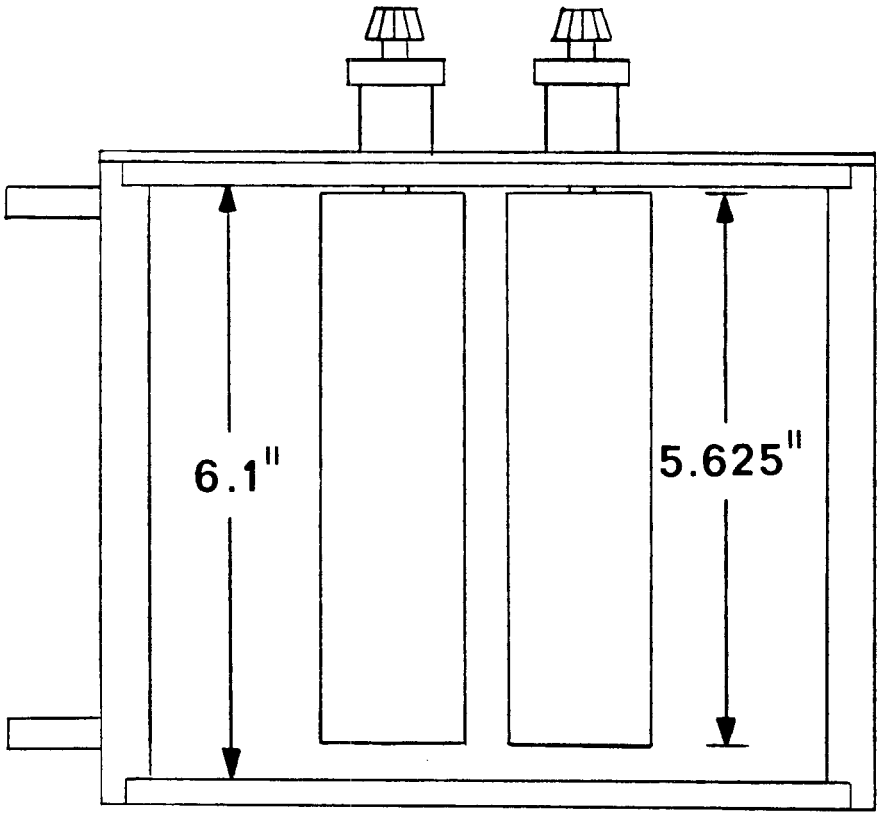

Figure 4

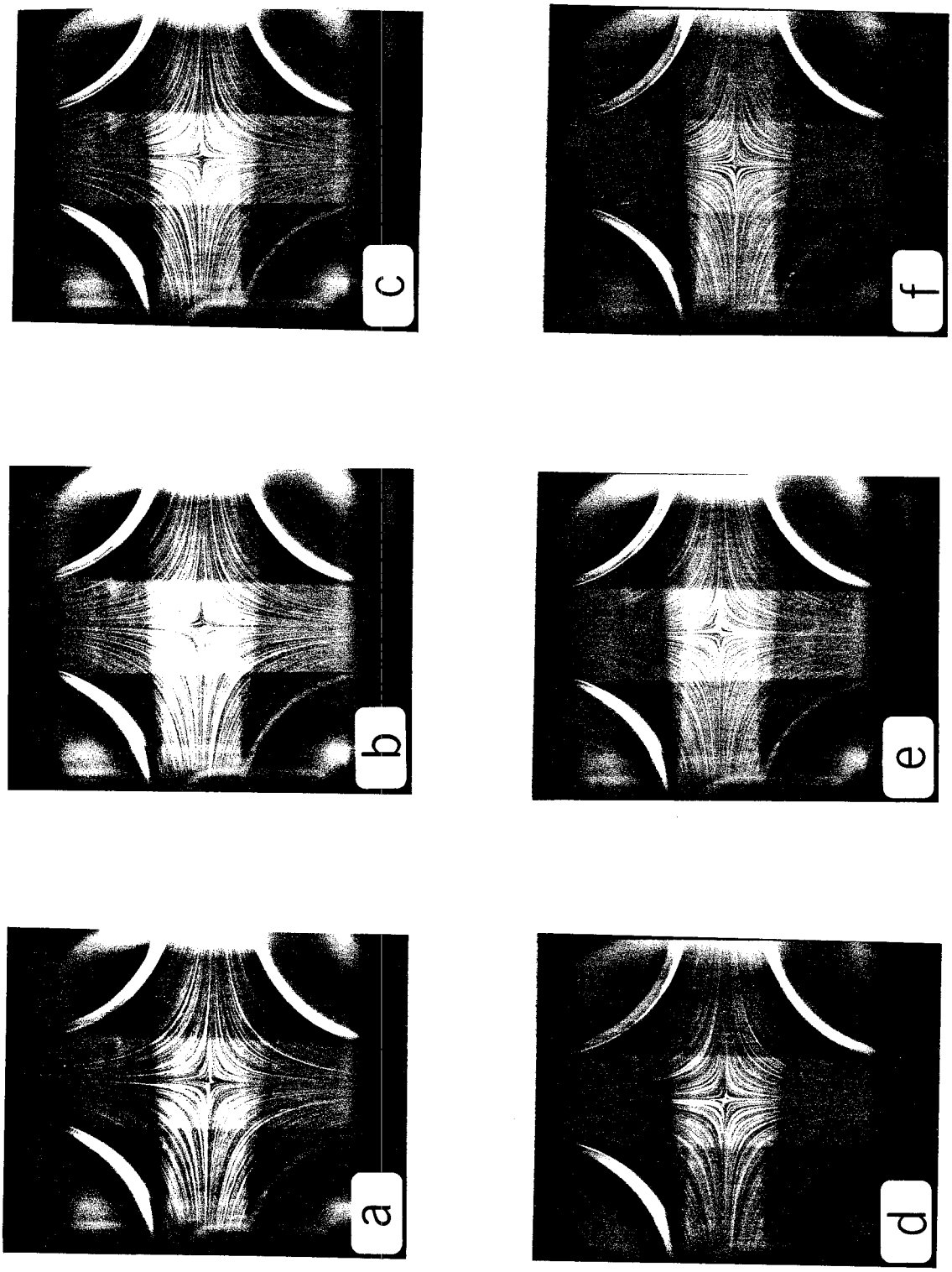

Figure 5

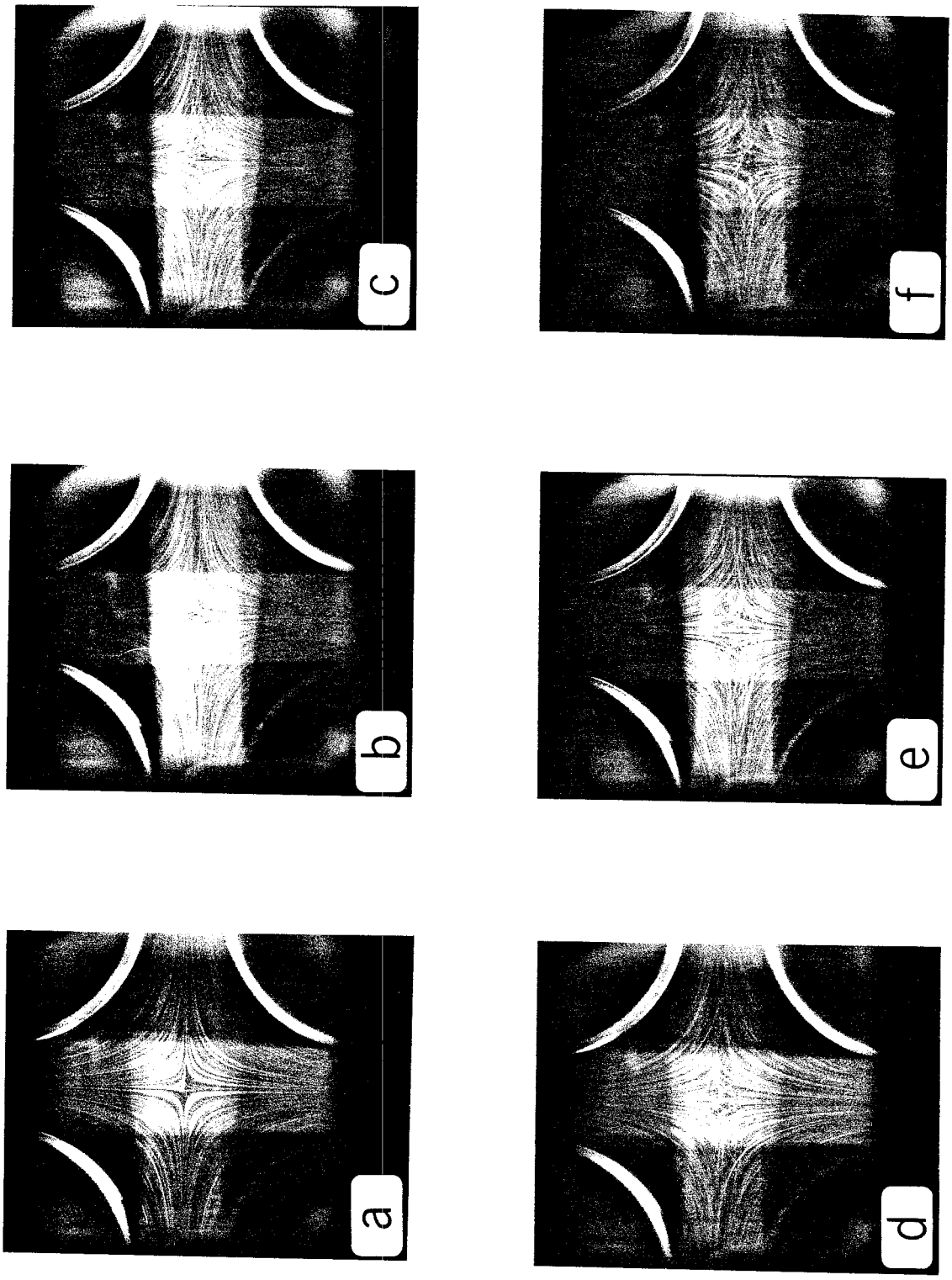

Figure 6

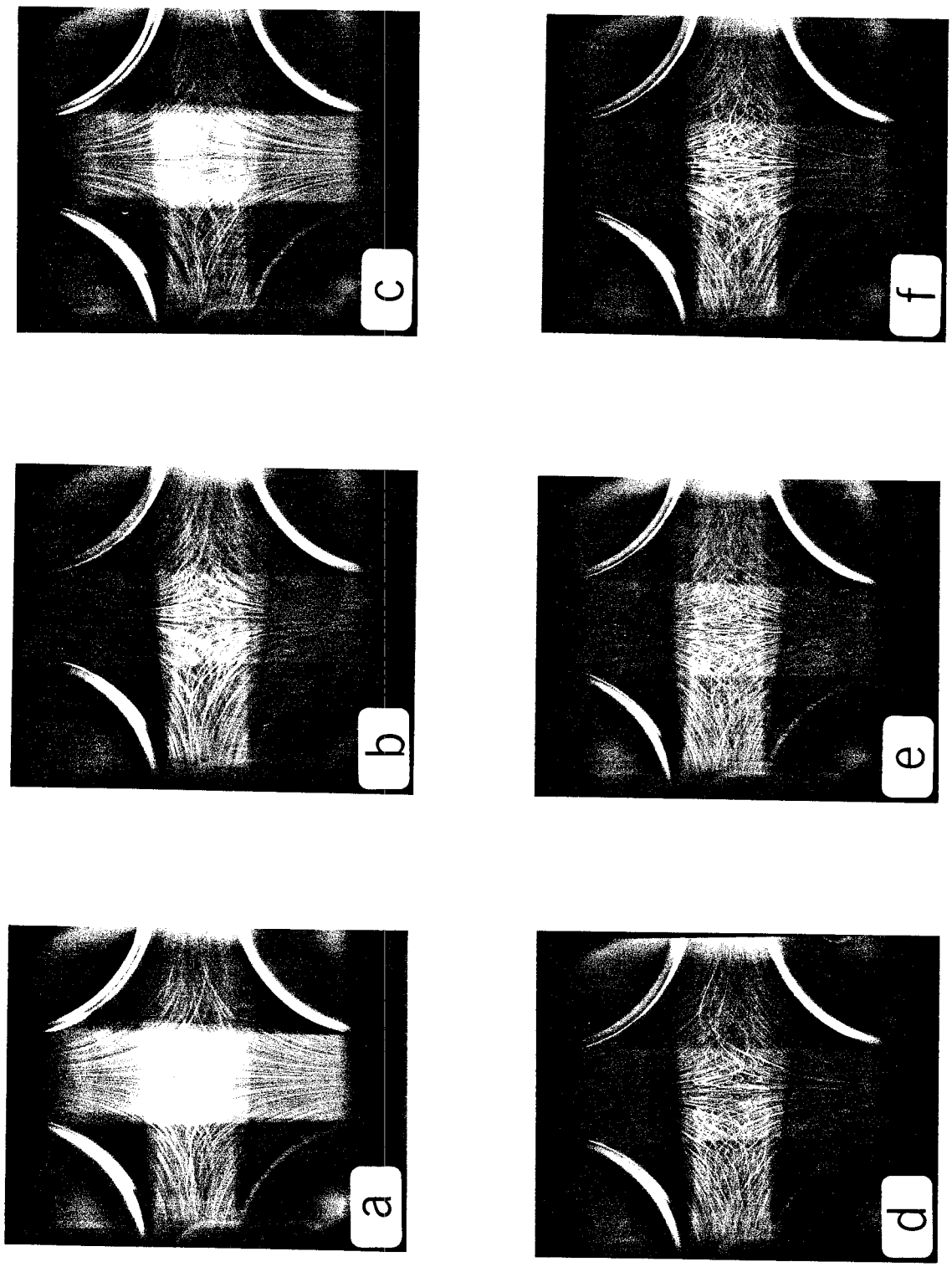

Figure 7

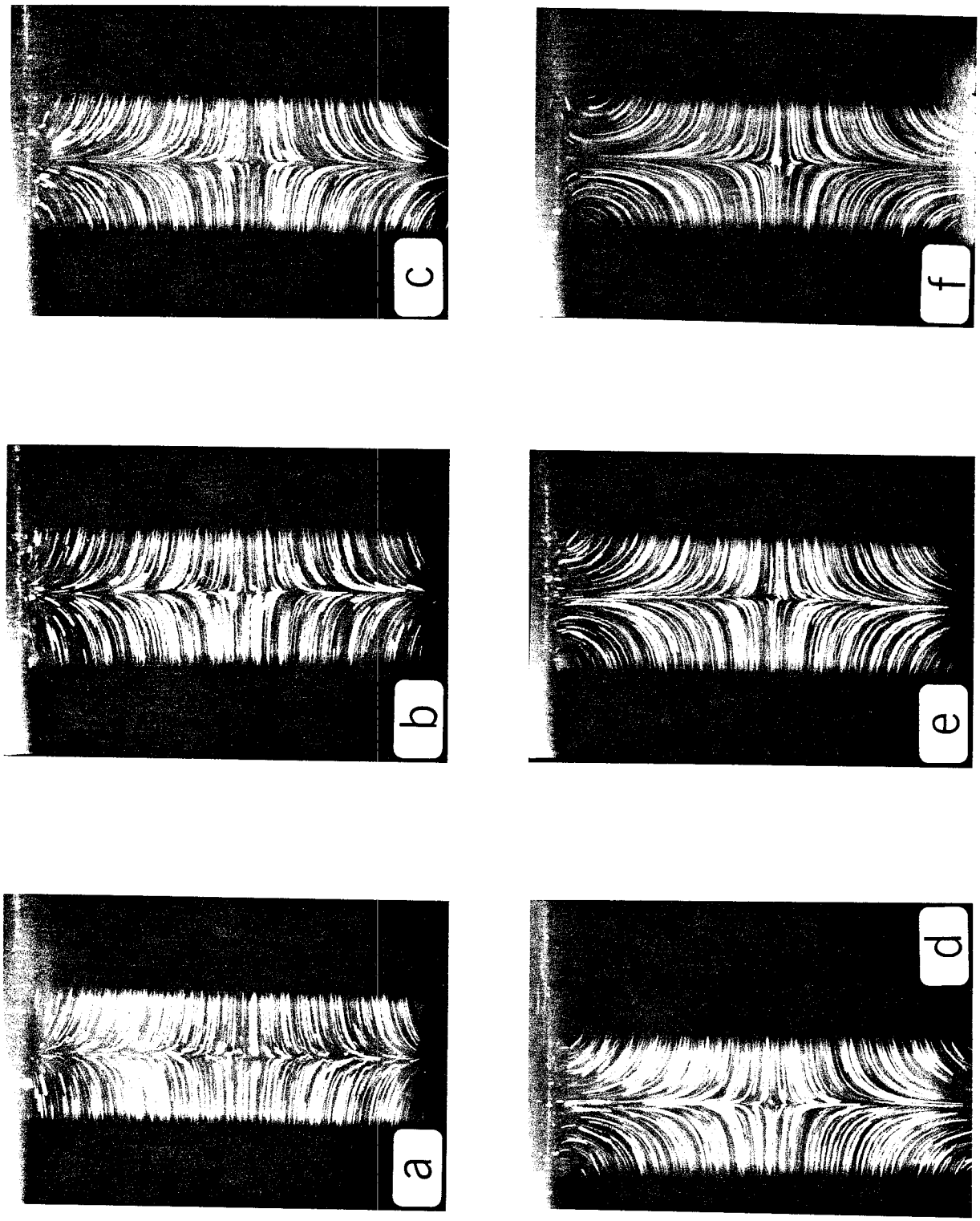

Figure 8

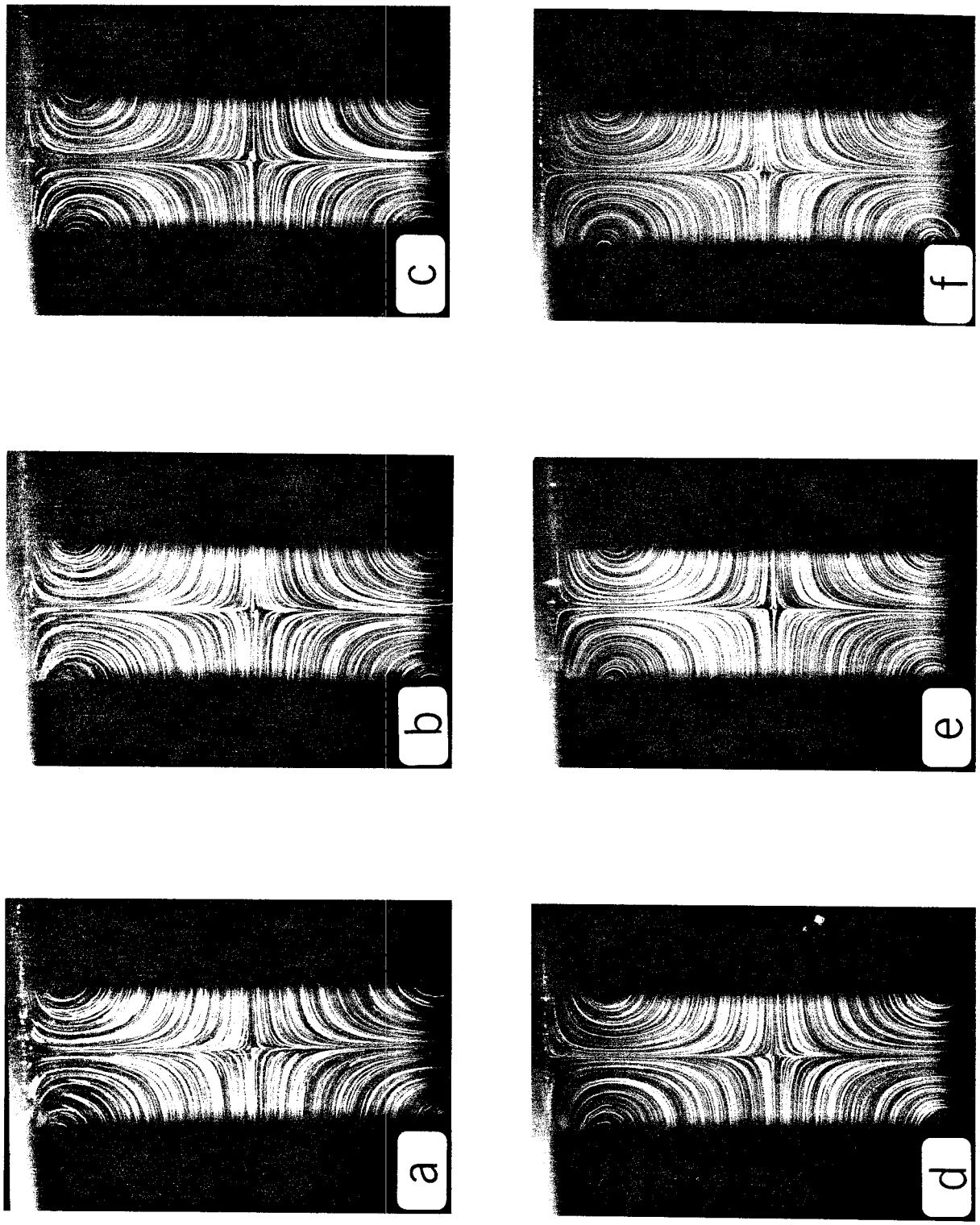

Figure 9

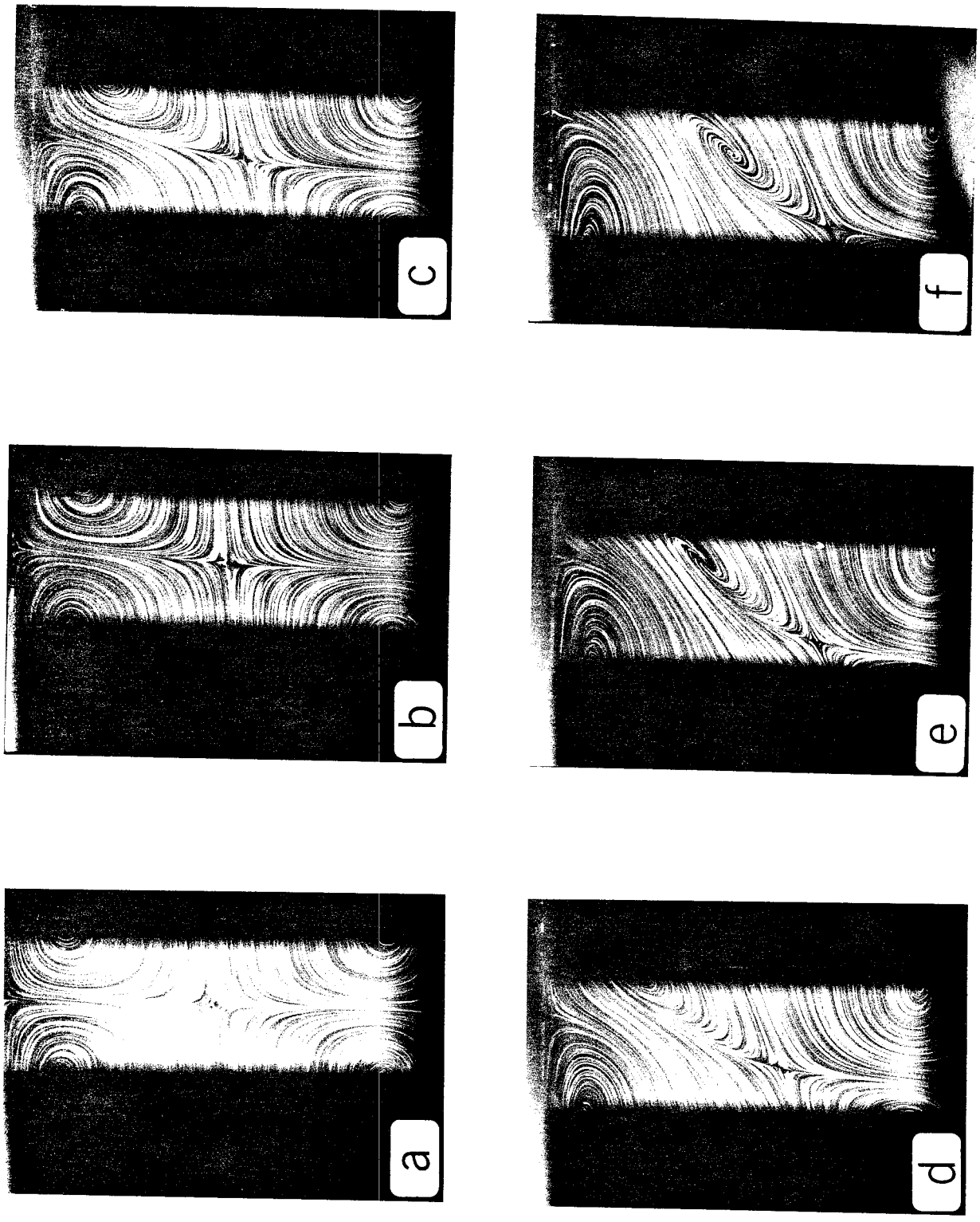

Figure 10

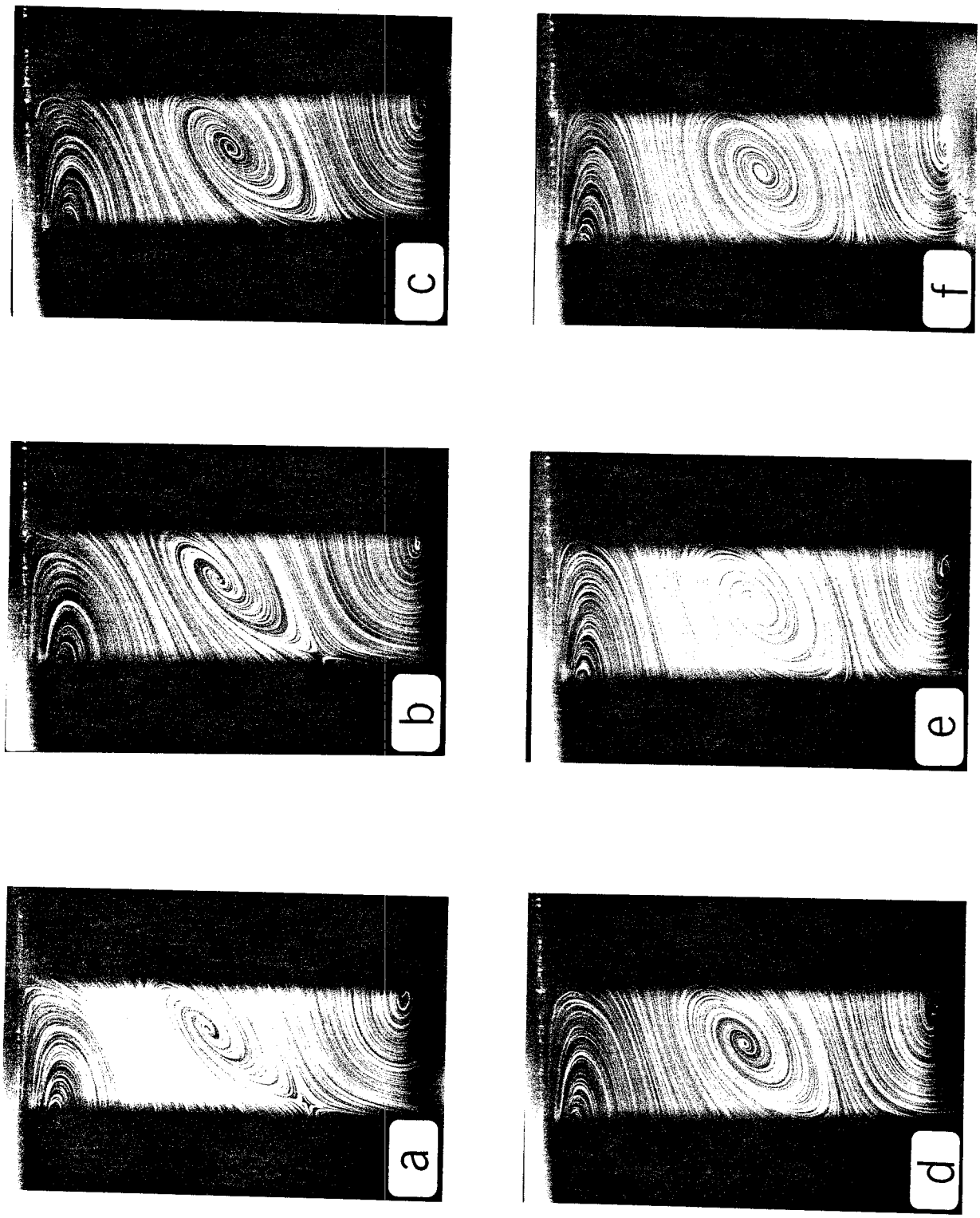

Figure 11

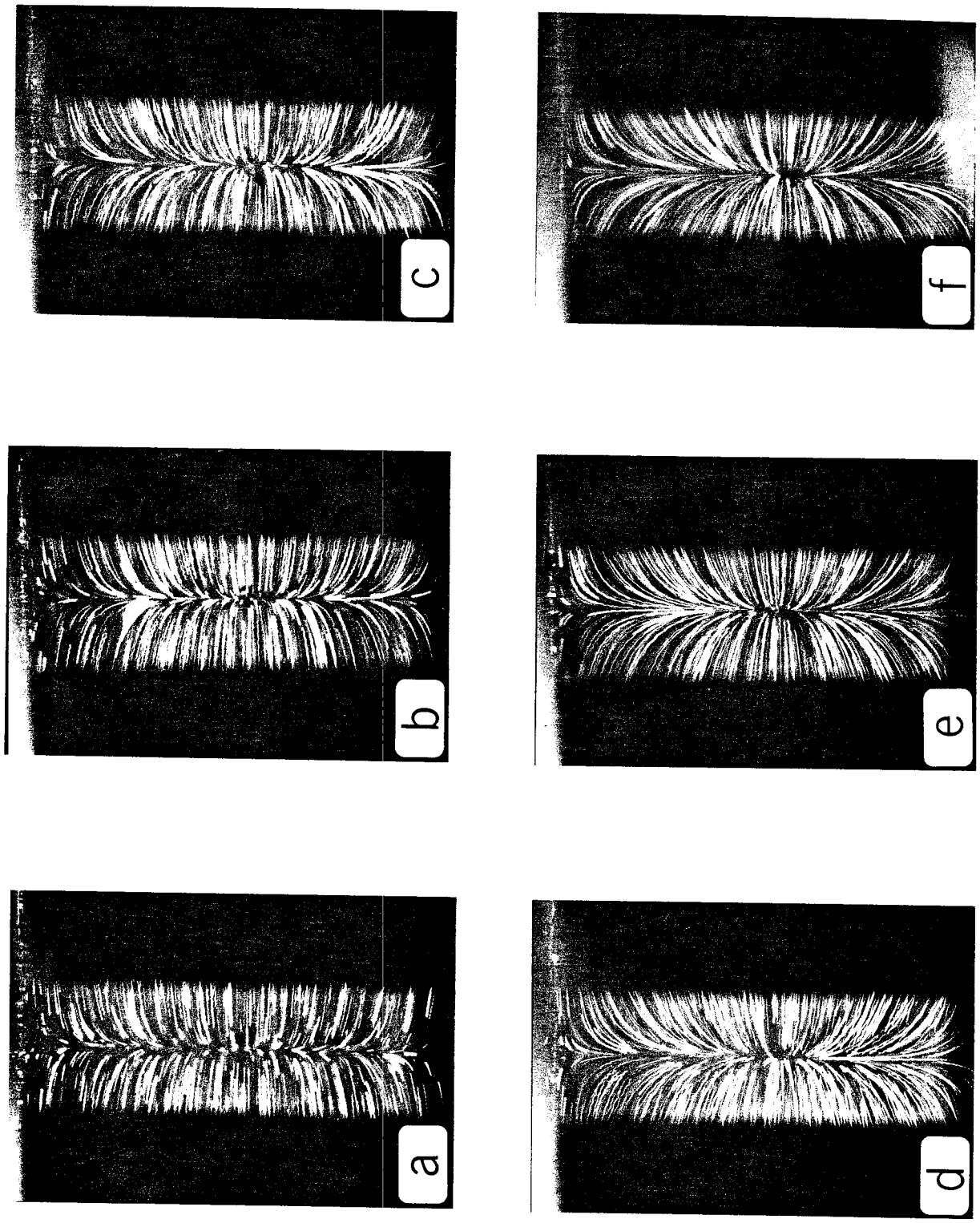

Figure 12

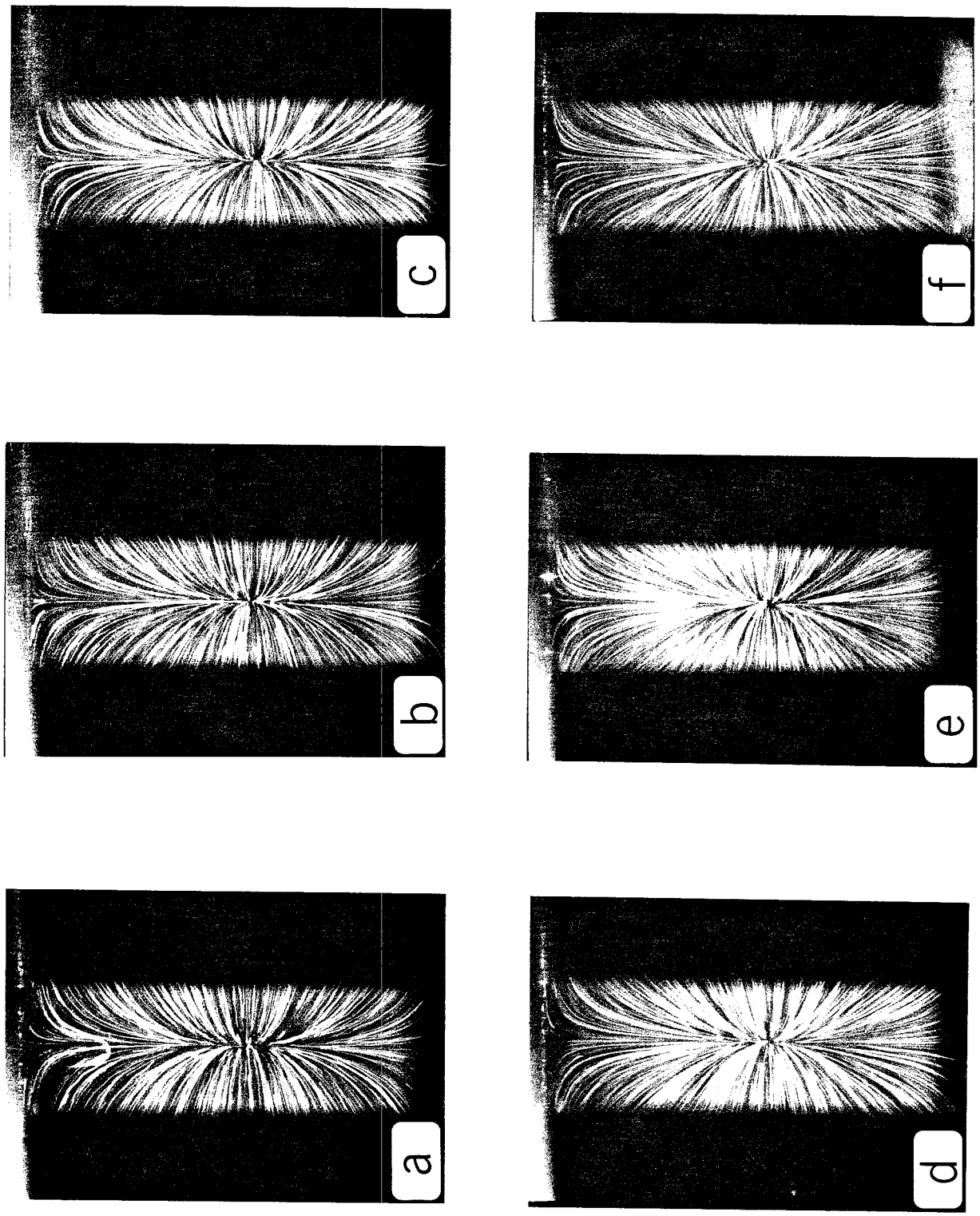

Figure 13

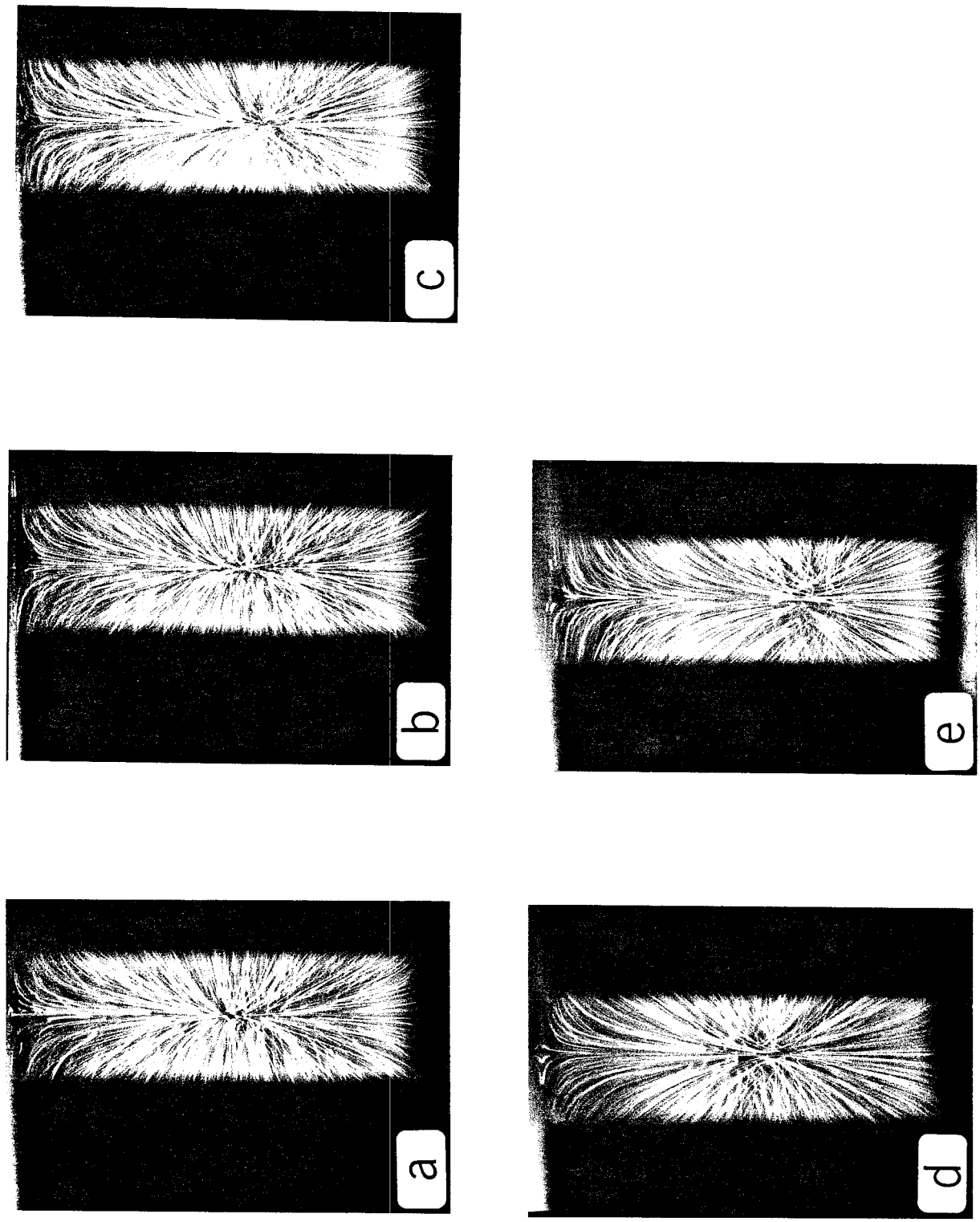

Figure 14

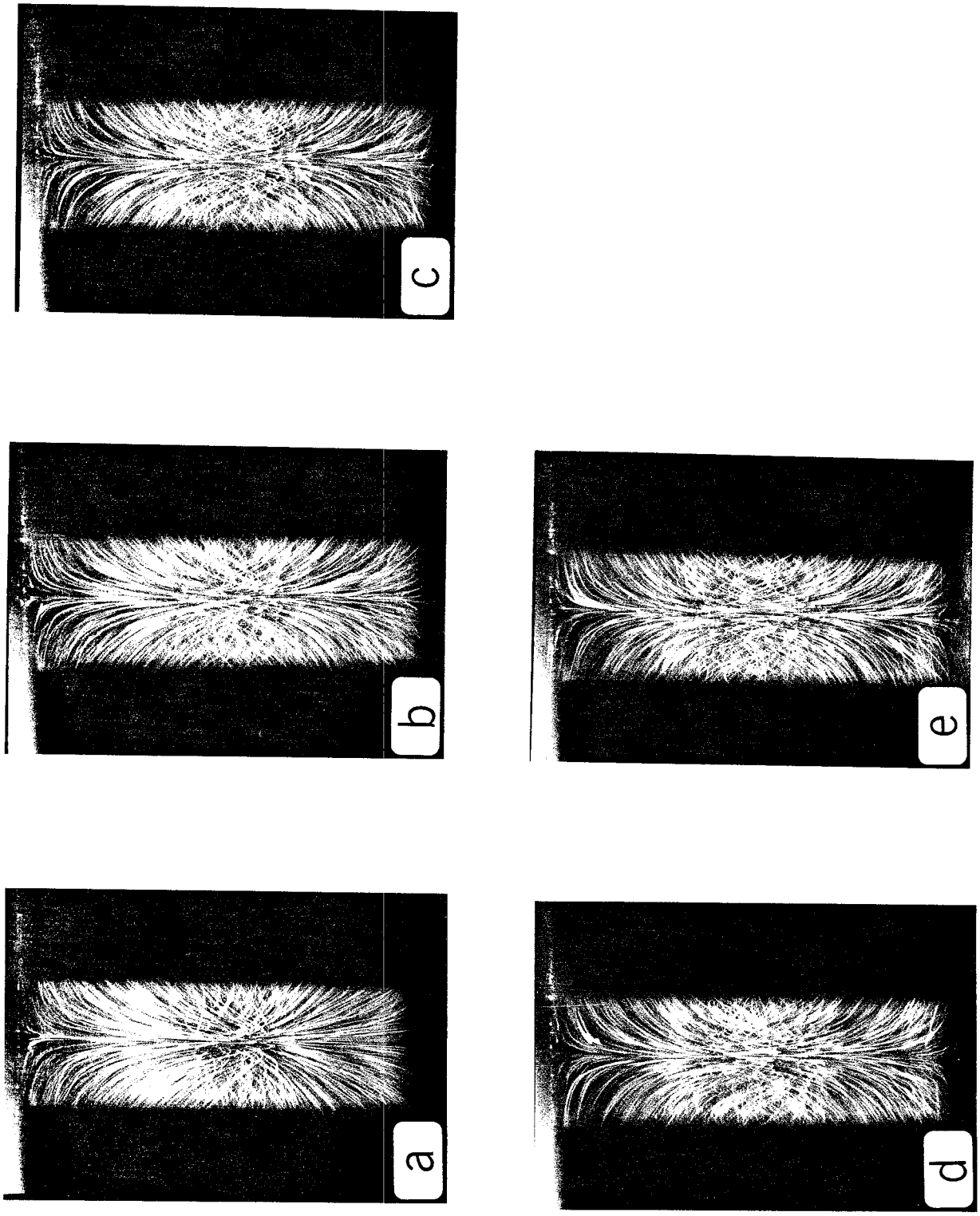

Figure 15

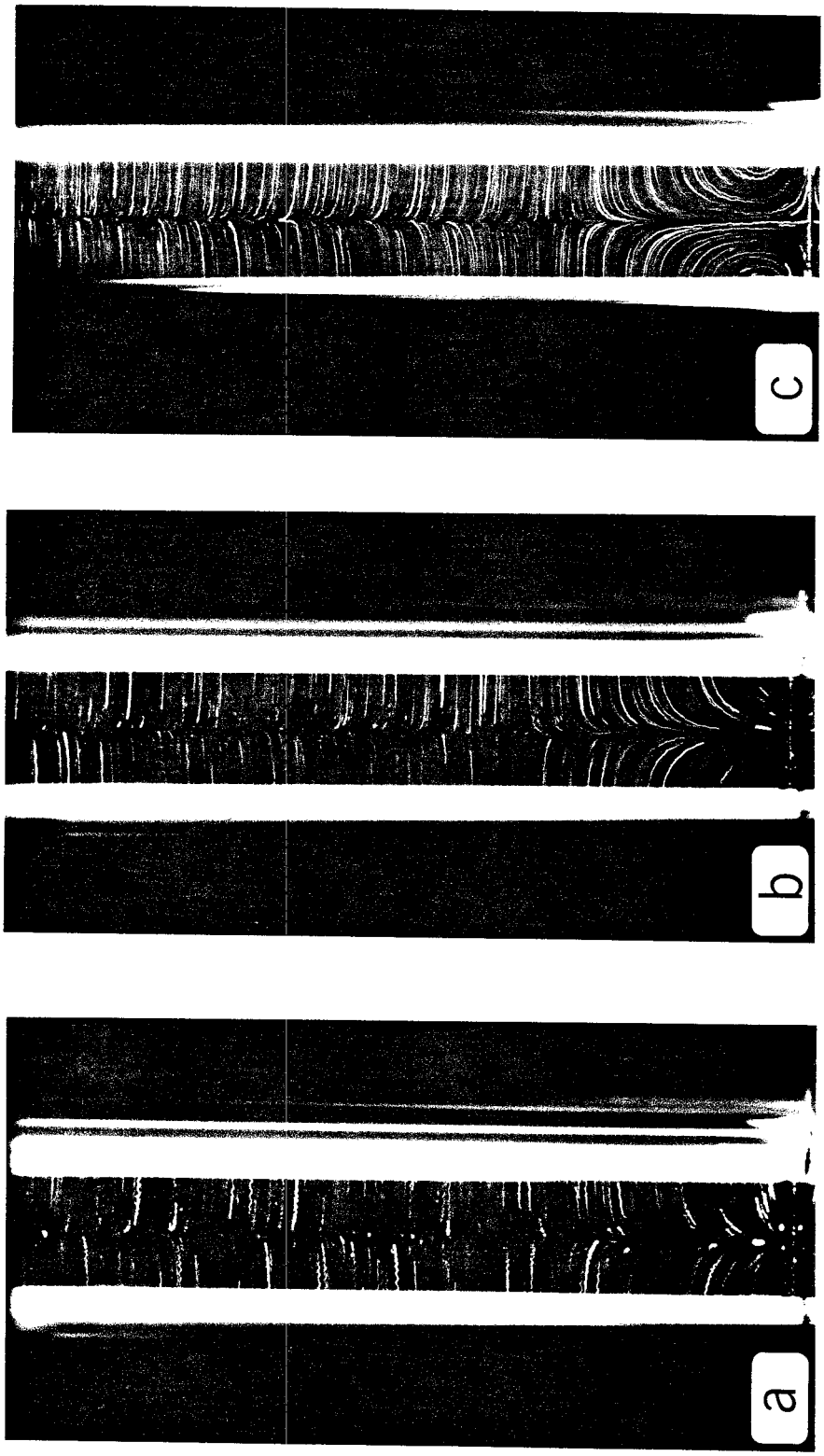

Figure 16

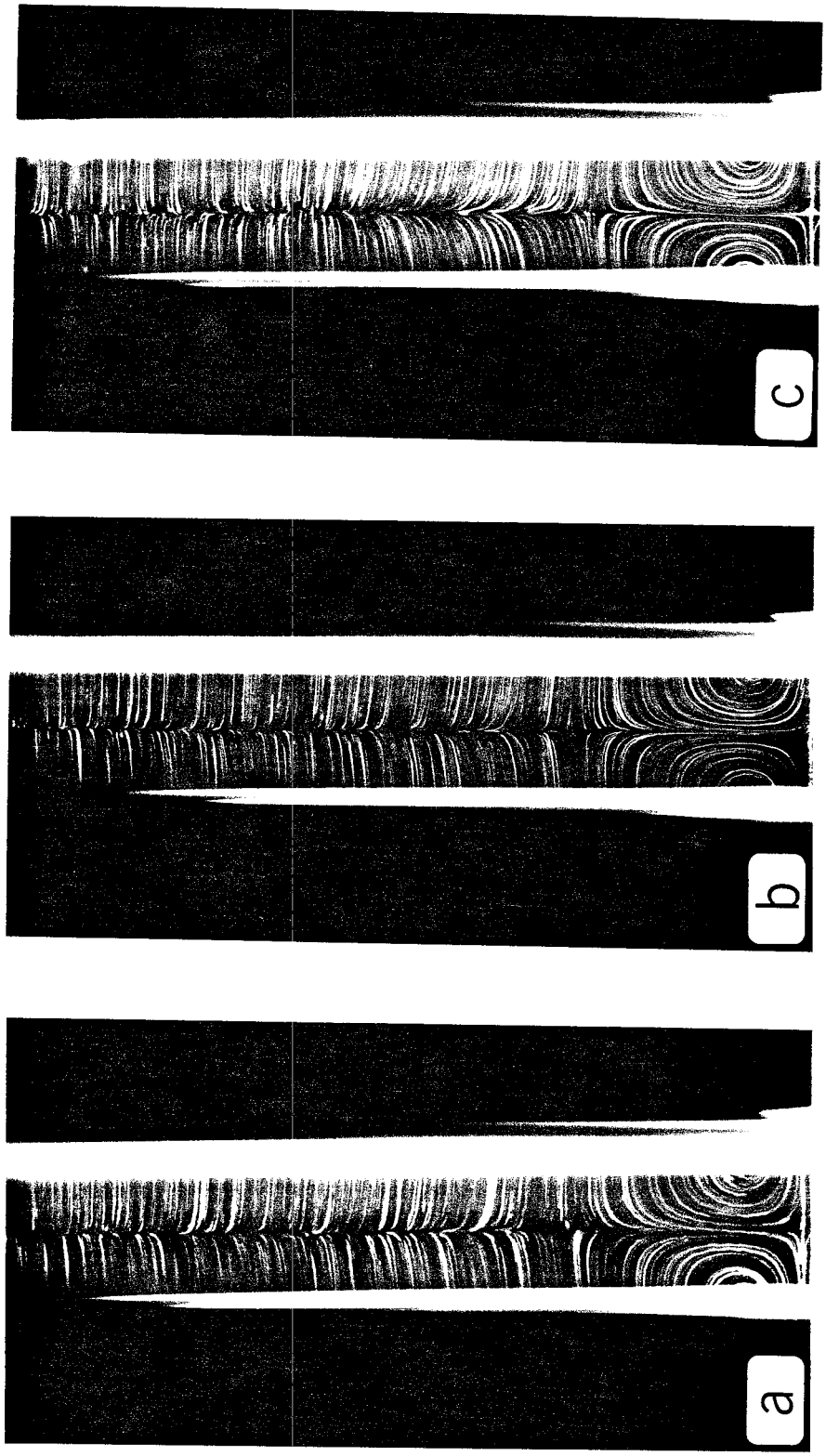

Figure 17

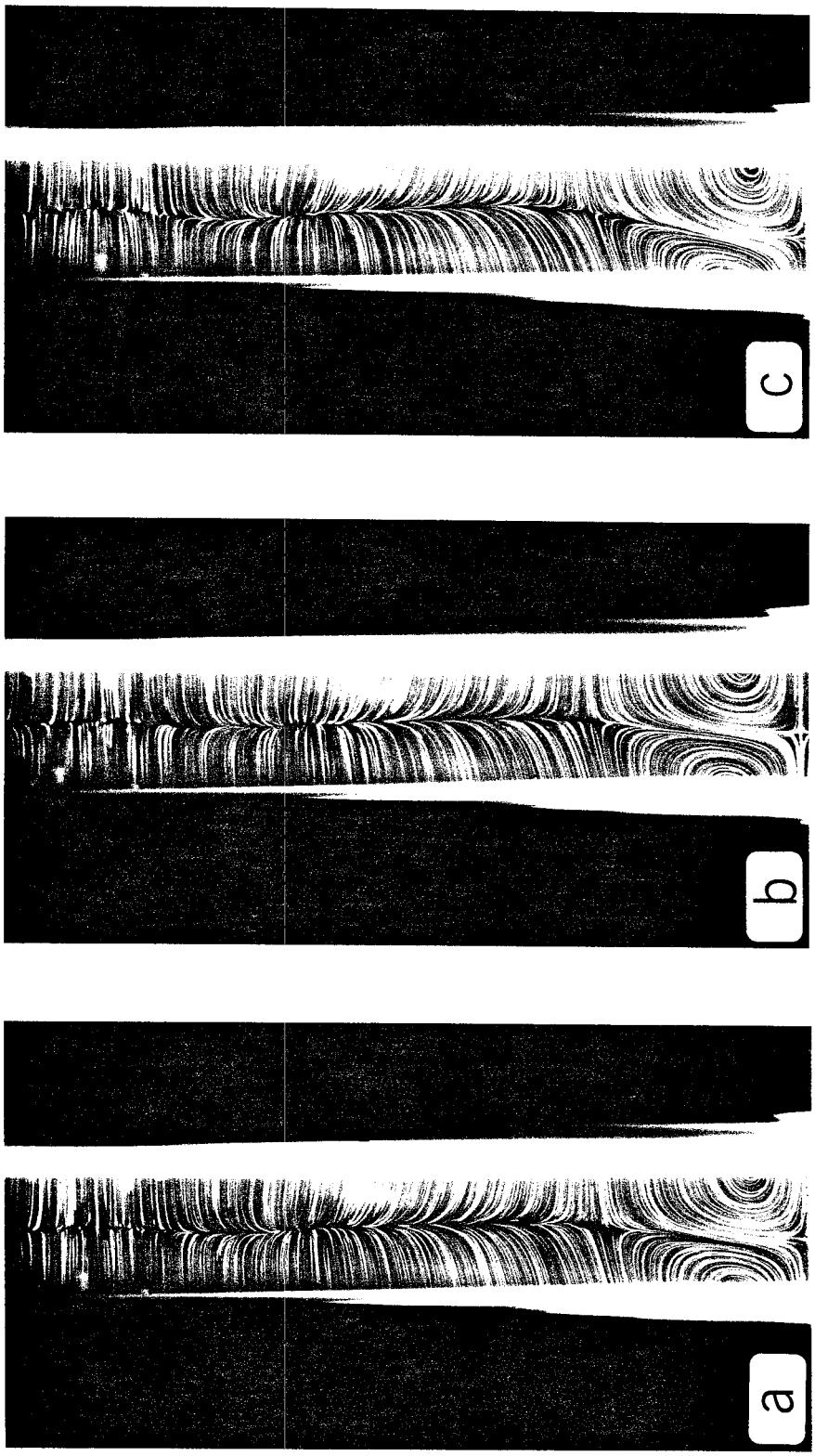

Figure 18

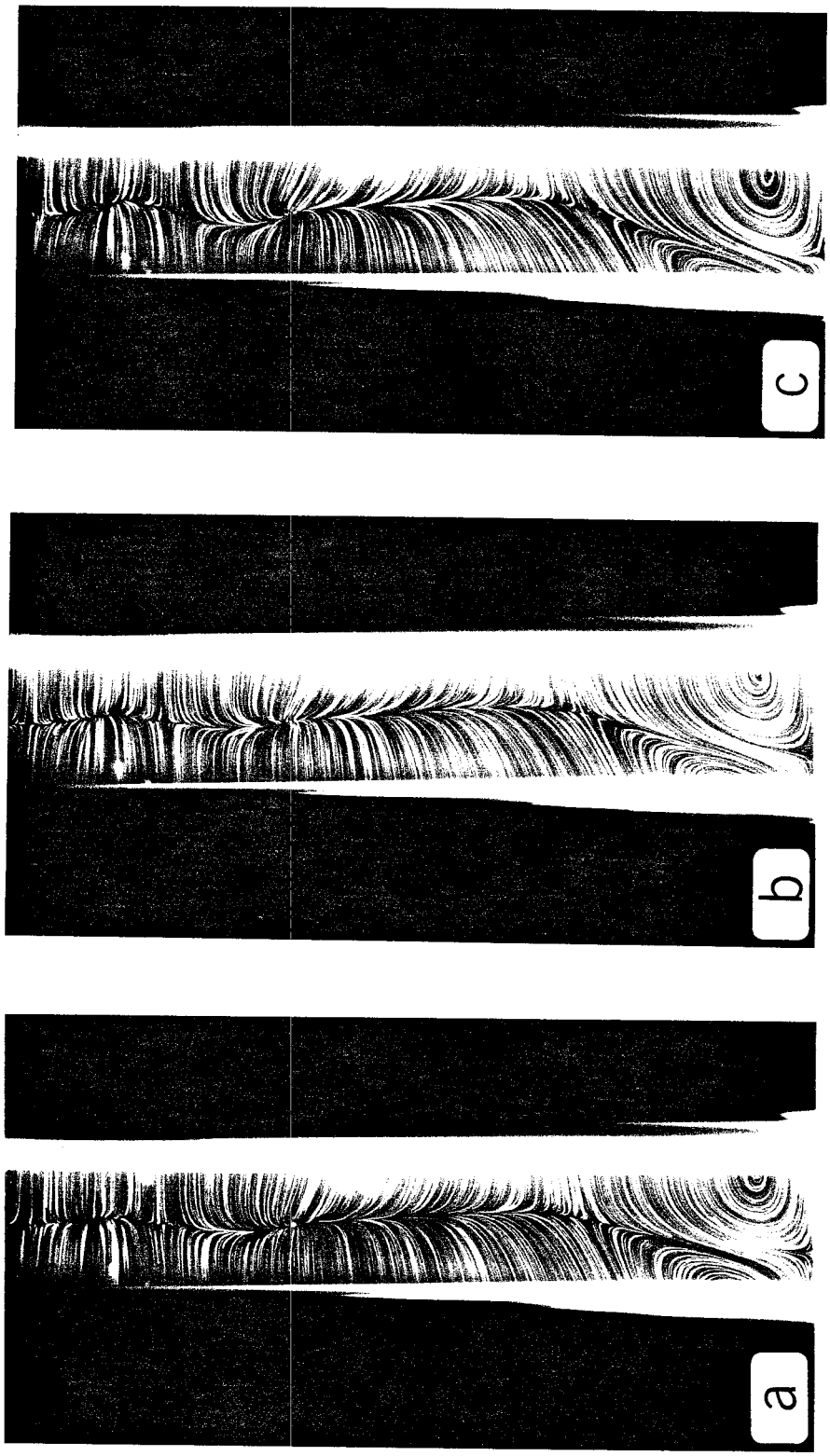

Figure 19

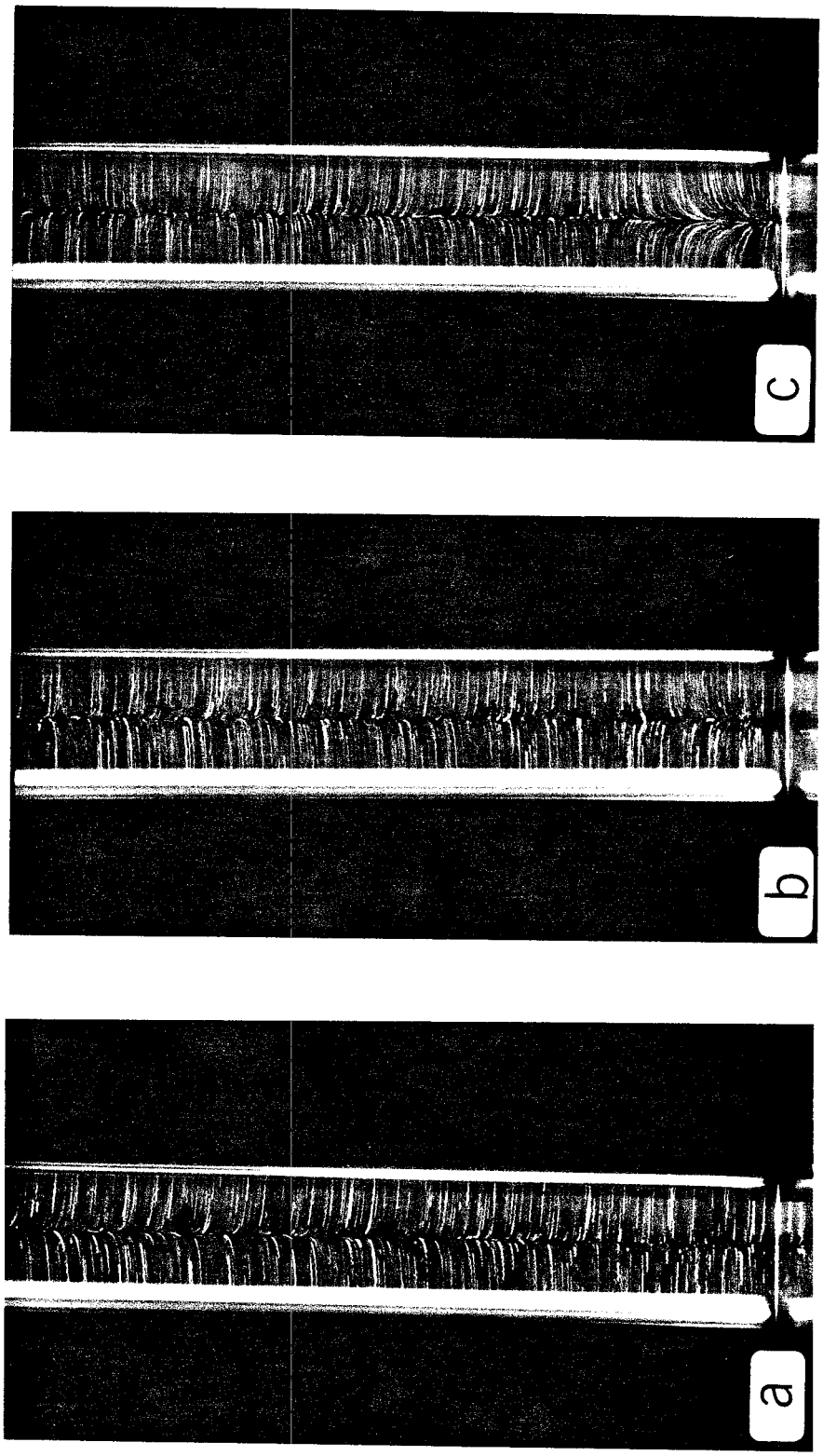

Figure 20

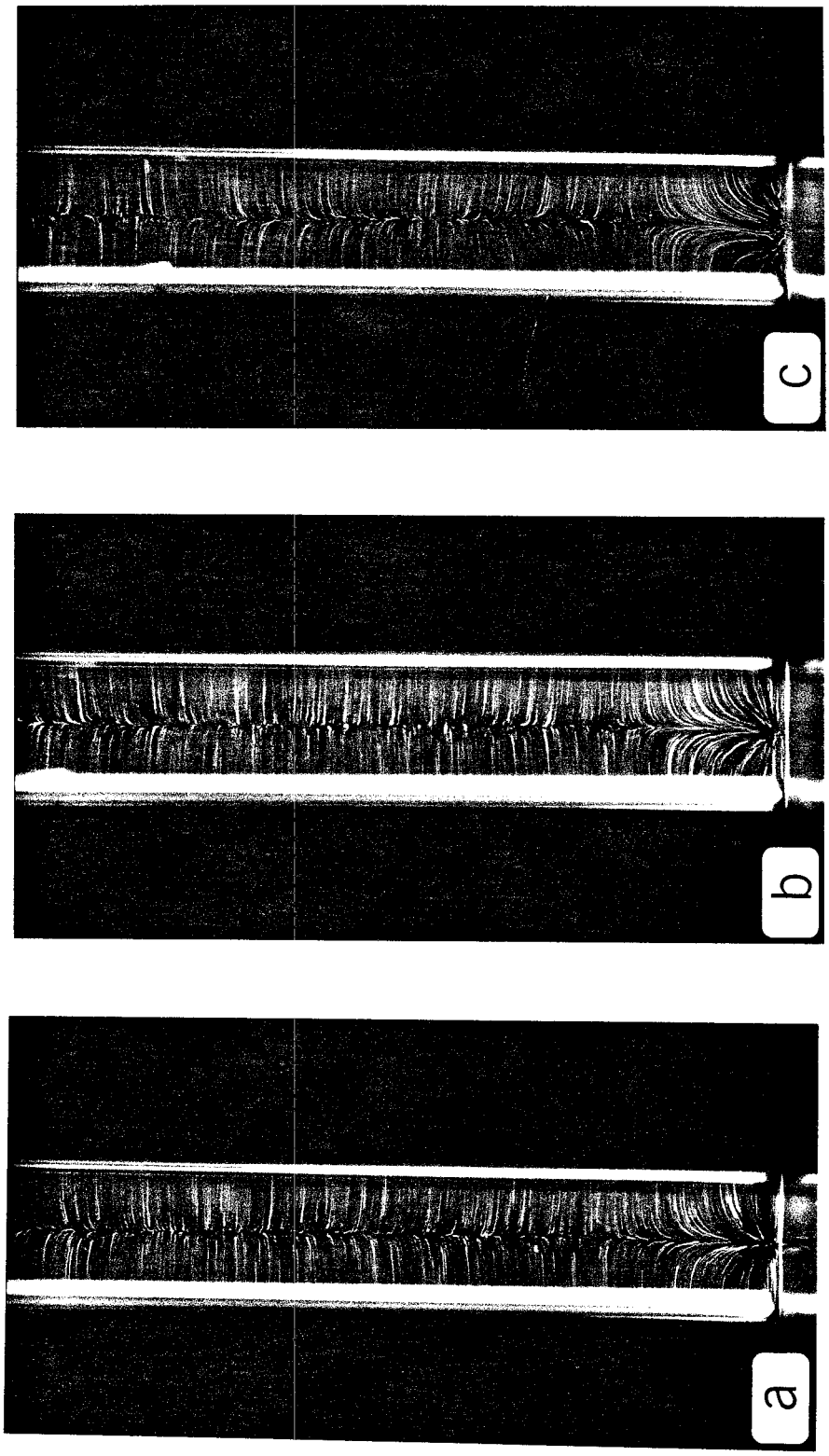

Figure 21

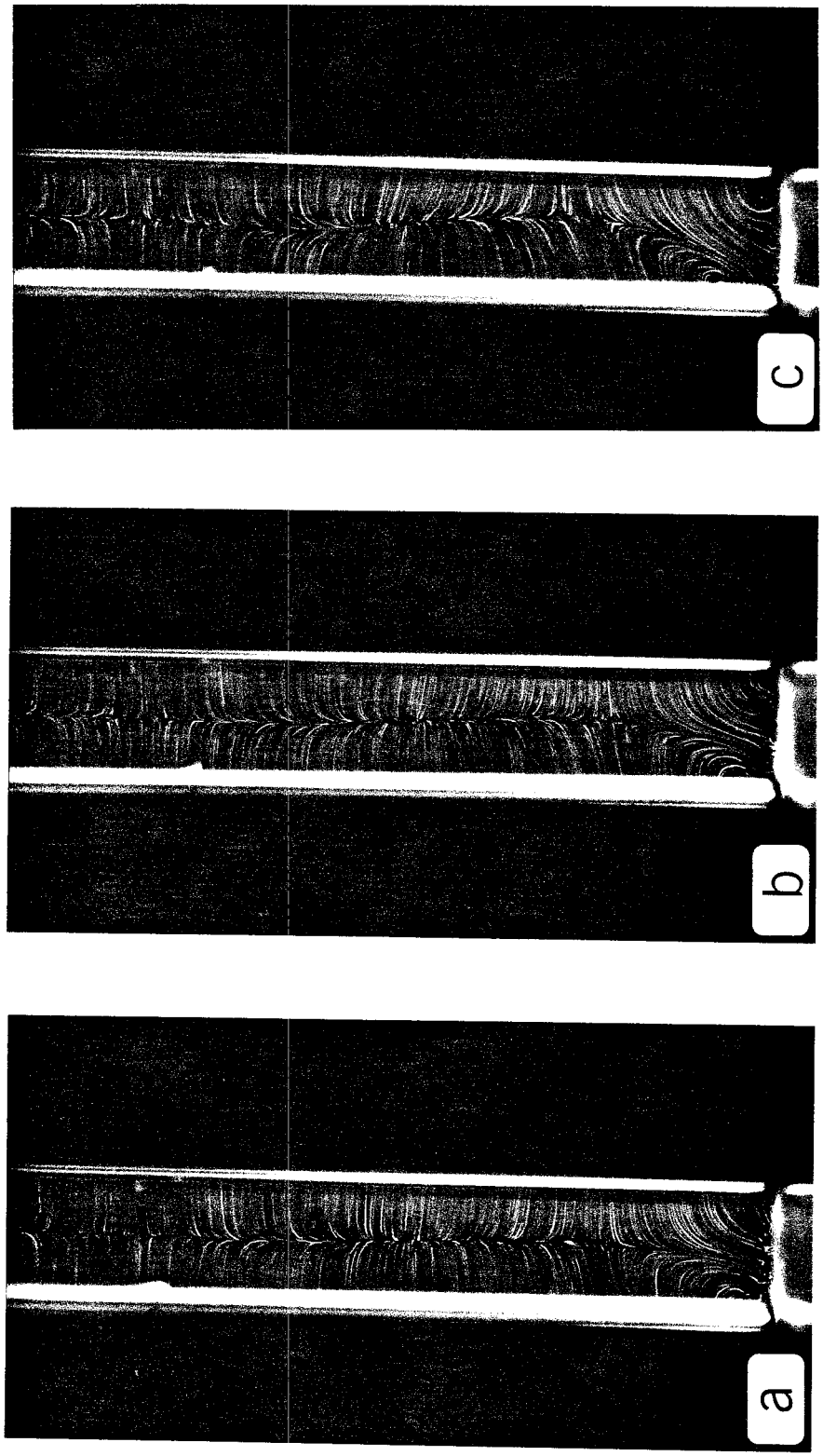

Figure 22